POST CRITICAL HEAT FLUX HEAT TRANSFER

by

EJUP N. GANIC

B.S., University of Belgrade
(1970)

M.S., University of Belgrade
(1972)

SUBMITTED IN PARTIAL FULFILLMENT
OF THE REQUIREMENTS FOR THE
DEGREE OF

DOCTOR OF SCIENCE

at the

MASSACHUSETTS INSTITUTE OF TECHNOLOGY

May 1976

Signature of Author Signature redacted
Department of Mechanical Engineering, May 25, 1976

Certified by Signature redacted
Thesis Supervisor

Accepted by Signature redacted
Chairman, Department Committee on Graduate Students

POST CRITICAL HEAT FLUX HEAT TRANSFER

by

EJUP N. GANIĆ

Submitted to the Department of Mechanical Engineering on May 25, 1976 in partial fulfillment of the requirements for the Degree of Doctor of Science.

ABSTRACT

An experimental and theoretical analysis of the post critical heat flux heat transfer has been performed. The transient experimental technique included a long tubular preheater section for creating a dispersed flow and a short tubular transient test section for collecting the heat transfer data (heat flux vs. wall superheat data). Liquid nitrogen was used as a test fluid. The mass velocities varied from 30,000 to 220,000 lb/ft^2hr.

Dispersed flow (a flow pattern associated with post critical heat flux heat transfer) consists of liquid drops dispersed in a continuous vapor phase. The theoretical study included: the analysis of the structure of a dispersed flow (the analysis of a drop size and drop size distribution); the analysis of the deposition motion of liquid drops (the migration of drops toward the wall); the analysis of the possible successive states of drops-wall interaction, and heat transfer to a drop deposited on the heated wall.

Based on the above analyses the expression for the heat flux from the wall to dispersed flow has been developed. It includes the heat flux to liquid drops deposited on the wall, the heat flux to vapor component of the flow, and radiative heat flux between the wall and dispersed flow. The developed expression for the heat flux has given good agreement with the experimental data.

The work, presented in this study, was undertaken as the post critical heat transfer has come to importance in recent years due to advancements in various technologies, such as in cryogenics, materials, rocketry, and especially in design and safety analysis of nuclear reactors.

Thesis Supervisor: Warren M. Rohsenow
Title: Professor of Mechanical Engineering

ACKNOWLEDGMENTS

My sincere thanks to my thesis supervisor, Professor Warren M. Rohsenow, for his advice, guidance, and encouragement, especially in the early days of my thesis research.

Professor Peter Griffith, Professor Ain A. Sonin, and Professor Philip Thullen, the members of my thesis committee, gave generously of their time to discuss various aspects of this work.

I wish to make a special note of thanks to Dr. M.G. Cooper, Cambridge University, England; Professor P.G. Saffman, California Institute of Technology; and Professor S.I. Rubinow, Cornell University, for comments related to a drop motion in a dispersed flow.

Discussions with my colleagues, Dr. O.C. Iloeje, Dr. D.N. Plummer, and Ms. G.E. Kendall, throughout this investigation, were very helpful.

Many thanks to all whose names did not appear here, but who have contributed to this work either directly or indirectly.

The thesis research was supported by a grant from the National Science Foundation.

Dedicated to my parents, my sisters, and my brothers

TABLE OF CONTENTS

PAGE

PAGE

LIST OF TABLES

LIST OF FIGURES

LIST OF FIGURES (continued)

LIST OF FIGURES (continued)

NOMENCLATURE

a	drop diameter, ft
a_c	drop deposition diameter, ft
A	surface, ft^2
B	transfer number [Eq. (4.4)]
C_D	drag coefficient
C_{D_0}	drag coefficient [Eq. (4.3)]
C_p	specific heat, Btu/lbm-°F
D	tube diameter, ft
f_g	friction factor [Eq. (4.44)]
$f(a_c)$	cumulative factor [Eq. (4.46)]
$\mathcal{f}$	gray body factor
F	interchange factor [Eq. (4.32)]
F	configuration factor [Eq. (4.35)]
F	force, lb
F_b	Basset Acceleration force, lb
F_d	drag force, lb
F_g	gravity force, lb
F_i	inertia force, lb
F_L	lift force, lb
F_p	force due to pressure gradient, lb
F_{cy}	reaction force [Eq. (4.30)], lb

F_{ry}	reaction force [Eq. (4.38)], lb
G	mass flux, lbm/ft^{2}hr
h	heat transfer coefficient, Btu/ft^{2}hr-°F
$H_{\ell g}$	latent heat of evaporation, Btu/lbm
k	conductivity, Btu/ft-hr-°F
K	constant [Eq. (4.15)]
N	drop deposition flux, # drops/ft^{2}hr
Nu	Nusselt number
P(a)	drop size distribution [Eq. (3.7)], 1/ft
Pr	Prandtl number
Q	heat transferred to single drop, Btu
q/A	heat flux, Btu/ft^{2}hr
Re	Reynolds number
S	slip ratio [Eq. (4.42)]
S_n	stability number [Eq. (3.2)]
t	time, s
T	temperature, °R, °F
U	gas or vapor velocity in the flow direction, ft/s
U*	friction velocity [Eq. (4.44)], ft/s
V	gas or vapor velocity (vector), ft/s
V_a	drop velocity, ft/s
V_g	vapor velocity [Eqs. (4.26)-(4.30)], ft/s
We	Weber number [Eq. (3.1)]
x	axial distance, ft

x	vapor quality
y	radial distance, ft
f	cumulative (deposition) factor [Eq. (4.46)]
v_0	drop deposition velocity, ft/s [Eq. (4.44)], $v_0 = 0.15 \frac{Gx}{\alpha\rho_g}\sqrt{f_g/2}$
U_0	mean gas (vapor) velocity, ft/s (Note: $U_0 = V_g$)
u_0	initial drop velocity in the flow direction at the edge of the laminar sublayer, ft/s [Eq. (4.41a)]

GREEK LETTERS

α	void fraction
γ	weight density, lb/ft^3
δ	boundary or laminar sublayer thickness, ft
ε	thermal emissivity
κ	constant
μ	viscosity, lbm/ft-hr
μm	micron
ρ	density, lbm/ft^3
ω	angular velocity, rad/s
	Stefan-Boltzmann constant, $Btu/ft^2hr\text{-}^\circ R^4$
	surface tension, lb/ft

SUBSCRIPTS

a	drop
d	drag
d	drop
e,E	equilibrium
g	gas or vapor
g	gravity
i	inertia
ℓ	liquid
L	lift
m	maximum
mp	most probable
r	radiation
s	surface
s	saturation
sv	volume-surface
sat	saturation
v	vapor
v	volume
w	wall or surface
wℓ	wall-liquid
wv	wall-vapor

CHAPTER I: INTRODUCTION

1.1 Post Critical Heat Flux Heat Transfer

The formation of a two-phase mixture by vapor generation in a vertical heated tube is shown in Figure 1.1. The presence of a heat flux through the tube wall alters the flow pattern from that which would have occurred in a longer unheated tube at the same local flow conditions [6].† At some position up the uniformly heated tube (Figure 1.1) the wall temperature exceeds the saturation temperature and vapor bubbles grow at the wall surface and by detaching form a bubbly flow. The bubble population increases with length and coalescence takes place forming slug flow. An annular flow then forms along the tube where now vapor generation is a result of evaporation at the liquid film-vapor core interface. Increasing velocities in the vapor core will cause entrainment of liquid in the form of drops. The depletion of the liquid from the film by this entrainment and by evaporation finally causes the film to dry out completely [6]. Drops continue to exist and are slowly evaporated until only single-phase vapor is present, Figure 1.1. The region between the dryout point and the transition to dry vapor has been termed the post critical heat flux heat transfer region (the post

---

†Numbers in parentheses refer to references, found on p. 122

critical heat transfer region, the liquid deficient region, the dispersed flow heat transfer region; the terms are used interchangeably), and is associated with the dispersed flow pattern. Figure 1.1 shows, in diagramatic form, the various flow patterns in addition to dispersed flow patterns encountered over the length of the tube, together with the heat transfer regions and wall and fluid temperatures variation and heat transfer coefficient variation. When dryout point is reached the wall temperature undergoes a sudden increase (Figure 1.1) due to a fundamental transition in the mechanism of heat transfer (the heated wall is no longer wetted by a thin liquid film through which heat is very efficiently carried away from the wall by forced convection in the film to the liquid film-vapor core interface, where evaporation occurs).

Dispersed flow is a particular but very important configuration of two-phase flow. In this configuration the liquid phase is the discontinuous phase, in form of drops, dispersed in the continuous vapor phase. The drops dimensions are very small, up to a few hundred microns, and therefore the surface tension acts in such a way that the drops behave as rigid spheres [10]. They are impelled by the vapor into a high turbulent motion; their velocity has transversal components, and the drops migrate toward the heated wall. Actually, only in the case of a heated wall does dispersed flow exist since in the case of an adiabatic wall, the drops deposited on the wall will form a thin liquid layer, changing the dispersed flow pattern into the annular flow pattern.

There is clear evidence [65,32] of a significant contribution of the

liquid drops to the heat transfer in dispersed flow but less clear are the mechanisms of this transfer. The mechanism of heat transfer to dispersed flow at wall temperatures below the Leidenfrost temperature is transition boiling, known as a mechanism where nucleate and film boiling both exist side by side. For the case where wall temperature is above Leidenfrost temperature the film boiling is the mechanism of heat transfer associated with dispersed flow. In this region the radiation heat transfer can be also significant, especially if the wall temperature is very high.

Post critical heat transfer has come to be important in recent years due to advancements in various technologies, such as in cryogenics, materials, rocketry, steam generators, and nuclear reactor design and safety. Much of the current interest in post critical heat transfer is due to its role in analysing and predicting heat transfer during a postulated loss of coolant accident in nuclear reactors.

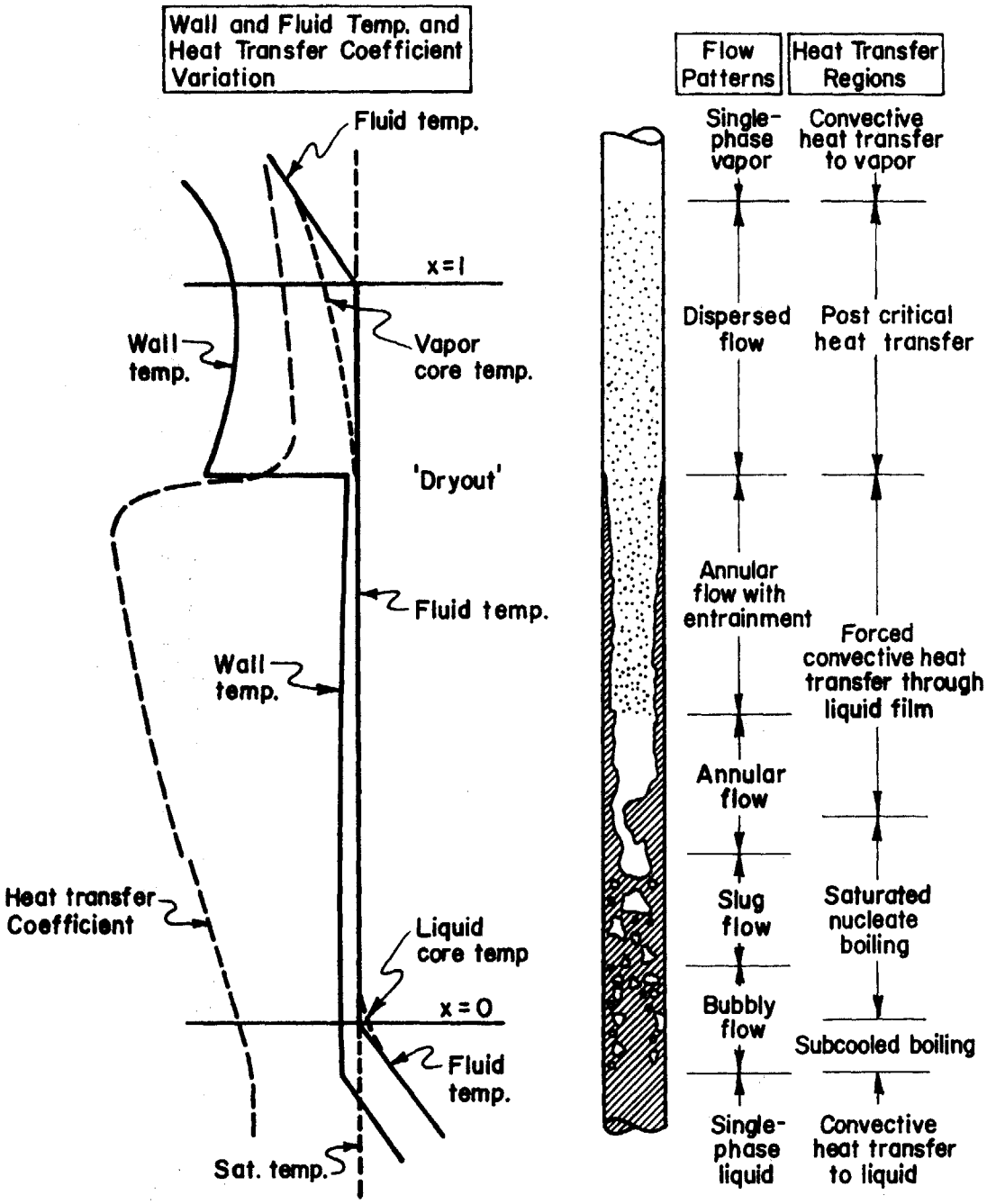

Figure 1.1 Regions of Heat Transfer in Convective Boiling (Uniformly Heated Tube, Low Heat Flux)[6, 68]

1.2 Literature Survey

Post critical heat transfer has been studied experimentally. Experimental data for steam-water mixtures in the pressure range 2000-3500 psi were published by Schmidt (1959), Swenson et al (1961), and Herkenrath et al (1967). Their data indicated the characteristic sharp increase in wall temperature at the dryout point followed by decreasing wall temperature as the vapor velocity increases with increasing vapor quality (Figure 7.11, ref. [6]). Wall temperatures increase once again in the superheat region as a result of the increase in bulk fluid temperature [6].

Similar studies to the above for cryogenic fluids flowing under forced convection in circular ducts are reported by Walters (1961), von Glahn and Lewis (1960), and Lewis et al (1962).

A number of empirical equations have been presented by various investigators for the estimation of heat transfer in the post critical region. Almost all of these correlations are modifications of the well-known Dittus-Boelter type relationship [6] for single-phase flow where various definitions of the "two-phase velocity" and physical properties are used. These correlations are listed in Table 1 of reference [24]. They generally predict a heat transfer coefficient based on the temperature difference between wall and saturation. As mentioned by Groeneveld (1975) they are simple to use but have a limited range of validity and should not be extrapolated outside the recommended range. Groeneveld's correlation, developed from post critical water data for tubes and annuli, is analyzed in reference [50]

where the region of applicability is mentioned. Recently published correlation by Tong and Young (1974) covers the transition and film boiling heat transfer in a steady water flow and provides good prediction of the experimental data from references [3,14].

Several MIT reports deal with a theoretical model for the prediction of the post dryout wall temperature as reported by Laverty (1964) and later by Forslund (1966) and Hynek (1969). In this model all parameters (drop size, vapor velocity, liquid velocity, void fraction, slip, etc.) are initially evaluated at the dryout location. It is assumed that heat transfer takes place in steps:

(a) from the heated wall to the vapor and then from the vapor to the drops;

(b) from the heated wall to liquid drops.

The heated channel is subdivided axially and the axial gradients in drop diameter, quality, vapor velocity, and liquid velocity are calculated at each node. The vapor superheat is evaluated from a heat balance at each node. The conditions at the downstream nodes are found by step-by-step integration along the heated channel. The wall temperature is then calculated at each node using superheated vapor heat transfer correlations. A similar model was independently developed by Bennett et al (1967).

Hynek (1969), in his thesis, clearly described two types of dryout which were experimentally observed. For the first type of dryout (Figure 6, reference [31]), low void fraction dryout, the inverted annual flow was observed downstream of dryout and a dispersed flow was created at certain

distance downstream after the liquid core was broken into liquid drops. The second type of dryout (Figure 1.1, or Figure 7 of ref. [31]) had all regimes of two phase flow existing upstream of dryout and dispersed flow starting from the dryout point.

Plummer et al (1974) and Iloeje et al (1974) extended work by Hynek by introducing the transient experiment for the experimental analysis of heat transfer in dispersed flow. They obtained experimental data in the film boiling region. In addition, Plummer presented a prediction scheme for correlating data in the film boiling region. Iloeje analysed the rewet phenomena in dispersed flow and proposed the additional mode of heat transfer in dispersed flow; heat transfer from the wall to liquid drops not touching the wall [32]. He also presented phenomenological prediction scheme of post critical heat transfer and compared it with the experimental data in the film boiling region.

The results of the work by Iloeje et al (1974) and Plummer et al (1974) stimulated this present study.

Further literature review was omitted in this section. It will be presented in the chapters III, IV, and V of this study where a closer look will be taken at some specific theoretical and experimental results, available in the literature and relevant to this study.

1.3 Objectives

The objectives of the present investigation include the following experimental and theoretical work:

1.3.1 Experimental work

The experimental work includes the analysis of the post critical heat flux heat transfer using transient experimental technique. Obtained experimental data will be presented in the boiling cure form (i.e., heat flux vs. wall superheat for a constant mass flux and vapor quality) covering both transition and film boiling regions.

1.3.2 Theoretical Work

The theoretical work includes the following analysis and derivations:

(1) Analysis of the structure of the fully-developed dispersed flow. Utilization of the relations for calculation of the maximum drop size, average drop size, and drop size distribution, in terms of mass flux and vapor quality.

(2) Analysis of the drop deposition in dispersed flow and development of drop deposition model capable of predicting a drop deposition flux (number of drops deposited on the heated wall per unit surface and unit time).

(3) Analysis of the experimental data in the literature concerning

the heat transfer to a single drop deposited on a wall. Characterization of the possible successive states of the drop-wall interaction and selection of an empirical relation for the heat transfer to a single drop.

(4) Derivation of the relation for the heat flux to dispersed flow which will cover both the transition boiling region and the film boiling region, applying results from (1), (2), and (3).

(5) Comparison of the experimental data with the relation which will be developed in Item (4).

CHAPTER II: EXPERIMENTAL PROGRAM

2.1 Apparatus

The loop diagram for the experimental apparatus is given in Figure 2.1. It is a once through system employing liquid nitrogen as the test fluid. It was constructed to allow for both a steady-state and transient test run, but the results analyzed here were obtained in the transient section.

The steady-state test section, a uniformly electrically-heated eight-foot long Inconel 600 tube 0.50 in. O.D. by 0.40 in. I.D., operates as a preheater for the transient test section. In this manner a two-phase flow mixture with a particular vapor quality and mass flux can be supplied to the transient section. The transient test section, Figure 2.2, consists of a one inch tube 0.40 in. I.D. by 1.00 in. O.D. supported and encased to be independently heated with steam supplied at a temperature of 220-250°F. The specimen is insulated from the supporting structure by micarta insulators (thermal conductivity of 0.2 Btu/ft^{2}hr). Three thermocouple holes 0.042 inches in diameter were drilled radially into the test pieces to a depth 1/32 of an inch from the inside radius [50]. The holes were spaced at three axial positions along each test piece with each hole circumferentially spaced 120 degrees apart. The thermocouples were coated with a conductivity gel and their leads were exited from the steam jacket through conex glands, to the recording devices. Further discussion of the apparatus and the instrumentation for monitoring of the test loop operations and data

acquisitions from the transient test section can be found in references [50] and [32]. In all cases copper-constantan thermocouples were utilized as the temperature sensing device.

2.2 Experimental Method

The following sequence of operations was carried out for obtaining dispersed flow heat transfer data. The steam supply to the transient section was turned on which allowed the specimen to reach an initial temperature of 220-250°F. Liquid nitrogen at 100 psia was allowed to flow through two heat exchangers that cooled it down sufficiently so that it remained liquid as it passed through the flow control valve. The subcooling was achieved by bleeding part of the main flow into a vacuum line, which forms the outer part of the two concentric-tube heat exchangers. The nitrogen subcooled 3-5°F was initiated into the preheater at about 20 psia. When the preheater thermocouples registered a temperature near the saturation temperature of the liquid, power was applied to the preheater. The flow rate and power were adjusted to give the desired value of mass flux and exit quality to the transient section for the particular run. When the steady state was achieved in the preheater the transient was initiated by closing off the steam flow to the transient section. The temperature transient was recorded following the data flow diagram in Figure 7, ref. [50]. Because of the nature of the test, all regimes of boiling existed on the test piece

during the transient. A run was terminated when nucleate boiling was re-established. Since the test piece was short, it was possible to assume that the quality variation with distance and time was negligible.

The nitrogen, before passing through the voltmeters (Figure 2.1), goes through one or two concentric-tube heat exchangers which serve to heat up the nitrogen to roughly room temperature. The steam or water that flows through the outer part of these heat exchangers also flows through another heat exchanger that heats up the vacuum line so that the vacuum pump does not freeze up.

2.3 Data Deduction

The three thermocouple outputs, the temperature-time history

$$T = T(t) \tag{2.1}$$

of the transient test section, did not differ significantly with the published thermocouple tables, within the published range. Figure 2.3 shows a typical temperature-time history curve with all regimes of boiling existing.

Considering the transient test section as a lumped heat source (no internal temperature gradients), the heat flux to the fluid during quenching is given as

$$q/A = \frac{V}{A} \rho C_p \frac{dT}{dt} \tag{2.2}$$

where

V = volume of the transient test section,

ρ = density of the test section material,

C_p = specific heat of the test section material,

A = heat transfer area of the test section,

and T = temperature.

The Biot number was calculated to be 0.01, 0.018, and 0.24 for the copper, aluminum, and inconel transient test section, respectively [32]. The characteristic dimension L on which Biot number was based was obtained by dividing the volume of the transient test section by its heat transfer area.

The heat flux to the two-phase mixture, for a particular quality and mass flux, was obtained by introducing the temperature-time data [Eq. (2.1)] into Eq. (2.2).

Figures 5.3 - 5.12 show the heat flux data obtained by the author. Appendix II-1 gives the estimate of the heat losses from the transient test section.

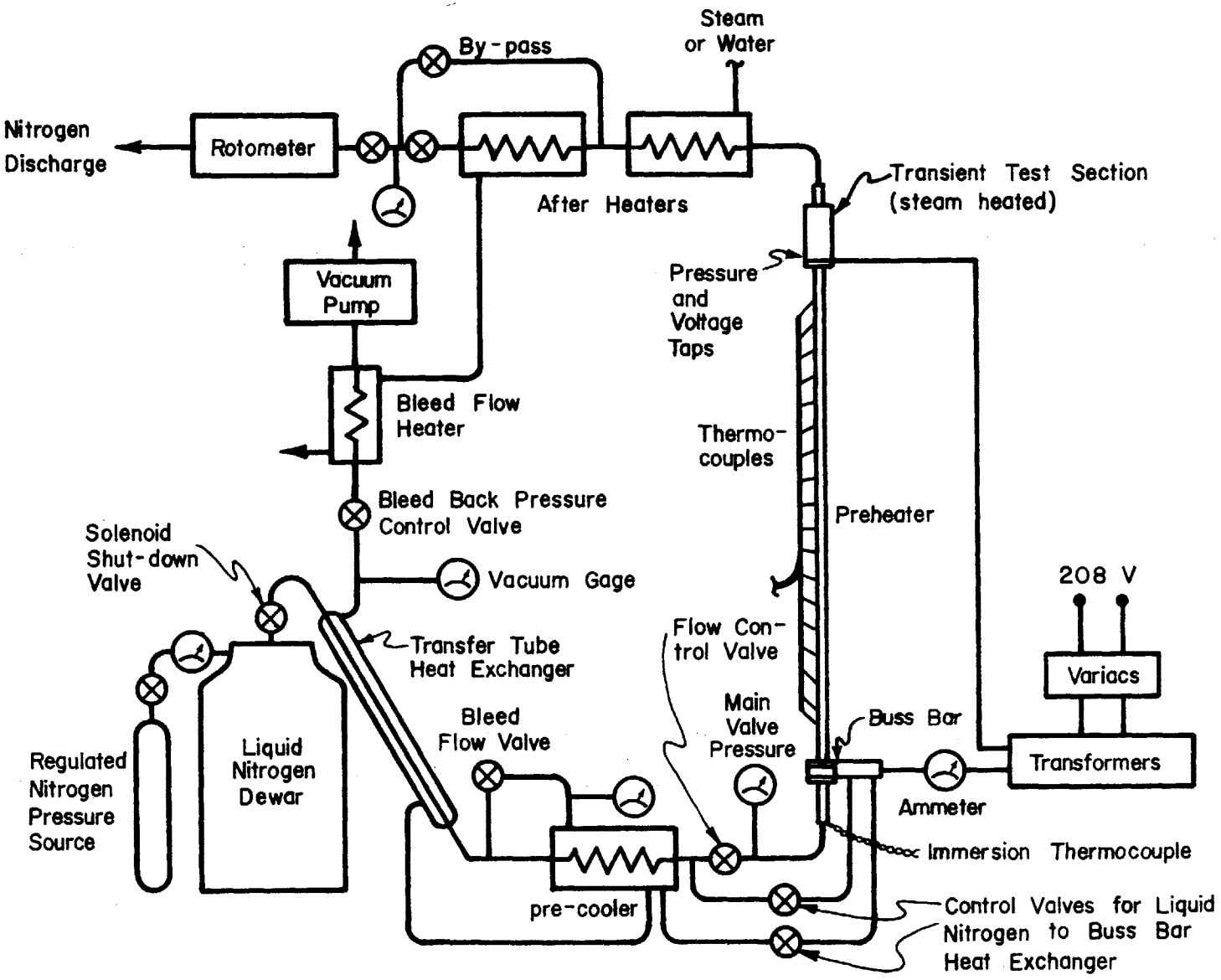

Figure 2.1 Nitrogen Test Loop

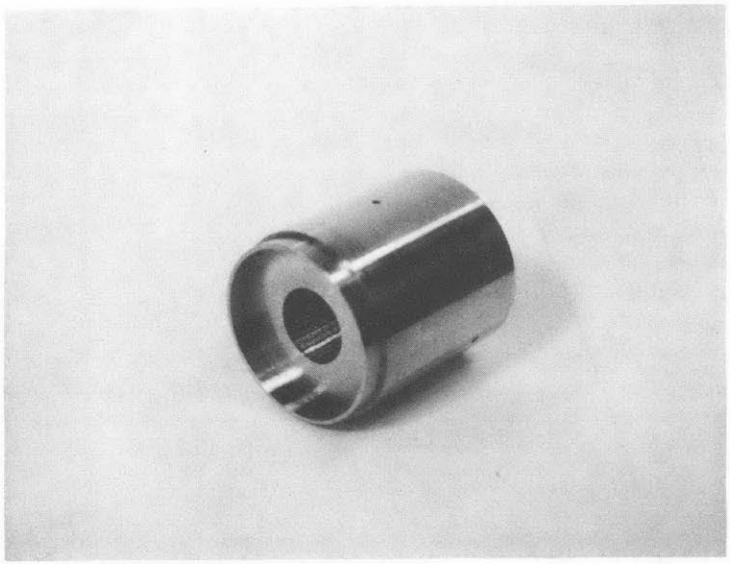

Figure 2.2 Transient Test Section

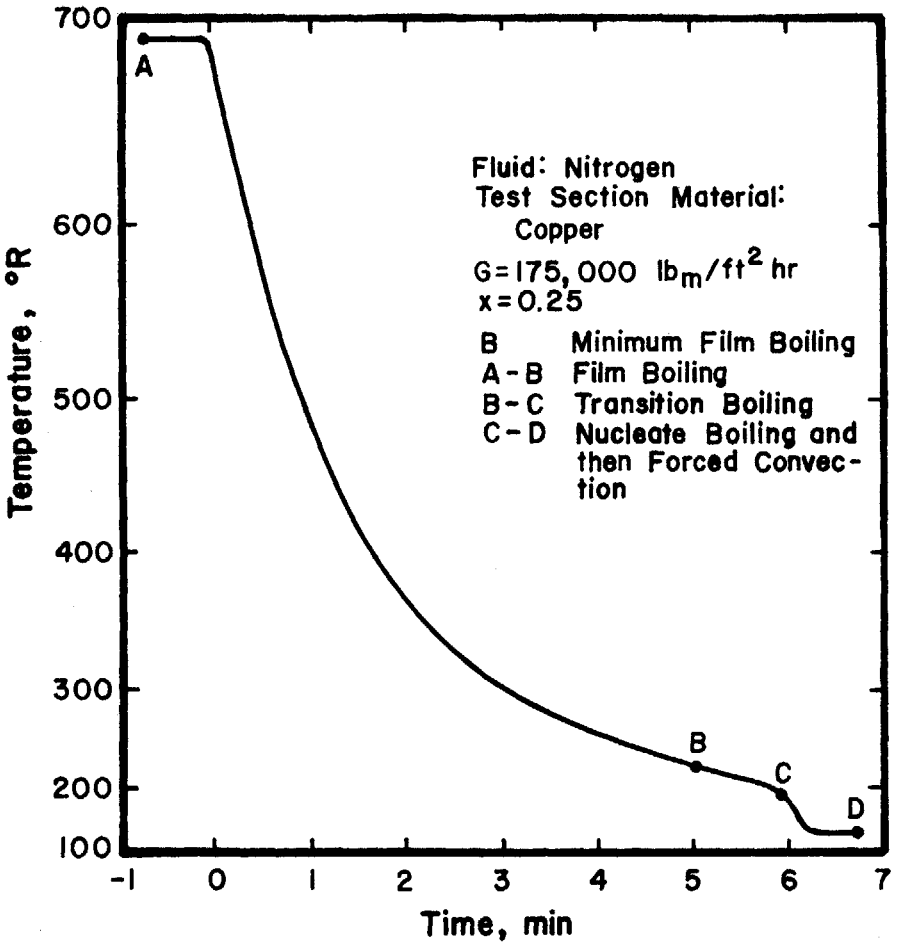

Figure 2.3 Temperature-Time History

CHAPTER III: STRUCTURE OF DISPERSED FLOW

The major concerns of this chapter are characterization of drop size and drop size distribution of a dispersed flow in terms of a mass flux and vapor quality. The distribution of mass of the liquid phase in a dispersed flow is important to the heat transfer and pressure drop characteristics of the flow.

Small liquid drops dispersed in a gas stream (dispersed flow) usually attain spherical shape due to surface tension. They are uniformly (statistically) mixed independently of their dimensions and the local gas velocity [10].

3.1 Maximum Drop Diameter

The maximum drop diameter is an important parameter because it evidently shows the maximum dimension that a drop can have in the particular conditions of dispersed flow. It constitutes in a certain sense a measure of the external forces which act on the drop, opposing surface-tension forces.

The most important dimensionless group for determining the stability of a single drop and its maximum size is the Weber number based on the relative velocity and the gas density [68],

$$We = \rho_g \frac{(V_g - V_\ell)^2}{\sigma} a \qquad (3.1)$$

where

σ = surface tension,

a = drop diameter,

ρ_g = gas density,

V_g = gas velocity,

and V_ℓ = liquid drop velocity.

A calculation of V_g and V_ℓ for a given mass flux G and quality x is presented in Appendix III-2.

Critical Weber numbers have been measured experimentally. Isshiki (1959) found that $We_c = 6.5$ agreed with his measured water drop diameters which were breaking up in an accelerating stream. This value agrees approximately with Forslund's (1966) value. He found $We_c = 7.5$ for liquid nitrogen drop in its vapor. Walles (1969) suggested that for nonviscous fluids the critical value of the Weber number above which drops will break up is about 12.

When a liquid drop is introduced into a gas stream at high value of We , several generations of drops will be produced by successive break up. In the eventual process of break up the drop is punched into a bag-like shape by the dynamic pressure of the gas acting at the stagnation point [68]. Liquid viscosity has a stabilizing effect on the drop shape which is scaled by the stability number S_n defined as [68]

$$S_n = \frac{\mu_\ell^2}{\rho_g a \sigma} \tag{3.2}$$

where μ_ℓ is the liquid viscosity.

If $S_n < 0.01$ a drop break up is not likely to occur unless the drop is suddenly accelerated [27,23].

In our dispersed flow study it was decided to use Forslund's value for the critical Weber number, so

$$a_m = \frac{7.5\ \sigma}{\rho_g (V_g - V_\ell)^2} \tag{3.3}$$

where a_m is the maximum drop diameter.

3.2 Mean Drop Diameter

A wide spectrum of drop diameters is present in dispersed flow. The mean drop diameter can be approximately predicted using Nukiyawa-Tanazawa equation [12,68,57],

$$\bar{a} = \frac{1.83}{(V_g - V_\ell)} \left(\frac{\sigma}{\gamma_\ell}\right)^{\frac{1}{2}} \tag{3.4}$$

where

$\bar{a}$ = mean drop diameter,

and γ_ℓ = liquid weight density.

Equation (3.4) has been widely used for predicting the mean drop diameter for atomization (shattering a continuous jet or sheet of liquid) with air. This equation is not dimensionless and care must be taken concerning the units which are a: m; V_g and V_ℓ: m/sec; σ: kg/m; and γ_ℓ: kg/m^3 . For a low mass flux G and quality x , $\bar{a}$ calculated from Eq. (3.4) is larger

than the experimentally observed mean drop diameter [58]. This is particularly true for a dispersed flow with heat addition, where a drop size is influenced not only by aerodynamics and surface forces, but also by evaporation at the drop interface (Appendix III-1). The correction factor C has been introduced into Eq. (3.4) so that a mean drop diameter in dispersed flow with heat addition is calculated using the relation

$$\bar{a} = \frac{1.83\ C}{(V_g - V_\ell)} \left(\frac{\sigma}{\gamma_\ell}\right)^{\frac{1}{2}} \tag{3.5}$$

The values for C , deduced from the experimental data† shown in Figures 5.3 - 5.12, are presented in Figure 5.13, which shows that C is a function of quality and mass flux.

3.3 Most Probable Drop Diameter

The most probable drop diameter a_{mp} satisfies the relation that $P(a)$ has a maximum value for $a = a_{mp}$ in the interval $0 < a < a_m$, where $P(a)$ is a drop size distribution. MacVean (1967) found that a great deal of data satisfied the relation

$$a_{mp} = \bar{a}/2 \tag{3.6}$$

---

†This will be explained in detail in Chapter V.

i.e., the mean drop diameter is twice as large as the most probable drop diameter.

3.4 Drop Size Distribution

The actual histogram of the size distribution of drops in a dispersed flow may, for purposes of this analysis, be replaced by a continuous curve, $P(a)$. The meaning of $P(a)$ is the probability of a drop having diameter between a and $a + da$. A large number of drop size distributions have been devised by experimenters in order to correlate data. Many authors [68,59] have used the normal and log-normal distributions which are also in common use for describing crushed particles.

In our study the following drop size distribution has been utilized:

$$P(a) = 4 \frac{a}{\bar{a}^2} e^{-2(a/\bar{a})^2} \tag{3.7}$$

where $\bar{a}$ is the mean drop diameter given by Eq. (3.5).

This type of distribution has been widely used for analyzing and solving mass transfer and evaporation problems of various dispersed flow systems [56,29,49]. It is important to mention here that the maximum drop diameter a_m calculated from Eq. (3.3) satisfies the relation

$$P(a_m) \simeq 0 \tag{3.8}$$

for $25000. < G < 220,000.$ lb/ft^{2}hr and $0.1 < x < 0.9$.

From Eqs. (3.7) and (3.8),

$$\int_0^{a_m} P(a)\, da \simeq 1.0 \qquad (3.9)$$

i.e., $P(a)$ has properties of a probability density function for $0 < a < a_m$.

The effects of the mass flux and quality on the drop size distribution [Eq. (3.7)] are presented in Figures 3.2 and 3.1, respectively. Figures 3.1 and 3.2 show that for higher mass fluxes and qualities, drops are smaller.

The above equations (3.3), (3.5), and (3.7) are sufficient to characterize the constitution of a dispersed flow, at least for the experimental conditions considered.

Experimental research on highly dispersed flow has been performed by Cumo et al (1973) employing Freon 12 at different pressures. The drops size distribution, and drops spatial concentration have been studied by means of a visualization technique for different thermohydraulic conditions (mass flux, quality and pressure). The drop size distribution expressed by the relationship

$$P(a) = \frac{a}{a_{mp}^2}\, e^{-a/a_{mp}} \qquad (3.9a)$$

has been deduced from their experimental data, where a_{mp} is the most probable drop diameter. Eq. (3.9a) is not very different numerically from Eq. (3.7).

Snyder (1959) also performed experimental study of drops size employing water at atmospheric pressure. The drops were trapped on a glass which was

coated with magnesium oxide and were measured by a traversing microscope. His three sets of the drop size distribution data, shown in Figure 1 of his thesis, follow basically the distribution law given by Eq. (3.7).

In the case when the drop size distribution is known (usually experimentally determined) the average (mean) drop diameters are defined according to [59],

$$\text{Mean diameter (length)} = \bar{a}_\ell = \frac{\int a\, P(a)\, da}{\int P(a)\, da} \tag{3.10}$$

$$\text{Mean volume diameter} = \bar{a}_v = \left[\frac{\int a^3\, P(a)\, da}{\int P(a)\, da}\right]^{1/3} \tag{3.11}$$

$$\text{Mean surface diameter} = \bar{a}_s = \left[\frac{\int a^2\, P(a)\, da}{\int P(a)\, da}\right]^{1/2} \tag{3.12}$$

$$\text{Mean volume-surface diameter} = \bar{a}_{sv} = \frac{\int a^3\, P(a)\, da}{\int a^2\, P(a)\, da} \tag{3.13}$$

Depending on the transport phenomena involved, $\bar{a}$ is given by one of these relations, Eqs. (3.10)-(3.13). For instance, when dealing with momentum transport of small drops at low relative velocity to fluid (Chapter IV), the mean diameter based on length is applicable. The mean surface diameter is related to heat and mass transfer and reaction at the fluid-particle interface.

The mean volume-surface diameter is related to rate processes affected by volume-to-surface ratio [59]. The mean volume diameter is related to determination of the void fraction (the total volume of drops per unit volume of space).

In the next two chapters we will be using drop size distribution $P(a)$ given by Eq. (3.7). The change of the mean drop diameter $\bar{a}$ [Eq. (3.5)] vs. vapor quality is demonstrated in Figure 3.3.

It is important to mention that even if there is no change in drop size because of the evaporation, the flow oscillations may produce the change of spectral distribution of sizes. For example, if the cloud of drops is accelerated, different sizes of drops will accelerate at different rates, and the differences in drop speeds will alter the relative concentrations per unit volume of the several drop sizes. These types of problems were not considered since no flow oscillations (except, of course, the small fluctuations that were masked by the throttling orifices) were present in any of the experimental data reported in this thesis.

In virtually all theoretical investigations of a dispersed flow the actual size distribution of drops was replaced by a simple model ("equivalent" size model) comprising a constant number of drops of uniform size. In some of these investigations the change in size of drops was allowed [3,23,17]. All these "equivalent" modes can give misleading results concerning drops-wall interactions (drops deposition). This will be discussed in more detail in the next chapter.

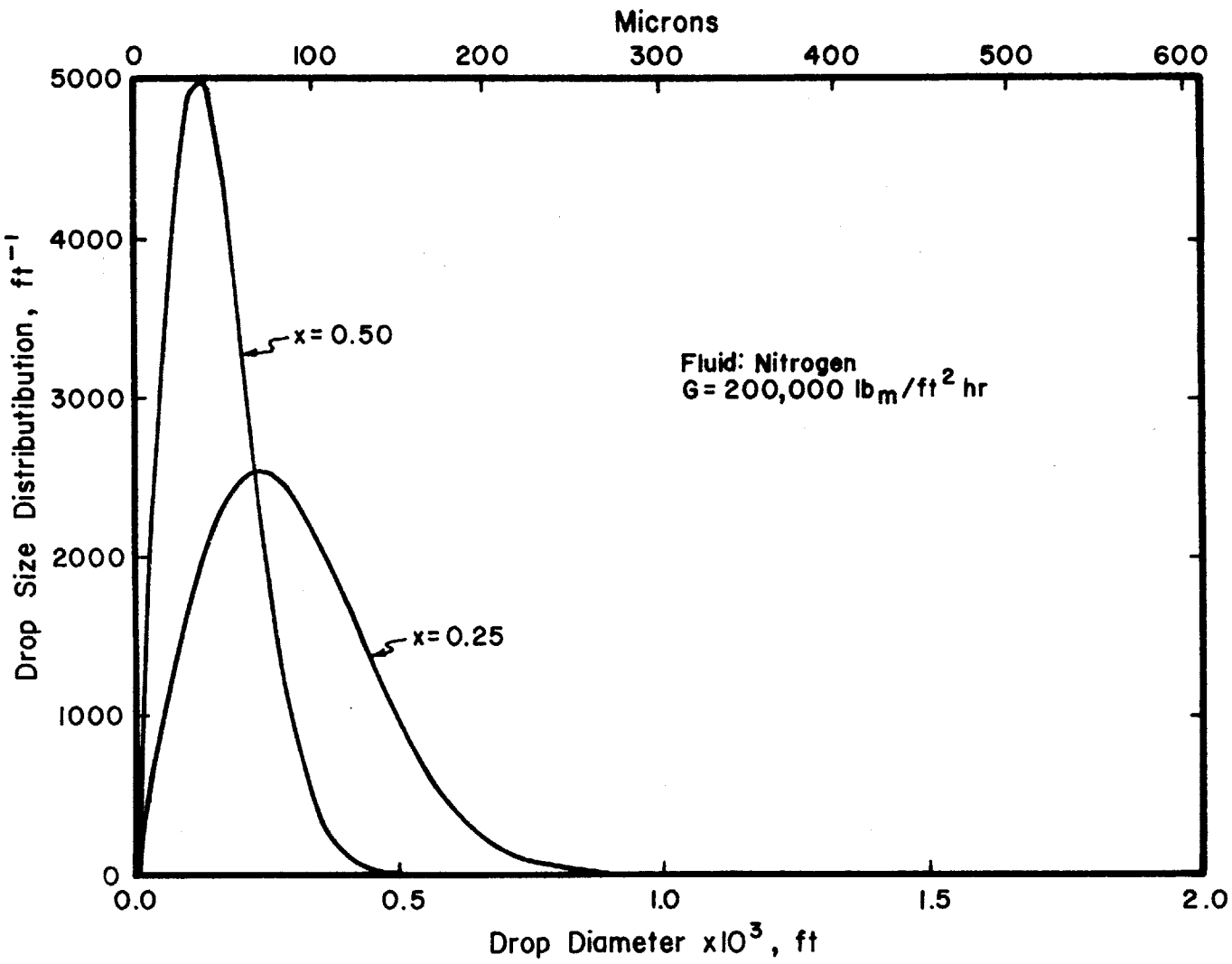

Figure 3.1 The Effect of Quality on the Drop Size

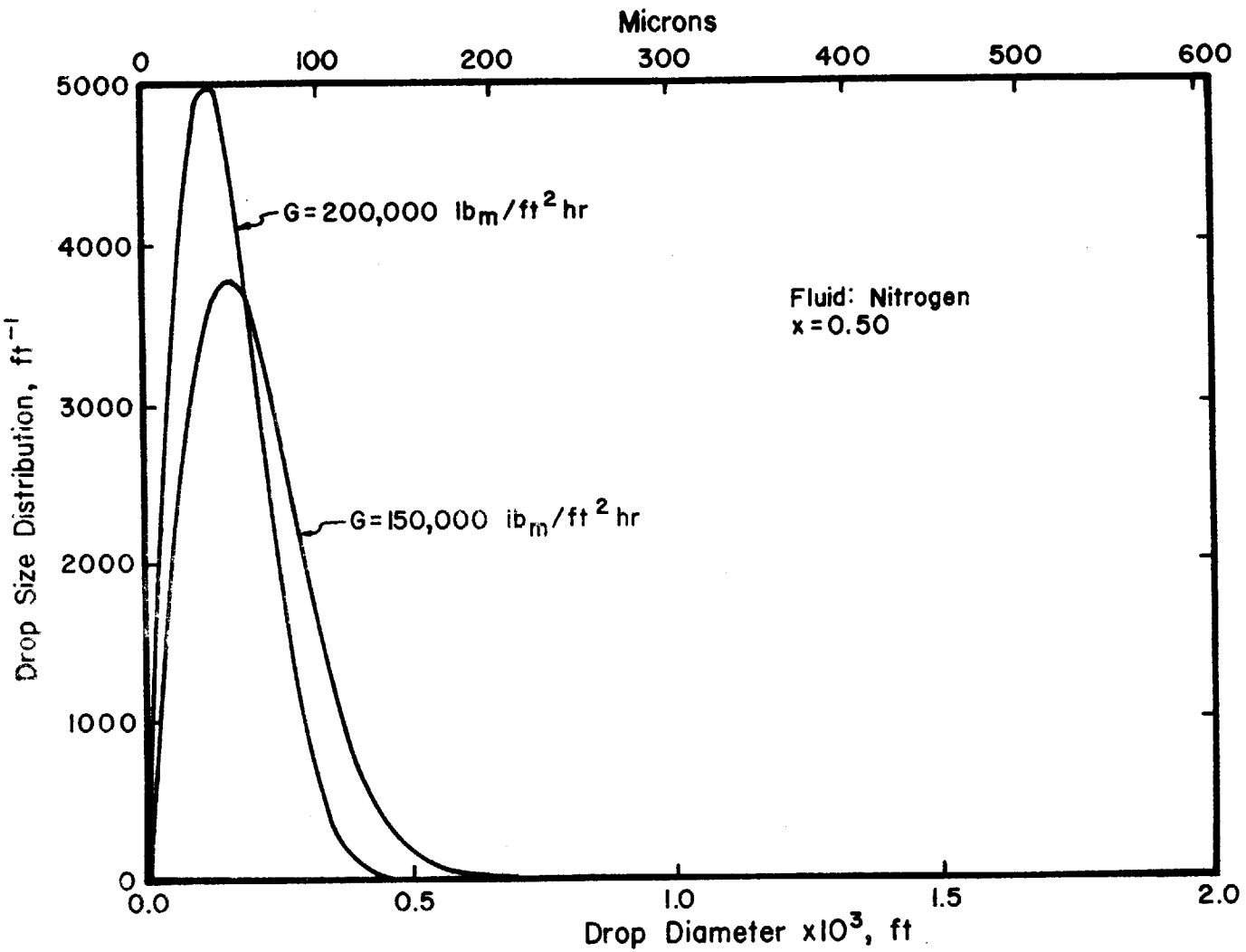

Figure 3.2 The Effect of Mass Flux on the Drop Size

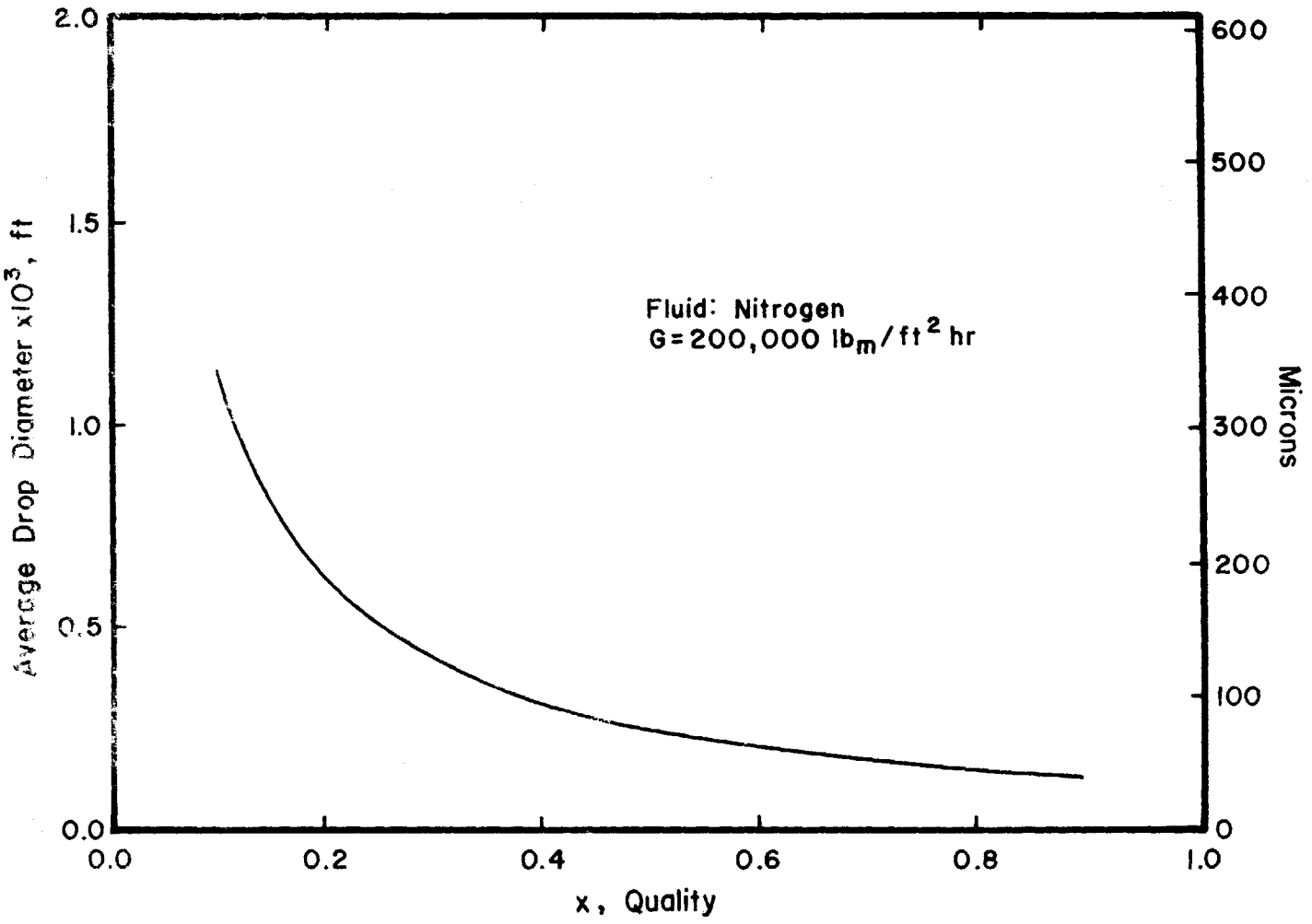

Figure 3.3 The Effect of Quality on the Mean Drop Diameter (Equation (3.5), C=0.26)

CHAPTER IV: MECHANISM OF LIQUID DROP DEPOSITION IN DISPERSED FLOW

The behavior of liquid drops suspended in a fluid stream (drop or dispersed flow) is of interest in a wide range of areas of technical importance. A knowledge of the trajectories of drops is important in the design of a number of industrial applications such as evaporators, nuclear reactors, spray coolers, and combustion devices involving sprays of liquid fuels. The theoretical approach in analyzing drop motion is generally similar to that of analyzing bubble motion. Equations of the motion of bubbles (bubbly flow) are analogous to drop motion. In spite of that, there are qualitative differences between the behavior of drops and bubbles. Those differences are most noticeable when the density difference between the components is high, as in gas-liquid systems at low pressure. In bubbly flow most of the inertia is in the continuous phase and as a result the drag forces on bubbles are large compared with their momentum. Bubbles therefore follow the motion of the surrounding fluid very closely in forced convection flow. Drops, however, take far longer to adjust to the motions of the surrounding gas. Also, for the dispersed flow heat transfer, some additional specific forces are associated with the drop motion.

The most important phenomenon in the dispersed flow is the deposition motion of drops. By deposition motion, we mean the migration of drops toward the wall. Up to now, a theoretical analysis of drop deposition from the gas stream on the hot wall has not been reported. The explanation of the deposition phenomena in the two-phase flow is associated with the theory of the

single drop motion inside the boundary layer.

4.1 Previous Work

The motion of the liquid drop inside the boundary layer is a well-known problem of particle migration in a shear field. In recent years there have been several investigations related to this problem. When a particle enters a shear flow it moves across fluid streamlines as a consequence of fluid dynamic forces. This kind of a particle motion can also be a consequence of the temperature gradient in the fluid stream, as we will show in this study. The forces on a particle in the fluid stream analyzed in most of the studies (Brenner, 1966) are inertia, drag, gravity, and buoyancy forces. In some of those studies, the lift force on a particle also has been considered but conclusions about the magnitude and importance of this force are not unique.

Deposition of water droplets in adiabatic turbulent downward air flow has been studied by Kondic (1970). The micron-size water droplets were generated at atmospheric pressure by the volumetric expansion of slightly superheated steam, mixed with the filtered atmospheric air. New techniques are introduced for the measurement of flow rates, drops deposition rate, and state variables of both components. No drop coagulation occurred. The balance of forces on the representative particle included the Magnus force (Swanson, 1961). A discussion of the magnitude and extension of validity of this force, for the conditions under which the experiment was performed, is presented. A reasonable agreement has been achieved between the computed and experimental results.

The theoretical analysis of the rigid particle motion within the laminar sublayer has been done by Rouhiainen and Stachiewicz (1970). The expression for the lift force developed by Saffman (1965) has been included in the analysis. The authors concluded that the lift force has a major effect on the trajectories of the particles in the certain range of the particle sizes. The numerical value of K [see Eq. (4.15) of this article] in Saffman's expression for the lift force was 81.2 instead of 6.46 . This numerical error, in the original Saffman paper of 1965 where a factor of $(4\pi)^{-1}$ is missing from the second line of the Eq. (4.11), was discovered by Harper and Chang (1968). Most of the numerical results in the Rouhiainen and Stachiewicz analysis are affected by the value of K .

The characteristics of the motion of a drop in a two-phase boundary layer on a flat plate have been reported by Deich and Ignat'evskaya (1970). In their study they included the lift force derived by Rubinow and Keller (1961). They obtained the experimental relationship of the change of liquid film thickness formed by drop deposition as a function of the initial parameters of a two-phase flow. The effect of the lift force on their experimental results has not been presented.

Denson et al (1966) analyzed the motion of a single rigid sphere entrained in a glycerine-water solution flowing downward through a cylindrical tube. A range of particle Reynolds numbers was from 6 to 120, tube Reynolds numbers of 208 to 890, and particle-to-tube diameter ratios of 0.12 to 0.19 . Trajectories of the sphere, calculated for various particle Reynolds numbers by using the Rubinow-Keller expression for the lift force, were found to agree

satisfactorily with experimentally determined trajectories when the particle Reynolds number was below 40.

A critical review of the work published prior to 1966 on investigations of the radial motion of particles and liquid drops in fluid stream has been presented by Brenner (1966).

The comparison of the theoretical and experimental values for the deposition velocities of liquid drops and solid particles in dispersed flow systems has been summarized by Liu and Ilori (1973). The experimental data obtained by Farmer (1970) are included in their analysis.

In a recent paper by Gauvin et al (1975) the work on spray dryers has been summarized and extended.

In spite of a large number of published studies, the theory of the drops deposition in dispersed flow with heat addition (dispersed flow heat transfer) has remained largely unexplored.

4.2 Analysis

Dispersed flow heat transfer is high void fraction flow. Because of this, the drop concentration is low, the interference of neighboring drops may be neglected, and the single drop may be treated as if it were alone in the medium.

Also, since we are focusing our analysis on the drop motion through the boundary layer (laminar sublayer), we are assuming that the drop diameter is small compared to the thickness of this layer. This is the kind of continuum

criterion to be satisfied. This basically means that the forces on the drop are dependent on the local vapor velocity and temperature of the stream.

In order to obtain some useful and reliable results the additional following simplifying assumptions for the motion inside the laminar sublayer are made:

(a) Drop has a spherical shape.

(b) Flow in the two-component, two-phase stream is laminar, two-dimensional, steady, and incompressible.

(c) The change of the drop diameter due to evaporation during deposition motion is not significant.

The list of forces during accelerated motion of the drop includes:

1. Inertia force
2. Drag force
3. Gravity and buoyancy forces
4. Lift force
5. Reaction force
6. Other forces.

4.2.1 Inertia Force

Inertia force acts on the drop as the resultant force

$$F_i = \frac{\pi a^3}{6} \rho_\ell \frac{dV_a}{dt} \tag{4.1}$$

where

a = drop diameter,

ρ_ℓ = density of the drop (particle),

and V_a = drop velocity.

4.2.2 Drag Force

Since the drop Reynolds number for our conditions is close to one, the drag of the medium due to viscosity μ_g is, according to Stokes Law,

$$F_d = 6\pi \mu_g \frac{a}{2} (V - V_a) \tag{4.2}$$

where V is the velocity of the fluid (vapor or gas).

The motion of the drop inside the boundary layer is unsteady, but it is customary to assume that the Stokes law may be used (Hidy, 1970). On the other hand, the drag problem becomes more complicated because of the evaporation of the drop and the possibility for circulation of liquid inside the drop. Evaporation can reduce the drag coefficient due to mass flux from the surface, for which Bailey et al (1970) suggests the following correlation:

$$C_{D_0} = C_D/(1 + B) \tag{4.3}$$

where B is the transfer coefficient (Spalding number), given by

$$B = C_g \frac{\Delta T}{H_{\ell g}} \tag{4.4}$$

where

C_D = drag coefficient corresponding to no evaporation,

C_g = specific heat of the diffusing vapor,

T_v = vapor temperature,

ΔT = $(T_v - T_s)$ = temperature difference,

and $H_{\ell g}$ = latent heat of evaporation.

The Spalding number is generally small compared to unity for an evaporating drop. This will be numerically proven below.

The circulation of the liquid inside the moving drop has been studied by Rybczynski and Hadamard and summarized by Hidy and Brock (1970). They found that the Stokes drag was modified by a factor involving the ratio of viscosities of two fluids, or

$$C_{D_0} = C_D f_\mu$$

where

$$f_\mu = \frac{1 + 0.75(\mu_g/\mu_\ell)}{1 + (\mu_g/\mu_\ell)} \tag{4.5}$$

For example, for a water drop in air, the correction f_μ is 0.994 at 20°C; for a liquid nitrogen drop $f_\mu = 0.99$ at atmospheric pressure. Therefore, for most practical considerations, one may disregard the correction due to the circulation inside the drop.

The Stokes drag for the sphere is derived for the case of uniform flow passing a sphere. On the other hand, the motion of a drop inside the boundary

layer is a shear flow problem as the velocity gradient is very high. This has been the subject of the experimental study by Kohlman and Mollo-Christensen (1965). They demonstrated that shear flow does not affect the drag for low Reynolds number. The reader is referred to their study for more details.

4.2.3 Gravity and Buoyancy Forces

The resultant force of these two forces is

$$F_g = \frac{\pi a^3}{6} (\rho_\ell - \rho_g)\, g \tag{4.6}$$

where g is the gravity vector and ρ_g fluid density.

4.2.4 Lift Force

Rotation of the drop occurs in the presence of a velocity gradient in the boundary layer (laminar sublayer). This is a well-known phenomenon that the velocity gradient can cause a solid particle to rotate. At low Reynolds numbers rotation causes fluid entrainment, increasing the velocity on one side of the body and lowering the velocity on the other side. This is known as the Magnus effect and tends to move the particle toward the region of higher velocity (Soo, 1967). The radial migration of solid particles and liquid drops in shear flow has been experimentally studied as we mentioned before. Most of the experimental data of this kind have been interpreted on the basis of Rubinow-Keller's Eq. (4.7) for the lift force on a spinning translating sphere in an unbounded fluid at rest (or in uniform flow) at

infinity.

By using Stokes' and Oseen's expansions and solving the Navier-Stokes equation, inertia term retained, Rubinow and Keller (1961) found that for the flow about a spinning sphere moving in a viscous fluid, the sphere experiences a force F_L (lift force) orthogonal to its direction of motion, in addition to the drag force determined by Stokes. The force is given by

$$F_L = \frac{\pi a^3}{8} \rho_g \omega \times (V - V_a) \left[1 + O(Re_a)\right] \tag{4.7}$$

Here a is the diameter of the sphere, ω is its angular velocity, $(V - V_a)$ is the linear velocity of the sphere relative to the fluid, ρ_g is the fluid density, and Re_a is the sphere Reynolds number,

$$Re_a = \frac{\rho_g (V - V_a) a}{\mu_g} \tag{4.8}$$

For the steady motion the angular velocity of the sphere is equal to the angular velocity of the flow. This is experimentally verified by Kohlman and Mollo-Christensen (1965) in the constant shear flow.

For the two-dimensional motion, the angular velocity of the flow is determined by the expression

$$\omega_g = \frac{1}{2} \left(\frac{\partial v}{\partial x} - \frac{\partial u}{\partial y} \right) \tag{4.9}$$

In the boundary layer,

$$\omega_g \simeq -\frac{1}{2} \frac{du}{dy} \tag{4.10}$$

so the spin of the drop is now given by Eq. (4.10). Rather remarkably, the Rubinow-Keller lift force is independent of viscosity for small values of Re_a . This force is comparable to the well-known Magnus force (Goldstein, 1938), arising at very high Reynolds numbers, usually invoked to explain such phenomena as the curving of a pitched baseball. Also, this force is very similar to the lift formula for two-dimensional potential flow about an airfoil.

Saffman (1965) derived the net force acting on a small translating sphere which is simultaneously rotating in an unbounded, uniform, simple shear very viscous flow, the translation velocity being parallel to the stream lines. In his analysis he applied the inner and outer solution technique to the equation of motion. Three independent Reynolds numbers based on sphere diameter arise in the analysis:

$$\text{Slip:} \qquad Re_a = \frac{\rho_g (V - V_a) a}{\mu_g} \tag{4.11}$$

$$\text{Shear:} \qquad Re_k = \frac{\rho_g a^2}{\mu_g} \frac{dV}{dy} \tag{4.12}$$

$$\text{Rotation:} \qquad Re_\omega = \frac{\rho_g a^2}{\mu_g} \omega \tag{4.13}$$

The analysis is valid when

$$Re_a , Re_k , Re_\omega << 1.0 \quad \text{and} \quad Re_k , Re_\omega >> Re_a{}^2 \tag{4.14}$$

and the transverse force is given by

$$F_L = K \frac{a^2}{4} (\rho_g \mu_g)^{\frac{1}{2}} \left(\frac{dV}{dy}\right)^{\frac{1}{2}} (V - V_a) \qquad (4.15)$$

plus a smaller term[†] perpendicular to the flow direction which acts to deflect the particle towards the streamlines. A numerical constant K has a value of $K = 6.46$ obtained by a numerical integration.

When the conditions given by Eq. (4.14) are met, the slip-shear Saffman lift force [Eq. (4.15)] can be an order of magnitude larger than the slip-spin Rubinow-Keller lift force [Eq. (4.7)]. On the other hand, these conditions [Eq. (4.14)] are not satisfied in many kinds of dispersed flow systems, specifically those with high flow Reynolds number, which makes the range of the possible applicability of Saffman's lift force limited.

The directions of the lift force on the small sphere (drop) inside the boundary layer are shown in Figure 4.1 for the cases:

(a) when the velocity component of the drop is less than the velocity of the fluid (slip flow);

(b) when the velocity component of the drop is greater than the velocity of the fluid.

[†]The smaller term which is due to rotation is given by

$$\pi \frac{a^3}{8} \rho_g \omega (V - V_a) \qquad (4.15a)$$

4.2.5 Reaction Force

As we mentioned before, this force is due to asymmetrical drop evaporation inside the boundary layer. There is a high temperature gradient in the fluid stream close to the wall because the wall temperature is much higher than the fluid temperature. Since the fluid temperature is larger than the drop temperature (saturation temperature assumed), the evaporation of the drop occurs. The difference in these two temperatures is larger for the drop side facing the wall than for the other side of the drop because of the temperature gradient in the fluid stream. This causes the vapor velocity generated on the drop side facing the wall (bottom side) to be higher than the vapor velocity generated on the other side. This produces a reaction force which tends to prevent a deposition of the drop on the wall.

The derivation of the reaction force is based on the following assumptions:

(a) The temperature profile inside the boundary layer is a linear one:

$$T = T_s + (T_w - T_s)\left(1 - \frac{y}{\delta}\right) \tag{4.16}$$

where y = the distance from the wall,

δ = laminar sublayer thickness,

T_w = wall temperature,

and T_s = saturation temperature.

The temperature gradient is now

$$\frac{dT}{dy} = -\frac{(T_w - T_s)}{\delta} \tag{4.17}$$

(b) The Nusselt number related to the drop heat transfer is given by the relation (Bird et al, 1960)

$$Nu_a = 2.0 + 0.6\, Re_a^{0.5}\, Pr^{0.33} \qquad (4.18)$$

and the circumferential variation of this number is negligible. Since the drop Reynolds number for our condition is close to one, then

$$Nu_a \simeq 2.6 \quad \text{as} \quad Pr \simeq 1 \qquad (4.19)$$

Equation (4.18) is good for small heat transfer rate. In the case of high evaporation rate (drop is very close to the hot wall), the correction to the Nusselt number is needed, similar to that suggested by Bailey (1970).

(c) The boundary layer thickness around the spherical drop moving in shear flow is approximately given by the potential flow theory. This thickness is then of the correct order of magnitude of drop diameter when the drop Reynolds number is close to one (Schlichting, 1970).

As we mentioned before, the drop diameter is much smaller than the thickness of the laminar sublayer. The above leads us to the conclusion that the drop stay time (deposition time or time measured from the moment a drop enters the boundary layer until it touches the wall) is much larger than the time for a heat diffusion through the drop boundary layer. As long as this conclusion is valid, the drop motion inside the boundary layer is influenced

by the temperature distribution in it.

The evaporation of the drops occurs due to convective heat transfer from the fluid stream (vapor) to the drop and radiative heat transfer from the hot wall to the drop. The vapor participation in radiant energy exchange is assumed to be small. We will first analyze the evaporation due to convective heat transfer.

Let the drop be at distance y from the wall (Figure 4.2). The corresponding vapor temperature at that distance is $T_i(y)$. As we assumed the linear temperature distribution, the average vapor temperatures for the upper and lower portions of the drop are then, respectively,

$$T_{i+1}(y) = T_i(y) + \frac{dT_i}{dy} \Delta y \tag{4.20}$$

$$T_{i-1}(y) = T_i(y) - \frac{dT_i}{dy} \Delta y \tag{4.21}$$

where $\Delta y = \frac{a}{\kappa}$ and $\kappa = 4$. The value of κ was obtained by calculating the average fluid (gas) temperature for the upper or lower surface portion of the sphere.

Introducing Eq. (4.17) in (4.20) and (4.21) gives

$$T_{i+1}(y) = T_i(y) - \frac{(T_w - T_s)}{\delta} \frac{a}{4} \tag{4.22}$$

$$T_{i-1}(y) = T_i(y) + \frac{(T_w - T_s)}{\delta} \frac{a}{4} \tag{4.23}$$

The average heat transfer rates for the upper and lower portion of the drop are, respectively,

$$(q/A)_1 = h\left[T_{i+1}(y) - T_s\right] \tag{4.24}$$

$$(q/A)_2 = h\left[T_{i-1}(y) - T_s\right] \tag{4.25}$$

where h is the heat transfer coefficient defined by Eq. (4.19). The average vapor velocities leaving the upper and lower portion of the drop are, respectively,

$$v_1 = \frac{(q/A)_1}{H_{\ell g}\rho_g} \tag{4.26}$$

$$v_2 = \frac{(q/A)_2}{H_{\ell g}\rho_g} \tag{4.27}$$

Here, $H_{\ell g}$ is the latent heat of evaporation, and ρ_g is the vapor density.

Introducing equations (4.22)-(4.25) into (4.26) and (4.27) gives

$$v_1 = \frac{h}{H_{\ell g}\rho_g}\left[(T_w - T_s)\left(1 - \frac{y}{\delta}\right) - \frac{(T_w - T_s)}{\delta}\,\frac{a}{4}\right] \tag{4.28}$$

$$v_2 = \frac{h}{H_{\ell g}\rho_g}\left[(T_w - T_s)\left(1 - \frac{y}{\delta}\right) + \frac{(T_w - T_s)}{\delta}\,\frac{a}{4}\right] \tag{4.29}$$

Since $v_2 > v_1$ the upward force on the spherical drop is produced. We choose the volume of the spherical drop as a control volume. The upward

force (reaction force) is then approximately given as the net rate of efflux of momentum through the control surface in the y direction,

$$F_{cy} = \iint_{c.s.} v_y \, (\rho_g \, \vec{v} \, dA) \tag{4.30}$$

where

$\vec{v}$ = vapor velocity (vector),

v_y = vapor velocity in y direction (scalar),

and A = surface of the sphere.

Introducing Eqs. (4.28) and (4.29) into (4.30) gives (Appendix IV-2),

$$F_{cy} = \frac{\pi a^2 h^2}{4 \, H_{\ell g}^{\,2} \, \rho_g} \, (T_w - T_s)^2 \, \frac{a}{\delta} \left(1 - \frac{y}{\delta}\right) \tag{4.31}$$

It is seen from Eq. (4.31) that the reaction force, F_{cy}, is a function of the drop distance y from the wall for the given wall temperature and drop diameter.

If the distance of the drop from the wall is less than the drop boundary layer thickness, the expression (4.31) is not valid any more. In that case, the thermal conduction through the vapor film existing between the wall and the bottom of the drop is the most important mechanism of heat transfer. If we assume that conduction is in the y direction only, then the velocity of the vapor leaving the lower portion of the drop due to evaporation is

$$v_2 = \frac{k_g}{\bar{y}} \, \frac{(T_w - T_s)}{H_{\ell g} \, \rho_g}$$

where $\bar{y}$ is the current mean film thickness through which heat is conducted and k_g is the thermal conductivity of vapor.

In this case the pressure increase in the vapor layer does influence saturation temperature T_s and the latent heat of evaporation $H_{\ell g}$. Also, the effect of the wall roughness may be important. Further details of this analysis include application of Eq. (4.30) and iterative evaluation of the saturation temperature (Appendix (IV-4). They are omitted here because the most critical effects of the resistance forces on the drop occur near the edge of the laminar sublayer, or sufficiently far away from the wall. More clearly, whenever a drop approaches the distance that is equal to or less than the drop boundary layer thickness, deposition of the drop will occur. This will be shown below.

The evaporation of the drop due to radiative heat transfer becomes more important as the wall temperature increases. Assuming that the wall and the lower half of the drop are separated by a non-absorbing, non-emitting medium, the rate of the radiative heat transfer between these two bodies is

$$q_2 = A_2 F_2 \sigma (T_w^4 - T_s^4) \tag{4.32}$$

where F_2 is the overall interchange factor for radiation between the hot wall and the lower half of the liquid drop. F_2 is given for a system of two-zone, source-sink surfaces as (McAdams, 1954),

$$\frac{1}{F_2} = \left(\frac{1}{\varepsilon_L} - 1\right) + \frac{A_2}{A_w}\left(\frac{1}{\varepsilon_w} - 1\right) + \frac{1}{\bar{F}_2} \tag{4.33}$$

where

A_w = area of hot wall,

ε_L = thermal emissivity of the liquid,

ε_w = thermal emissivity of the wall,

σ = Stefan-Boltzmann constant,

and A_2 = surface area of the lower half of the drop.

Since $A_2 << A_w$, Eq. (4.33) can be further simplified to

$$\frac{1}{\bar{F}_2} = \left(\frac{1}{\varepsilon_L} - 1\right) + \frac{1}{\bar{F}_2} \tag{4.34}$$

Similarly, the overall interchange factor for radiation between the wall and the upper half of the liquid drop is

$$\frac{1}{\bar{F}_1} = \left(\frac{1}{\varepsilon_L} - 1\right) + \frac{1}{\bar{F}_1} \tag{4.35}$$

$\bar{F}_1$ and $\bar{F}_2$ are the average configuration factors for radiation between the lower and upper halves of the spherical drop and wall, respectively. The value for $\bar{F}_1$ and $\bar{F}_2$ are 0.318 and 0.682, respectively (Gottfried, 1966).

Substituting the value for $\bar{F}_2$ into Eq. (4.34), and then into Eq. (4.32), the radiation heat transfer between the wall and the lower half of the drop is

$$q_2 = \frac{A_2 \sigma (T_w^4 - T_s^4)}{[(1/\varepsilon_L) - 1] + 1/0.682} \tag{4.36}$$

Similarly, the radiative heat transfer between the wall and the upper half of

the drop is

$$q_1 = \frac{A_1 \sigma (T_w^4 - T_s^4)}{[(1/\varepsilon_L) - 1] + 1/0.318} \tag{4.37}$$

where A_1 is the surface area of the upper half of the drop.

Introducing Eqs. (4.36) and (4.37) into (4.26) and (4.27) and then into Eq. (4.30) gives approximately the reaction force on the spherical drop due to radiation heat transfer,

$$F_{ry} = \frac{\pi a^2 \sigma^2}{4H_{\ell g}^2 \rho_g} (T_w^4 - T_s^4)^2 \left\{ \frac{1}{\left[\left(\frac{1}{\varepsilon_L} - 1\right) + \frac{1}{0.682}\right]^2} - \frac{1}{\left[\left(\frac{1}{\varepsilon_L} - 1\right) + \frac{1}{0.318}\right]^2} \right\} \tag{4.38}$$

The total reaction force on the drop due to non-uniform evaporation is then the sum of the forces given by Eqs. (4.31) and (4.38). It is not likely that the shape of the spherical drop will be changed due to evaporation. As we mentioned before, a drop rotates inside the boundary layer due to velocity gradient. Because of the rotation the whole surface of the drop is equally exposed to the hot wall during deposition.

For the case of the single drop motion inside the tube the component of the reaction force due to radiation heat transfer, F_{ry} is zero as the average configuration factors $\bar{F}_1$ and $\bar{F}_2$ have the same numerical values.

4.2.6 Other Forces

A full list of forces known to influence the drops motion in addition to the forces we analyzed so far includes:

(6a) Force on the drop due to the pressure gradient in the fluid stream. For a drop of radius a in a pressure gradient $\frac{dP}{dx_i}$ this force is given by (McCormack, 1973)

$$F_p = -\frac{\pi a^3}{6} \frac{\partial P}{\partial x_i}$$

where x_i is the spatial coordinate in the direction of F_p and is in the opposite direction to the pressure gradient. Unless there is a very large pressure gradient this force will be very small.

The local increase in pressure when an evaporating drop is approaching the hot wall can produce this type of force. However, this is already included in the derivation of the expression for the reaction force due to non-uniform drop evaporation.

(6b) Basset Acceleration force due to the deviation of the flow pattern from the steady state (McCormack, 1973). It is an instantaneous flow resistance and accounts for the acceleration history of the particle. The expression for this force is

$$F_b = \frac{3}{2} a^2 (\pi \rho_g \mu_g)^{\frac{1}{2}} \int_{t_{p_0}}^{t_p} \frac{(d/d\tau)(V - V_a)}{(t_p - \tau)}$$

where τ is the time constant for the effect. This force becomes significant only when the drop (particle) is accelerated at high rate, when the observed drag force becomes many times the steady drag coefficient (Hughes, 1952). So only in cases of extreme

particle accelerations should this force be considered.

(6c) Forces arising from proximity to the wall and the effects of irregularities in the wall surface on the local flow.

(6d) Forces produced by possible fluctuations in pressure.

(6e) Intermolecular forces. They are symmetrical in action and their influence on the drop motion is unimportant.

(6f) Forces arising because of thermophoresis and photophoresis phenomena (Waldmann, 1966).

(6g) Forces arising because of diffusiophoresis phenomenon (Waldmann, 1966).

All these forces are important only for the motion of the submicron drop size and they are omitted in our analysis.

4.3 Drop Deposition Model

Denoting the coordinates of the center of a spherical drop by x and y and applying Eqs. (4.1), (4.2), (4.6), (4.7), and (4.31), we write the equations of motion of a drop moving in the laminar sublayer when the main flow in the channel is directed vertically upward:

$$\rho_\ell \frac{\pi}{6} a^3 \frac{d^2x}{dt^2} = \frac{\pi}{16} a^3 \rho_g \frac{dU}{dy}\left(\frac{dy}{dt}\right) - 6\pi \mu_g \frac{a}{2}\left(\frac{dx}{dt} - U\right) - \\ - (\rho_\ell - \rho_g) g \frac{\pi}{6} a^3 \tag{4.39a}$$

$$\rho_\ell \frac{\pi}{6} a^3 \frac{d^2y}{dt^2} = -\frac{\pi}{16} a^3 \rho_g \frac{dU}{dy}\left(\frac{dx}{dt} - U\right) - 6\pi \mu_g \frac{a}{2}\left(\frac{dy}{dt}\right) + \\ + \frac{\pi a^2 h^2}{4 H_{\ell g}^2 \rho_g} (T_w - T_s)^2 \frac{a}{\delta}\left(1 - \frac{y}{\delta}\right) \tag{4.39b}$$

Equation (4.39a) is obtained from the equilibrium of forces acting on the drop in the direction of flow (x-direction), x being taken as positive upward. Forces acting upwards in the x direction are taken as positive. Equation (4.39b) is obtained from the equilibrium of forces acting on the drop in the y-direction, y being taken as zero at the wall, increasing positively toward the center line of the channel (tube). Subscripts ℓ and g refer to liquid drop and stream (gas or vapor), respectively. The first terms on the right side of Eqs. (4.39a) and (4.39b) represent the lift forces (Rubinow-Keller expression used) of the stream flow acting on the periphery of the drop with variation in velocity around the drop, i.e., in the gradient of the stream flow.

The second terms on the right side of Eqs. (4.39a) and 4.39b) represent the drag forces on the drop. The third term on the right side of Eq. (4.39a) represents the gravity and buoyancy force. The third term on the right side of Eq. (4.39b) represents the reaction force on the drop due to non-uniform evaporation of the drop inside the laminar sublayer. The terms on the left side of Eqs. (4.39a) and (4.39b) represent the inertial forces acting on a drop of mass $m = \frac{\pi a^3}{6} \rho_\ell$.

In order to solve the equations (4.39a) and (4.39b) the linear velocity profile of the gas stream across the laminar sublayer was assumed:

$$U = U_0 \left(\frac{y}{\delta} \right) \tag{4.40}$$

where U_0 is the mean gas velocity. Also, the following initial boundary

conditions were used:

$$t = 0 \quad , \quad x = 0 \quad , \quad \frac{dx}{dt} = u_0 \tag{4.41a}$$

$$t = 0 \quad , \quad y = \delta \quad , \quad \frac{dy}{dt} = v_0 \tag{4.41b}$$

where $\frac{dx}{dt}$ and $\frac{dy}{dt}$ are the velocity components of the drop in x and y directions, respectively. The slip ratio S at $y = \delta$, the ratio of U_0 and u_0, is defined as

$$S = \frac{U_0}{u_0} \tag{4.42}$$

The initial velocity in the radial direction v_0 is usually called the deposition velocity of the drop. Equations (4.39a) and (4.39b) were solved analytically (Appendix IV-1).

The main results of calculating the trajectories of the drops in the region of the laminar sublayer are presented on Figures 4.3 - 4.6. The effects of the drop diameter, wall temperature, initial drop velocities in the x and y directions, and the flow Reynolds number on the drop trajectories are separately analyzed. Also, the magnitude of all forces on the drop are calculated. The drop Reynolds number during the drop motion inside the laminar sublayer is calculated. Nitrogen data were used in the calculation.

A. Effect of Initial Drop Velocity on the Flow Direction (Slip Effect)

The trajectories of the drop of 20 μm diameter for two different values of the initial drop velocity in the flow direction at the edge of laminar sublayer are presented on Figure 4.3. The other parameters of drop motion, the wall temperature T_w, drop deposition velocity v_0, and the thickness of a laminar sublayer δ, are specified (Figure 4.3). For the first case where $S = 1.18$ [S is the slip, from Eq. (4.42)], the deposition of the drop was not achieved. From the shape of the corresponding trajectory one can see that the drop starts moving toward the wall and after a few milliseconds reverses direction and starts moving away from the wall. Since the initial velocity of the drop in the flow direction is less than the local stream velocity at the edge of the laminar sublayer ($u_0 < U_0$, i.e., $S > 0$), the lift force has been directed toward the center line. The drop then has been decelerated because of the additive effect of lift, Stokes, and reaction forces. After the drop reverses direction of motion it starts accelerating toward the center line. It is important to mention here that the intensity of the lift force is proportional to the intensity of $(V - V_a)$ as is evident from Eq. (4.7).

For the second case where $S = 1.11$ (Figure 4.3), the drop was deposited on the wall. In this case the slip is less compared to the previous case. Because of this, the drop penetrated sufficiently close to the wall, so that it entered the region in which its velocity in the direction of flow $\frac{dx}{dt}$ becomes greater than the local fluid velocity. The lift force is now being

directed towards the wall and becomes larger than the sum of the Stokes and reaction forces, causing the drop to travel to the wall.

B. Effect of Drop Diameter

The effect of drop diameter on the drop trajectory is presented on Figure 4.4. Other parameters of drop motion for this case are specified (Figure 4.4). Since drop deposition velocity is the same for a = 20 μm and a = 50 μm , the larger drop enters the boundary layer with the higher momentum. Because of this the drop of a = 50 μm reaches a region where $(U - \frac{dx}{dt})$ becomes negative and the direction of the lift force is reversed, i.e., the lift force now is directed toward the wall, assisting deposition. The drop of a = 20 μm returns to the main stream.

C. Effect of Wall Temperature

The reaction force on the drop due to non-uniform drop evaporation inside the sublayer is proportional to the square of the wall superheat $(T_w - T_s)$, Eq. (4.31). The effect of the wall temperature on the drop motion inside the sublayer is presented in Figure 4.5. Three trajectories are plotted in this figure for the three different wall temperatures, 400°R, 450°R, and 500°R. The parameters v_0 , u_0 , U_0 and δ are kept the same for the three different trajectories. As can be seen in Figure 4.5, the drop of a = 20 μm penetrates the sublayer to some depth and then is forced back into the main stream if the wall temperature is equal to or greater than 450°R. For the wall temperature of 400°R the same drop is deposited.

D. Effect of Deposition Velocity

The effect of the deposition velocity on the drop trajectory is presented in Figure 6. For the higher value of the deposition velocity, v_0 = 371 ft/hr, the drop is deposited as it enters the sublayer with higher momentum, overcoming the resistance of the Stokes and reaction forces and the initial resistance of the lift force until $(U - \frac{dx}{dt})$ is positive. As we mentioned before, the lift force is directed toward the main stream (center line) when $(U - \frac{dx}{dt})$ is positive.

E. Effect of Reynolds Number

As the Reynolds number (flow Reynolds number) increases, the boundary layer becomes very thin, the velocity gradient $\frac{dU}{dy}$ becomes steeper. Now the distance that the drop must travel into the sublayer for the lift force to reverse directions is very small. As $\frac{dU}{dy}$ is now very large, the lift force becomes very large in both regions: in the region where $(U - \frac{dx}{dt})$ is positive, especially at the beginning of this region, and the lift force is directed toward the center line; and in the region where $(U - \frac{dx}{dt})$ is negative and the lift force is directed toward the wall. Also, as the Reynolds number increases, the drop deposition velocity v_0 , which is imparted to the drop by the transverse velocity fluctuations of the gas stream which carries it, increases.

On the figures 4.3-4.6 the radial position of the drop was plotted

against time, instead of the axial position. This was done to make evident the regions of the drop acceleration and deceleration.

In order to summarize the studies on the drop motion inside the sublayer the history of the drop that penetrated the sublayer to a certain depth and was forced back to the main stream is presented in Figure 4.7 and Table 1. On the Figures 4.7b-c the forces on the drop in the y and x directions during drop motion are plotted against time. In Table 1 the radial position of the drop, the axial and radial velocities of the drop, and the difference between the axial velocities of the stream and drop are tabulated as functions of time. The drop Reynolds number is calculated and plotted in Figure 4.7d.

The same analysis for the drop that has been deposited on the wall is presented in Figure 4.8 and Table 2.

From Figures 4.7a-b one can see that the direction of the lift force has been changed at $y = 0.8865 \times 10^{-3}$ft as $(U - \frac{dx}{dt})$ becomes negative (see Table 1), but the lift force has been overcome by the reaction and Stokes forces and the drop returned to the main stream.

So if $(U - \frac{dx}{dt})$ is negative the lift force on the drop is directed toward the wall as we mentioned before, but this is not sufficient condition for the deposition of the drop. From Figure 4.8 and Table 2 one can see that the drop penetrates sufficiently far into the sublayer where, at $y = 0.88 \times 10^{-3}$ ft, the lift force overcomes the reaction and Stokes forces, and the drop begins to accelerate toward the wall.

When the drop is approaching a wall the drop Reynolds number is becoming

larger than 1.0 due to drop acceleration (Figure 4.8d). The same is true for the drop leaving the sublayer (Figure 4.7d). In this case the Stokes expression for the drag of the drop is not applicable, but since the lift force dominates in these regions, the correction to the drag coefficient does not play a significant part in the drop trajectory.

By analyzing the values for the lift force and the drop Reynolds number along the drop trajectory we can conclude that the lift force increases with increased drop Reynolds number (Figure 4.7 and 4.8).

The analysis of the drop trajectories on Figures 4.3, 4.4, 4.5, 4.6, and 4.7, and the numerical values for the drop deposition in Table 2, lead to the conclusion that the drops are being deposited on the wall with a definite impact. This is in qualitative agreement with the results of Cousin and Hewitt (1968). Their results of the photographic studies in two-phase up-flow of water drops suspended in air indicate that drops reach the surface with high velocities without being slowed as they enter the region of low gas velocity adjacent to the surface.

The significant conclusion concerning the drop trajectories in Figures 4.3-4.8 is that since the most critical effects of the lift, reaction, and drag forces on the drop deposition take place sufficiently far away from the wall, the effect of the wall may be neglected, as was assumed in Eqs. (4.39a,b). Also, the effect of the evaporation on the drag coefficient and drop Nusselt number is negligible as the values of the transfer coefficient B for $y > y_{cr}$ are small (y_{cr} is the critical distance, i.e., the distance where

the critical effects of the forces occur). For example, the values of B for the trajectories in Figures 4.3, 4.6, 4.7a at $y = y_{cr}$ are 0.007, 0.098, and 0.106, respectively.

Since the vapor superheat increases when a drop is approaching a wall, then B , which is a function of the local vapor superheat, increases and effects of the evaporation on the drag coefficient and drop Nusselt number may be significant. On the other hand, the lift force dominates when the drop is approaching a wall, as we mentioned before, and any corrections for the drag coefficient and drop Nusselt number do not play a significant part in the drop trajectory.

The equations (4.39a,b) were solved assuming that decrease of the drop diameter due to evaporation during deposition motion inside the sublayer was negligible. This assumption holds very well for larger drops ($d > 10$ μm) since their stay time inside the sublayer is very short (Appendix IV-5). For a small drop, a diameter of the order of magnitude of 1 μm, the effect of the curvature on the surface tension should be included when analyzing the rate of decrease of drop mass due to evaporation. This was omitted in our study because small drops do not usually penetrate the sublayer (Figure 4.9).

Little error is introduced in the analysis by assuming that the angular velocity of the drop is the same as that of the fluid stream. The actual angular velocity of the drop is given by the following relation (Rubinow-Keller, 1960);

$$\omega = -\frac{1}{2}\frac{dU}{dy}\left[1 - \exp\left(-\frac{60\mu_g}{a^2\rho_\ell}t\right)\right] \tag{4.43}$$

For the drop of a = 20 μm (Figure 4.8, Table 2), the angular velocity of the drop and stream are becoming practically the same within two milliseconds. The time of two milliseconds is much smaller than the drop stay time (Table 2) and the fact that the drop undergoes unsteady motion can be neglected. The same drop made 23 revolutions before being deposited. This was calculated using Eq. (4.43) and the drop deposition history from Table 2.

In our study of the drop deposition through the sublayer the lift force on the drop derived by Rubinow and Keller is applied instead of Saffman's lift force. The fact is that we are dealing with the dispersed flow gas (vapor) drops where flow Reynolds number is very high. For such types of flow (drops of size from 1 μm to several hundred microns) the conditions for the validity of Saffman's expression for the lift force as specified by Eq. (4.41) are satisfied only for small drops with a diameter of the order of magnitude of 1 μm. The same was concluded and discussed with more details by Rouhiainen and Stachiewicz (1970). The reader is referred to Figure 5 of their article. It is also important to mention here that the cumulative mass of drops with a diameter of 1 μm and less is negligible compared to the total cumulative mass of the drops in the dispersed flow under consideration.

The Rubinow-Keller lift force was not derived for a shear flow but on

the other hand, the experimental and theoretical studies of the drop trajectories by Denson et al (1966), Goldsmith (1962), Repetti (1964), and Kondic (1970) indicated that it yields a force of the correct order of magnitude for such a flow.

It is interesting to mention that Saffman's and Rubinow-Keller's lift forces become numerically the same for the larger drops ($a > 10$ μm) for the dispersed flow considered in this study (Appendix IV-3).

4.4 Application of Drop Deposition Model

So far we have been analyzing the motion of the single drop through the sublayer. In order to determine the drops deposition rate on the wall (i.e., the number of drops deposited per unit area of the wall and unti time), a drops size spectrum $P(a)$ was introduced into the analysis.

Predictions of drops trajectories for $a_0 \leq a \leq a_m$ (where a_0 and a_m are minimum and maximum drop diameter, respectively, in dispersed flow under consideration) was done by increasing initial drop diameter a_0 step by step and solving the equations (4.39a,b) for each value of a .

The initial boundary condition given by Eq. (4.41b) was expressed as a function of the friction velocity,

$$v_0 = k\,U^* = k\,U\sqrt{f_g/2} \tag{4.44}$$

where

k = constant,

U^* = friction velocity ($U^* = U\sqrt{f_g/2}$),

and f_g = friction factor.

Relation (4.44) was obtained from the summarized study of deposition of solid particles and liquid drops in two-phase mixtures by Liu and Ilori (1973). On the Figure 2 of their article, particle deposition velocity was plotted vs. particle relaxation time. The particle dimensionless relaxation time t^* was defined in terms of particle diameter, particle density, and viscosity of the main stream, i.e., $t^* = a^2\rho_\ell/18\mu_g$. By careful examination of Figure 2 of their article one can see that the particle (drop) deposition velocity is independent of the particle diameters, ranging from several microns to several hundred microns. The value of k [Eq. (4.44)], related to the deposition velocity of drops at the edge of the sublayer, is always less than one but is actually a parameter. In this analysis we used $k = 0.15$ as suggested by Iloeje et al (1974).

The initial drop velocity in the flow direction, u_0, at the edge of the sublayer, can be approximately determined by equating the drag force on the drop and its weight. Cumo et al (1972) performed visual observations of the dispersed flow employing high speed cinematography. Analyzing more than 10,000 drops, they found that the drop velocity in the direction of flow is independent of drop diameter and almost equal for all drops. They also found that the drop transversal velocity profile in the flow channel is very close to the vapor velocity profile with local slip ratio close to

one (see for instance Figure 9 in their article). Since their observation was basically outside of the laminar sublayer one can assume that the drop velocity in the flow direction at the edge of the sublayer is

$$u_0 = \frac{U}{S} \tag{4.45}$$

where S is the slip ratio at the edge of the laminar sublayer. The methods of the evaluation of the slip ratio S are referenced in the Appendix III-2.

For a given mass flux G and vapor quality x the initial boundary conditions, Eqs. (4.44) and (4.45), were evaluated. Equations (4.39a,b) were then solved and trajectories obtained for each value of a, $a_0 < a < a_m$, for one particular value of the wall temperature. The summarized results of calculation for $G = 215{,}000$ lb/ft^{2}hr and $x = 0.49$ are presented in Figure 4.9.

For example, if the wall temperature was equal to the saturation temperature (no heat addition) then drops with a diameter $a \geq 10$ μm were deposited on the wall and drops with a diameter $a < 10$ μm were returned to the main stream (Figure 4.9). The diameter $a = 10$ μm for this case is so called the deposition diameter a_c, i.e., $a_c = 10$ μm.

For the same conditions and the wall temperature of 700°R, $a_c = 260$ μm, etc. (Figure 4.9). The curve in Figure 4.9, deposition diameter vs. wall temperature, was obtained for the step increase in drop diameter of $\Delta a = 5$ μm, for one particular value of the wall temperature. The step increase in wall temperature was $\Delta T_w = 20°R$.

The important point to be noted here is that small drops, $a < 10$ μm, were not deposited. Their trajectories were obtained assuming that deposition velocity at the edge of the sublayer was given by Eq. (4.44) but the actual deposition velocity of such small drops is less as it can be seen from Figure 2 of Liu and Ilori's article. This leads to the conclusion that small drops, of a diameter of the order of magnitude of 1 μm, do not penetrate the sublayer under normal conditions, i.e., when their deposition velocities are imparted to them by the transverse velocity fluctuations of the main stream. Because of this, the detailed analysis of the evaporation and its effect on the drop trajectory for such small drops was omitted in our study.

The deposition model, Eqs. (4.39a,b), related to the drop motion inside the sublayer, is applicable in the buffer layer too, where quasi-laminar motion can be assumed, i.e., velocity fluctuations of the main fluid can be neglected. The constant k [Eq. (4.44)] will have a greater value at the edge of the buffer zone than that at the edge of the sublayer. As soon as we move out in the turbulent core, velocity fluctuations of the main fluid (gas) cannot be neglected and the application of the model is questionable. On the other hand, the drop deposition occurred along trajectories mainly developed in the laminar sublayer.

The effect of the wall temperature on the drops deposition is once again demonstrated in Figure 4.9.

For the known value of the deposition diameter a_c, and drop size distribution law $P(a)$, Eq. (3.7), we define the cumulative factor $f(a_c)$

as

$$f(a_c) = \frac{\int_{a_c}^{a_m} a^n P(a)\, da}{\int_{0}^{a_m} a^n P(a)\, da} \qquad (4.46)$$

For $n = 3,2,1$, $f(a_c)$ represents mass, surface, and momentum cumulative factor, respectively.

From Eq. (4.46) one can see that $0 \leq f(a_c) \leq 1.0$. If the wall temperature increases a_c increases (Figure 4.9) and $f(a_c)$ as defined by Eq. (4.46) decreases since the number of drops deposited on the wall decreases. For any value of a_c, $f(a_c)$ is calculated using Eq. (3.7) for $P(a)$. The value of $f(a_c)$ is used in calculating drop deposition flux (number of drops deposited per unit area of the wall and unit time) as explained later in section 5.2.

The accuracy of the deposition model developed in this study in determining the deposition diameter a_c is based on the validity of several assumptions mentioned before, related to the magnitude of the forces of the drop.

The region of the model inaccuracy, as indicated in Figure 4.10, may produce a small consistent overestimate or underestimate in calculating the cumulative factor f. On the other hand, the drops deposition phenomenon is in general well described by the model.

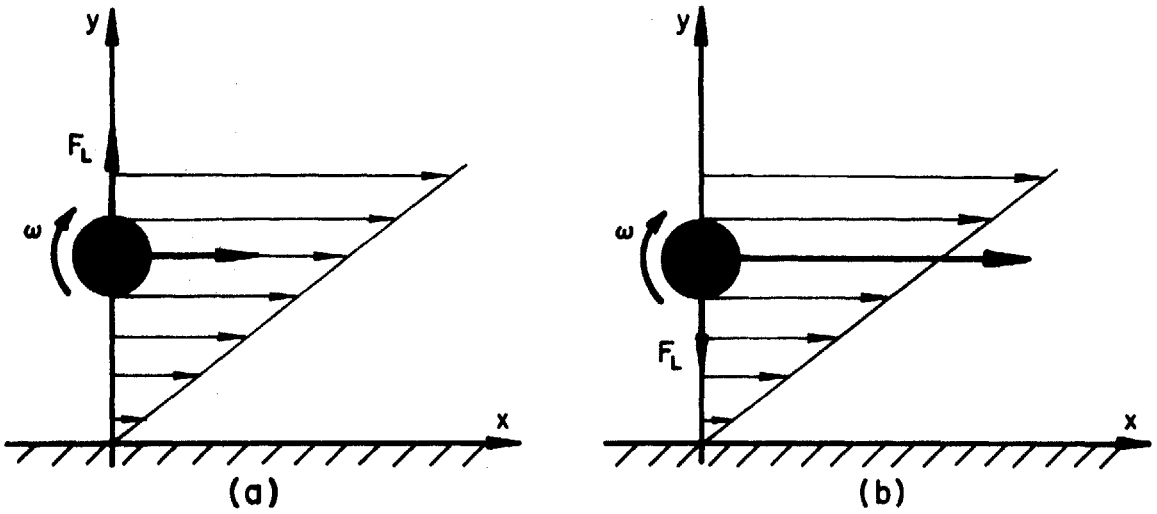

Figure 4.1 Direction of the Lift Force Acting on the Drop in a Boundary Layer

a. Velocity Component of the Drop is Less Than the Velocity of the Fluid (gas)

b. Velocity of the Drop is Greater Than the Velocity of the Fluid

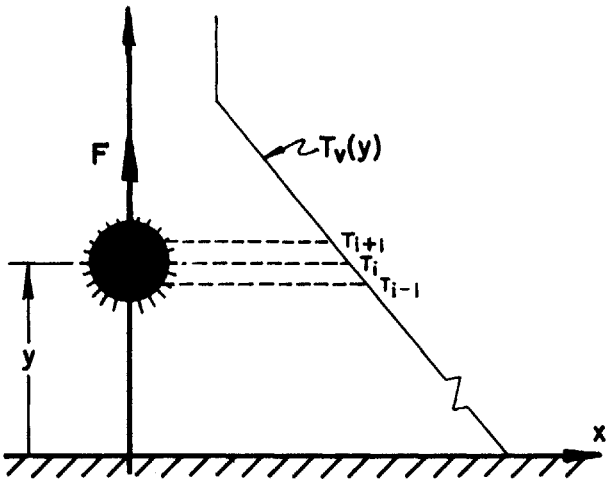

Figure 4.2 Direction of the Reaction Force Acting on the Evaporating Drop in a Thermal Boundary Layer

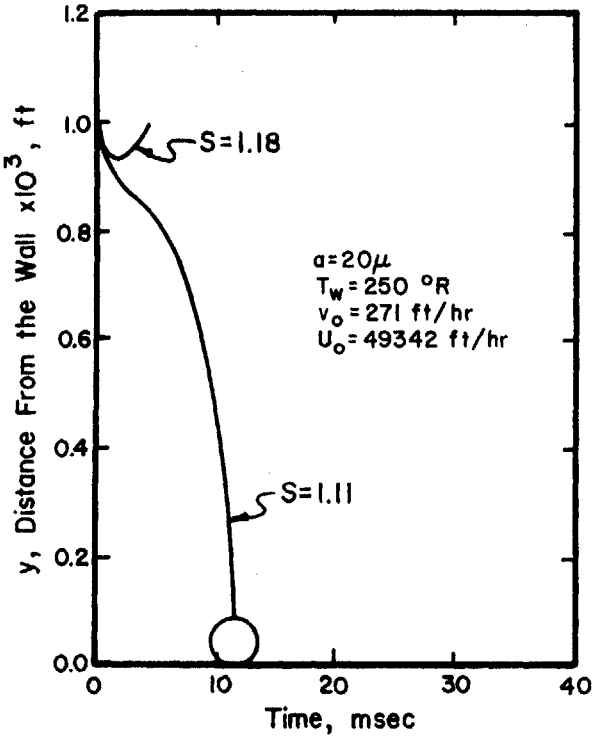

Figure 4.3 The Effect of the Slip Ratio on the Drop Trajectory

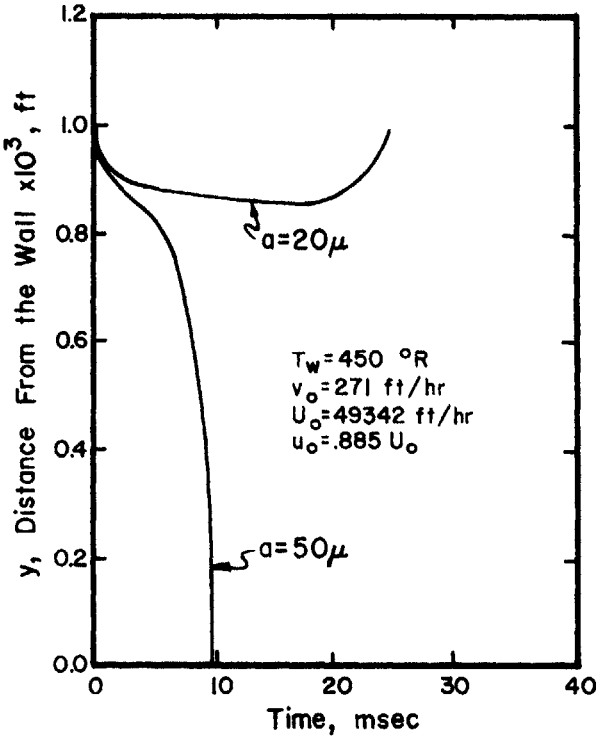

Figure 4.4 The Effect of Drop Diameter on the Drop Trajectory

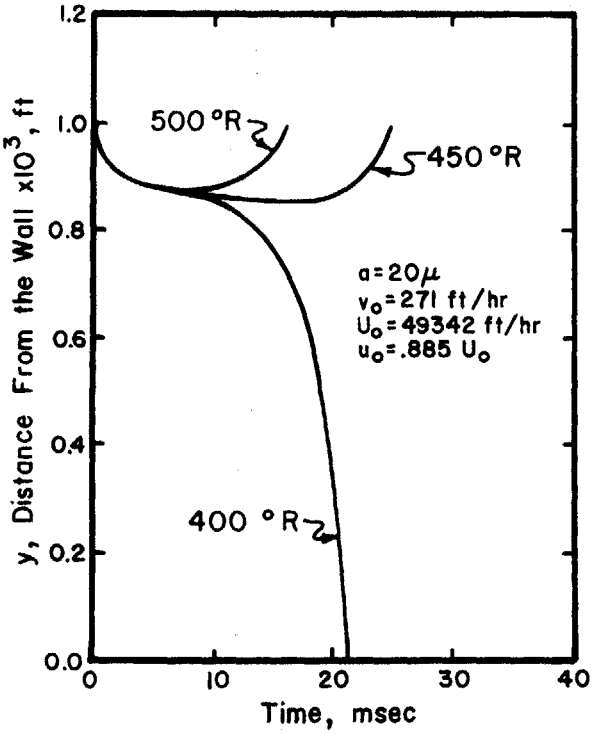

Figure 4.5 The Effect of the Wall Temperature on the Drop Trajectory

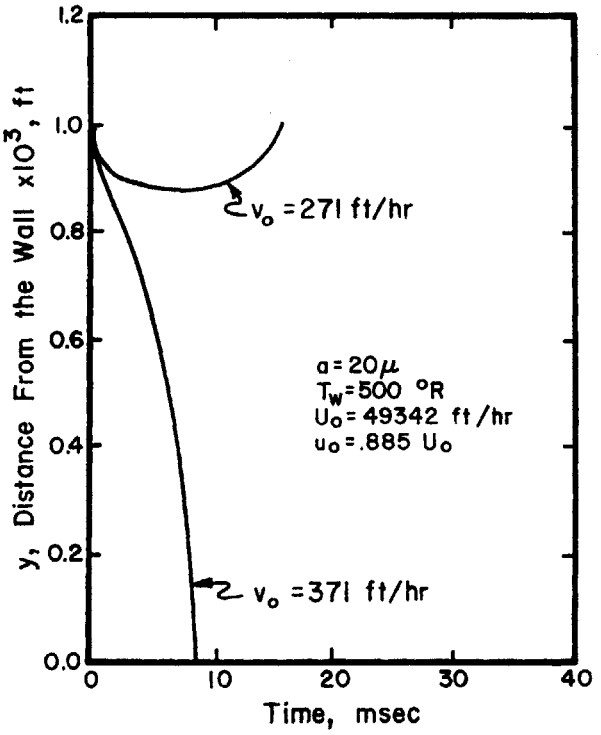

Figure 4.6 The Effect of Drop Deposition Velocity on the Drop Trajectory

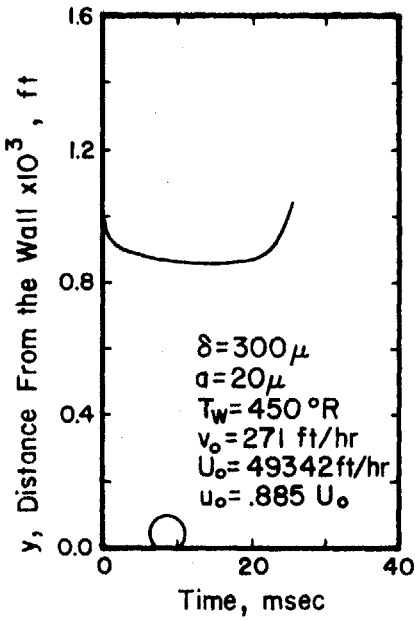

Figure 4.7a Trajectory of Drop

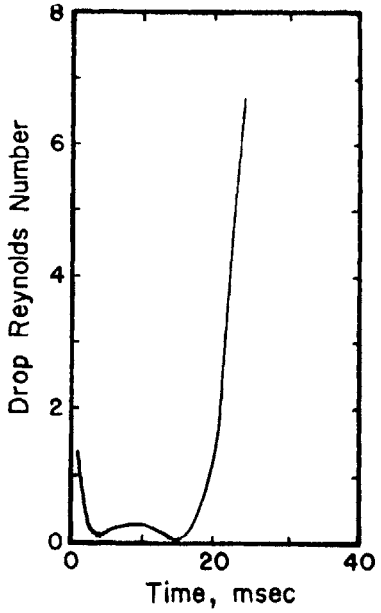

Figure 4.7d Drop Reynolds Number

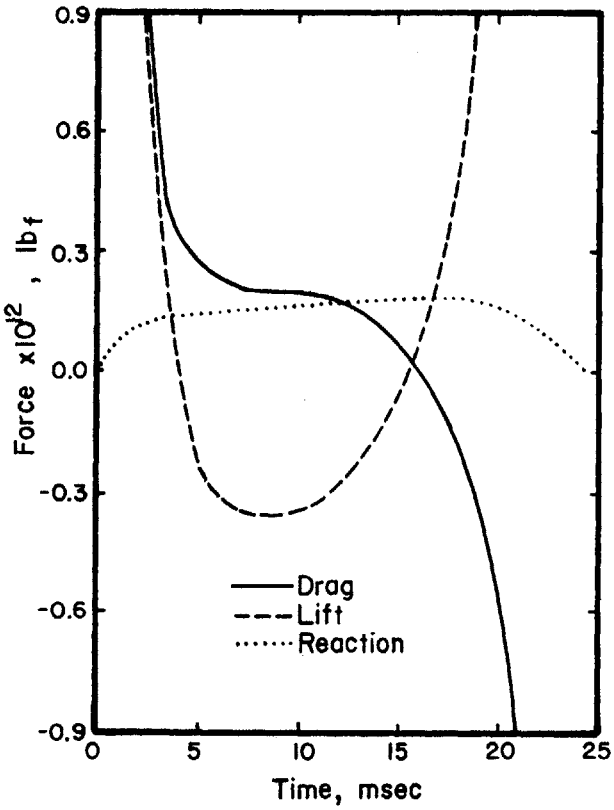

Figure 4.7b Forces on the Drop in the y-Direction

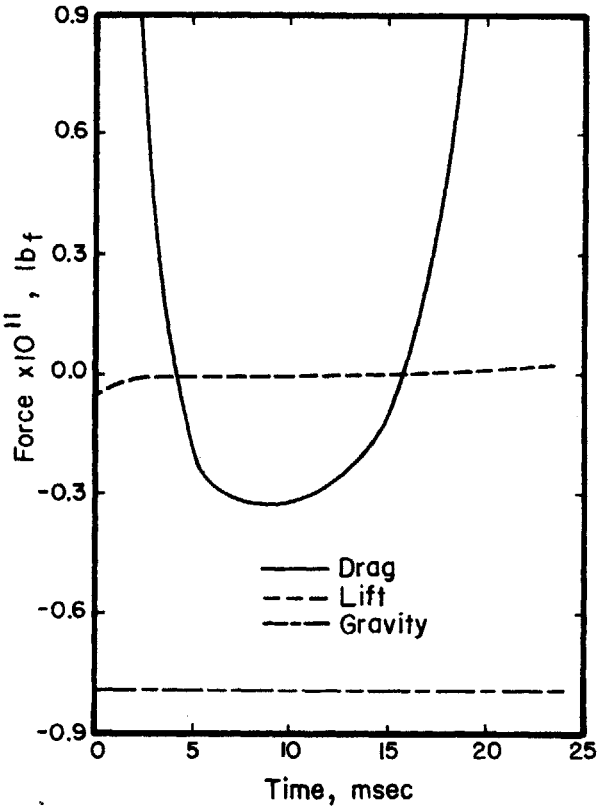

Figure 4.7c Forces on the Drop in the x-Direction

t (ms)	y (ft)	$\frac{dy}{dt}$ (ft/hr)	$\frac{dx}{dt}$ (ft/hr)	U (ft/hr)	$\left[U - \frac{dx}{dt}\right]$ (ft/hr)
0.	0.9840E-03	-0.2710E 03	0.43668E 05	0.49342E 05	0.5674E 04
1.	0.9328E-03	-0.1196E 03	0.44524E 05	0.46774E 05	0.2250E 04
2.	0.9096E-03	-0.5666E 02	0.44784E 05	0.45610E 05	0.8230E 03
3.	0.8980E-03	-0.3053E 02	0.44796E 05	0.45029E 05	0.2330E 03
4.	0.8912E-03	-0.1967E 02	0.44704E 05	0.44691E 05	-0.1300E 02
5.	0.8865E-03	-0.1513E 02	0.44570E 05	0.44453E 05	-0.1170E 03
6.	0.8826E-03	-0.1321E 02	0.44417E 05	0.44257E 05	-0.1600E 03
7.	0.8791E-03	-0.1233E 02	0.44257E 05	0.44080E 05	-0.1770E 03
8.	0.8757E-03	-0.1184E 02	0.44095E 05	0.43912E 05	-0.1830E 03
9.	0.8725E-03	-0.1144E 02	0.43931E 05	0.43750E 05	-0.1810E 03
10.	0.8694E-03	-0.1099E 02	0.43769E 05	0.43594E 05	-0.1750E 03
11.	0.8664E-03	-0.1037E 02	0.43609E 05	0.43445E 05	-0.1600E 03
12.	0.8636E-03	-0.9503E 01	0.43453E 05	0.43306E 05	-0.1470E 03
13.	0.86125-03	-0.8255E 01	0.43302E 05	0.43182E 05	-0.1200E 03
14.	0.8591E-03	-0.6464E 01	0.43160E 05	0.43079E 05	-0.8100E 02
15.	0.8576E-03	-0.3904E 01	0.43031E 05	0.43005E 05	-0.2600E 02
16.	0.8570E-03	-0.2520E 00	0.42919E 05	0.42975E 05	0.5600E 02
17.	0.8576E-03	0.4945E 01	0.42833E 05	0.43006E 05	0.1730E 03
18.	0.8600E-03	0.1233E 02	0.42784E 05	0.43123E 05	0.3390E 03
19.	0.8648E-03	0.2281E 02	0.42788E 05	0.43363E 05	0.5750E 03
20.	0.8731E-03	0.3768E 02	0.42867E 05	0.43779E 05	0.9120E 03
21.	0.8863E-03	0.5876E 02	0.43052E 05	0.44442E 05	0.1390E 04
22.	0.9065E-03	0.8864E 02	0.43388E 05	0.45456E 05	0.2068E 04
23.	0.9367E-03	0.1310E 03	0.43938E 05	0.46969E 05	0.3031E 04
24.	0.9809E-03	0.1909E 03	0.447925 05	0.49186E 05	0.4394E 04
25.	0.1045E-02	0.2758E 03	0.46077E 05	0.52403E 05	0.6326E 04

t = time
x = axial position of drop
y = radial position of drop

$\frac{dx}{dt}$ = drop velocity in x direction
$\frac{dy}{dt}$ = drop velocity in y direction
U = vapor velocity

TABLE 1. History of Drop Motion (a = 20 μ; T_w = 450°R)

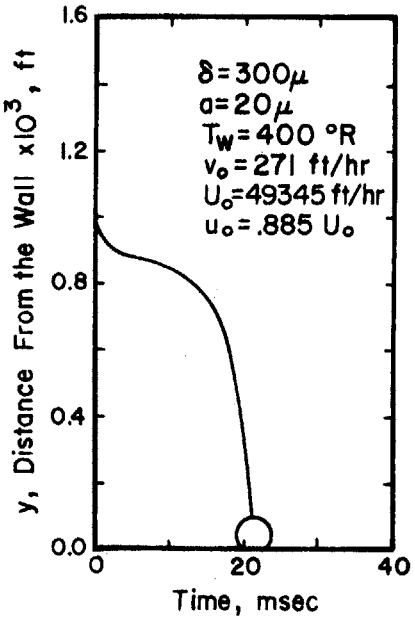

Figure 4.8a Trajectory of Drop

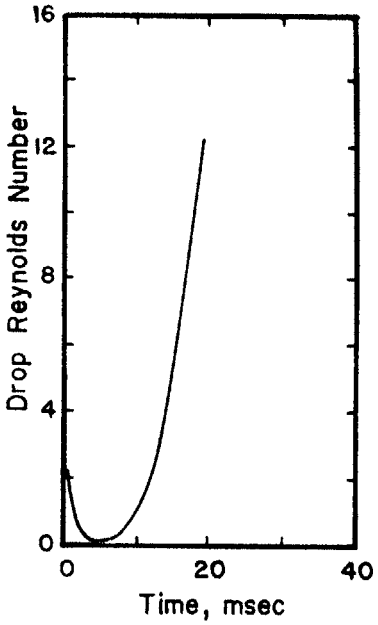

Figure 4.8d Drop Reynolds Number

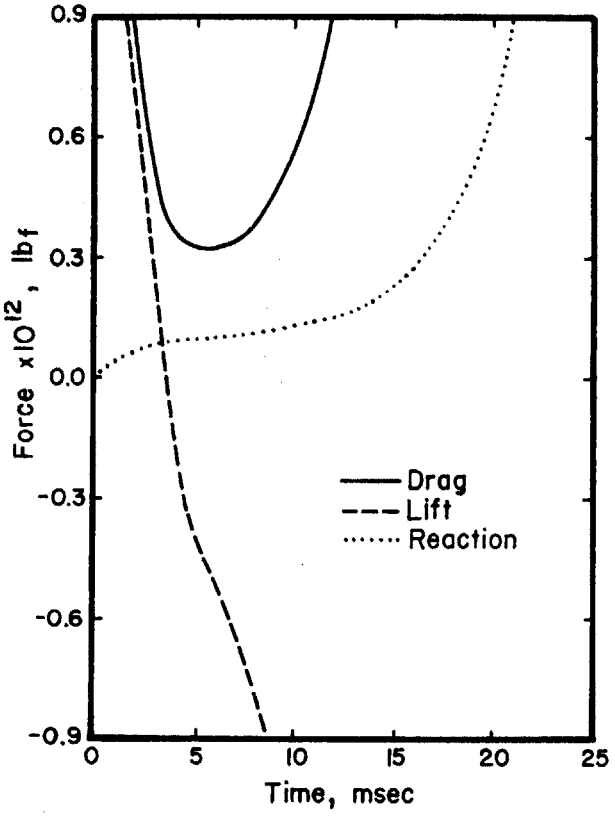

Figure 4.8b Forces on the Drop in the y-Direction

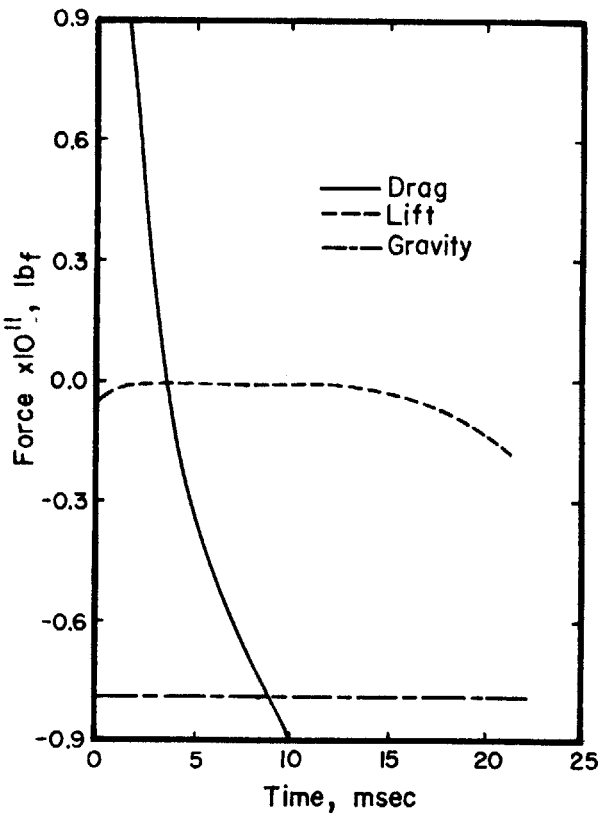

Figure 4.8c Forces on the Drop in the x-Direction

t(ms)	y(ft)	$\frac{dy}{dt}$ (ft/hr)	$\frac{dx}{dt}$ (ft/hr)	U (ft/hr)	$\left[U - \frac{dx}{dt}\right]$ (ft/hr)
0.	0.9840E-03	-0.2710E 03	0.43668E 05	0.49342E 05	0.5674E 04
1.	0.9328E-03	-0.1197E 03	0.44524E 05	0.46774E 05	0.2250E 04
2.	0.9095E-03	-0.5722E 02	0.44783E 05	0.46774E 05	0.8220E 03
3.	0.8977E-03	-0.3164E 02	0.44793E 05	0.45012E 05	0.2190E 03
4.	0.8905E-03	-0.2153E 02	0.44696E 05	0.44653E 05	-0.4300E 02
5.	0.8851E-03	-0.1806E 02	0.44551E 05	0.44382E 05	-0.1690E 03
6.	0.8802E-03	-0.1763E 02	0.44381E 05	0.44136E 05	-0.2450E 03
7.	0.8751E-03	-0.1888E 02	0.44193E 05	0.43884E 05	-0.3090E 03
8.	0.8696E-03	-0.2142E 02	0.43987E 05	0.43604E 05	-0.3830E 03
9.	0.8631E-03	-0.2532E 02	0.43759E 05	0.43281E 05	-0.4780E 03
10.	0.8553E-03	-0.3098E 02	0.43501E 05	0.52891E 05	-0.6100E 03
11.	0.8457E-03	-0.3906E 02	0.43202E 05	0.42406E 05	-0.7960E 03
12.	0.8333E-03	-0.5052E 02	0.42844E 05	0.41787E 05	-0.1057E 04
13.	0.8172E-03	-0.6679E 02	0.42404E 05	0.40977E 05	-0.1427E 04
14.	0.7956E-03	-0.8986E 02	0.41847E 05	0.39895E 05	-0.1952E 04
15.	0.7664E-03	-0.1226E 03	0.41125E 05	0.38429E 05	-0.2696E 04
16.	0.7262E-03	-0.1691E 03	0.40167E 05	0.36416E 05	-0.3751E 04
17.	0.6706E-03	-0.2350E 03	0.38876E 05	0.33629E 05	-0.5247E 04
18.	0.5931E-03	-0.3285E 03	0.37112E 05	0.29743E 05	-0.7369E 04
19.	0.4845E-03	-0.4613E 03	0.34678E 05	0.24296E 05	-0.1038E 05
20.	0.3317E-03	-0.6498E 03	0.31292E 05	0.16634E 05	-0.1465E 05
21.	0.1163E-03	-0.9172E 03	0.26554E 05	0.58296E 05	-0.2072E 05

t = time
x = axial position of drop
y = radial velocity of drop

$\frac{dx}{dt}$ = drop velocity in x direction

$\frac{dy}{dt}$ = drop velocity in y direction

U = vapor velocity

TABLE 2. History of Drop Motion
(a = 20 μ, T_w = 400°R)

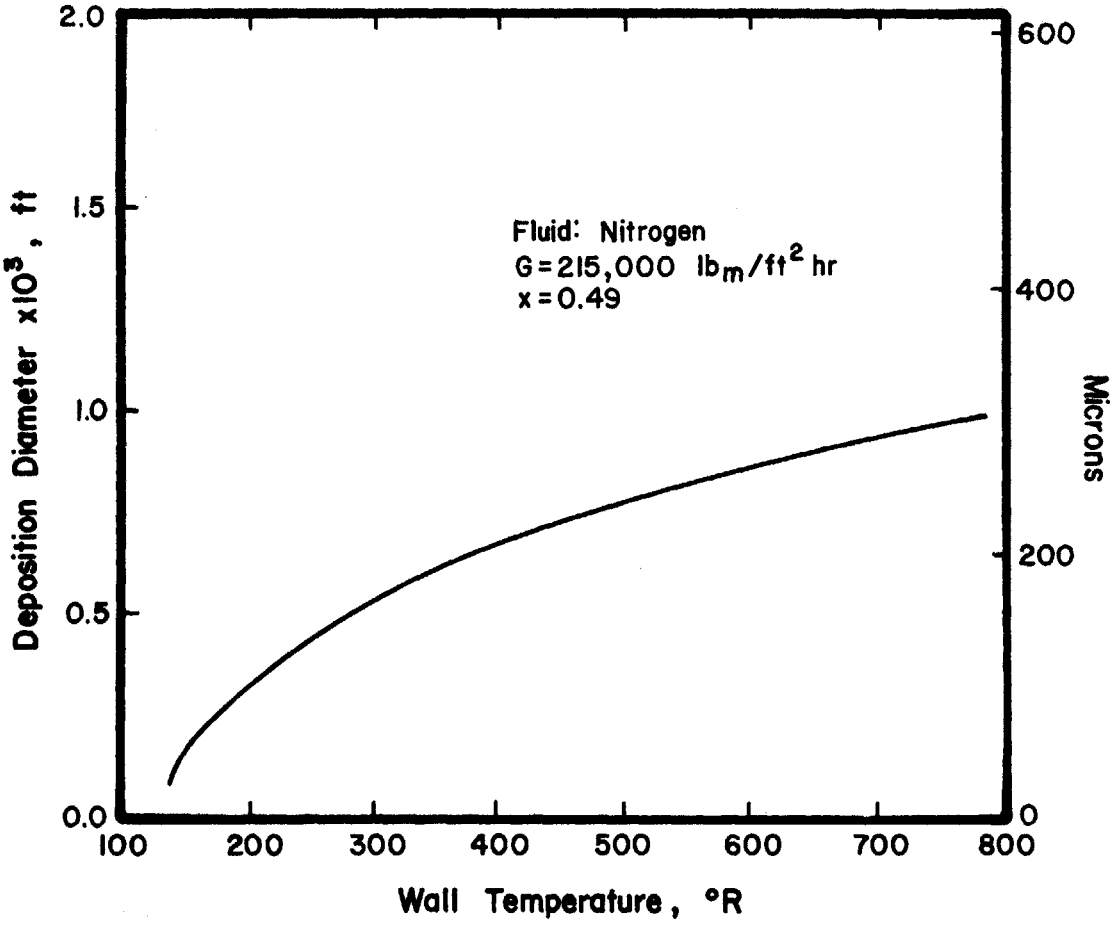

Figure 4.9 Effect of Wall Temperature on the Drop Deposition Diameter

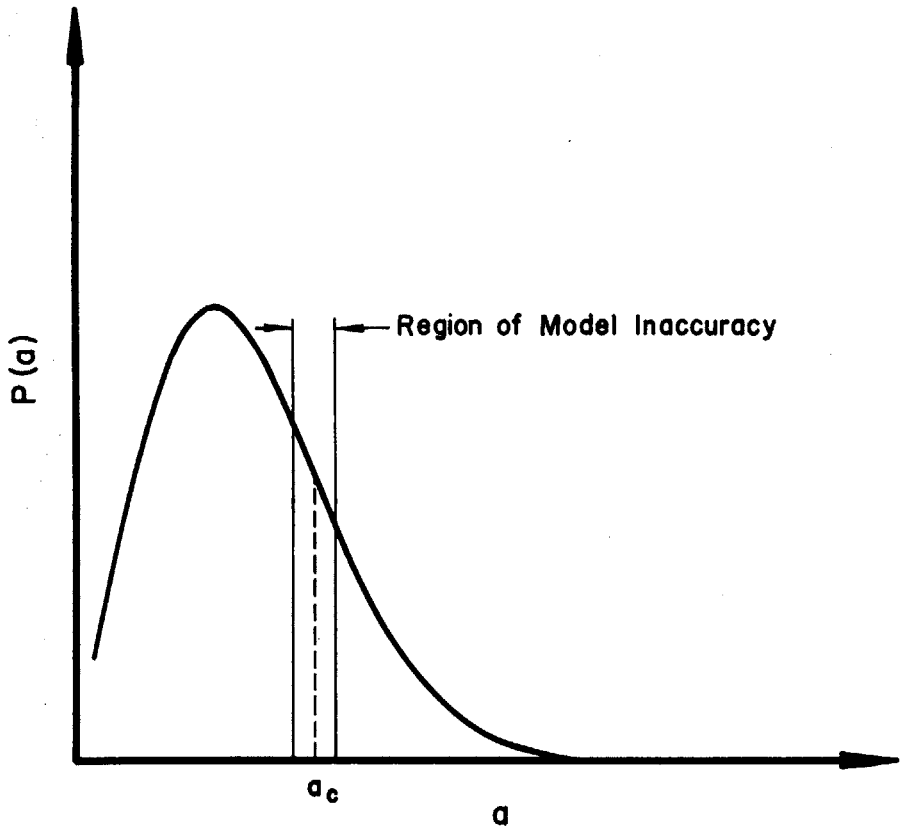

Figure 4.10 Drop Size Distribution

CHAPTER V: DISPERSED FLOW HEAT TRANSFER

As was mentioned in Chapter I, heat transfer from the wall to the dispersed flow is the sum of

(a) heat transfer to liquid drops deposited on the wall, $(q/A)_d$;

(b) heat transfer to the bulk vapor component of the flow, $(q/A)_v$;

(c) radiation heat transfer between the wall and dispersed flow, $(q/A)_r$;

or

$$q/A = (q/A)_d + (q/A)_v + (q/A)_r \qquad (5.1)$$

In deriving an expression for $(q/A)_d$ we will apply our results concerning the structure of dispersed flow (Chapter III) and dynamics of drops deposition on the hot wall (Chapter IV). First, however, we will analyze the heat transfer to the single drop deposited on the wall.

5.1 Heat Transfer to Single Drop

In dispersed flow with heat addition liquid drop penetrating the boundary layer collides with the heated wall and cools it by its evaporation. The physical variables which characterize the drop-wall collision and drop evaporation are very numerous, including all thermal and dynamic properties of the gas and liquid phase of the fluid, the thermal properties and surface conditions of the heated wall. A shape of the liquid drop in contact with solid wall varies with its dimensions. When the drop is very

small it will keep its spherical shape because of the surface tension effect. In the case of a large drop (diameter of the order of several hundred microns or more) it will form disc-shaped liquid film. When liquid drop touches the wall a contact boundary temperature is immediately established which depends [32] on the initial liquid and wall temperature and on the nature of the liquid and wall. Approximately [45],

$$\frac{T_c - T_\ell}{T_w - T_c} = \left[\frac{(k\,\rho\,C_p)_w}{(k\,\rho\,C_p)_\ell}\right]^{\frac{1}{2}} \tag{5.2}$$

where

T_c = contact boundary temperature,

T_w = initial wall temperature,

T_ℓ = initial liquid temperature,

k = conductivity,

ρ = density,

C_p = specific heat,

and subscripts ℓ and w refer to liquid and wall, respectively.

In spite of the above information, very little is known exactly, in technical literature, about thermal behavior of liquid drop deposited on the wall, over a wide range of the wall temperature and the drop impact velocity. In reference [10], where the experimental study of the dispersed flow drop behavior has been performed using high speed photography, it has been concluded that:

(a) As the wall temperature increases, the pictures show fewer and fewer drops touching the wall. The deposition model presented in Chapter IV of this study predicts this phenomenon.

(b) Drop-wall contact time is decreasing with wall temperature increase.

Several other investigators have studied wall-drop interaction [23].

Parker and Grogh (1961) studied steam-water dispersed flow heat transfer at qualities above 89% at 30 psia. In their study they concluded that if the wall temperature was below the minimum film boiling temperature (Leidenfrost† temperature, the temperature where the wall is so hot that the momentum of the rapidly generated vapor between the liquid drop and the hot surface forms a steam cushion to support the drop and prevent the liquid from wetting the surface), the heat transfer coefficients were three to six times the dry steam value. For wall temperature above the minimum film boiling temperature the heat transfer coefficients were almost identical to those for dry steam [47,23].

The drop splattering process, defined as the disintegration of drops

---

†Leidenfrost temperature, as described in technical literature, is usually related to the phenomenon of the evaporation of the stationary liquid drops deposited on the wall. The drops are of the order of several thousand microns or more [2]. In our case the drops are of the order of tens of microns and drop-wall contact times are very short (few milliseconds or less) [10,2]. Although there is a difference in the experimental conditions the existence of the Leidenfrost phenomenon appears also in the dispersed flow under consideration.

striking a hot wall without significantly wetting the wall was studied by McGinnis (1969). Splattering was found to occur at the higher drop velocities. The heat transferred per drop was expressed as a function of fluid properties and reached a maximum at surface temperature of 329°F above saturation for water, acetone, and alcohol drops. This maximum, for the impact angle of 27°, was given by the following correlation:

$$\frac{Q_{max}}{\rho_\ell \, a^3 \, H'_{\ell g}} = 8.44 \times 10^{-4} \left| \frac{\rho_\ell^{\,2} \, v_0^{\,2} a}{\rho_{\ell g} \, \sigma} \right|^{0.341} \tag{5.3}$$

where

$\rho_{\ell g}$ = density of the vapor at the film temperature,

$H'_{\ell g} = H_{\ell g} + C_p(T_w - T_{sat})/2$,

ρ_ℓ = liquid density,

a = drop diameter,

σ = surface tension,

and $H_{\ell g}$ = latent heat of evaporation.

Equation (5.3) has a limited applicability to dispersed flow heat transfer since it is based on very large drops ($a > 2.5$ mm).

Dispersed flow heat transfer has been studied by Forslund (1966) and later by Hynek (1969). Forslund's work is one of the first studies where drops-wall heat transfer has been analytically treated applying Baumeister's (1966) equation for the heat transfer coefficient for a stationary drop on the hot surface.

Wachters and Westerling (1966) also studied heat transfer from individual drops. They obtained data for drops 2300μ in diameter, approach(impact) velocities varying from 3.54 to 4.82 ft/s, and surface temperatures varying from 410°F to 662°F. Their data indicated a very low effectiveness [effectiveness is defined by Eq. (5.4) below] ranging from a maximum of 1.5 percent at 410°F to a minimum of 0.15 percent at 660°F.

Corman (1966) and Gauglev (1966) also studied drop-hot wall heat transfer. Their data will be shown below.

Cumo and Farello (1967) made a significant contribution to the understanding of disperses flow heat transfer phenomena. From a photographic study they concluded that between heated surface temperatures of 320°F and 482°F there is a sudden reduction in surface wettability [10,23]. Above 482°F his photographic results do not permit distinction between drops touching the surface or being insulated from it by a thin vapor blanket [10,23]. The reader is referred to their study for more details.

Pederson (1967) obtained heat transfer data for individual water drops impinging upon a heated surface. The drop diameters ranged from 200μ to 400μ, and the approach velocities from 8 to 33 ft/s. The effect of surface temperature variation from the saturation temperature to 1800°F was studied. Photographs of the impingement process are presented which show that even the small drops studied break up upon impingement at moderate approach velocities. These results, effectiveness of evaporation ε , are shown on Figure 5.1 together with results of other investigators. The effectiveness of evaporation ε is defined as:

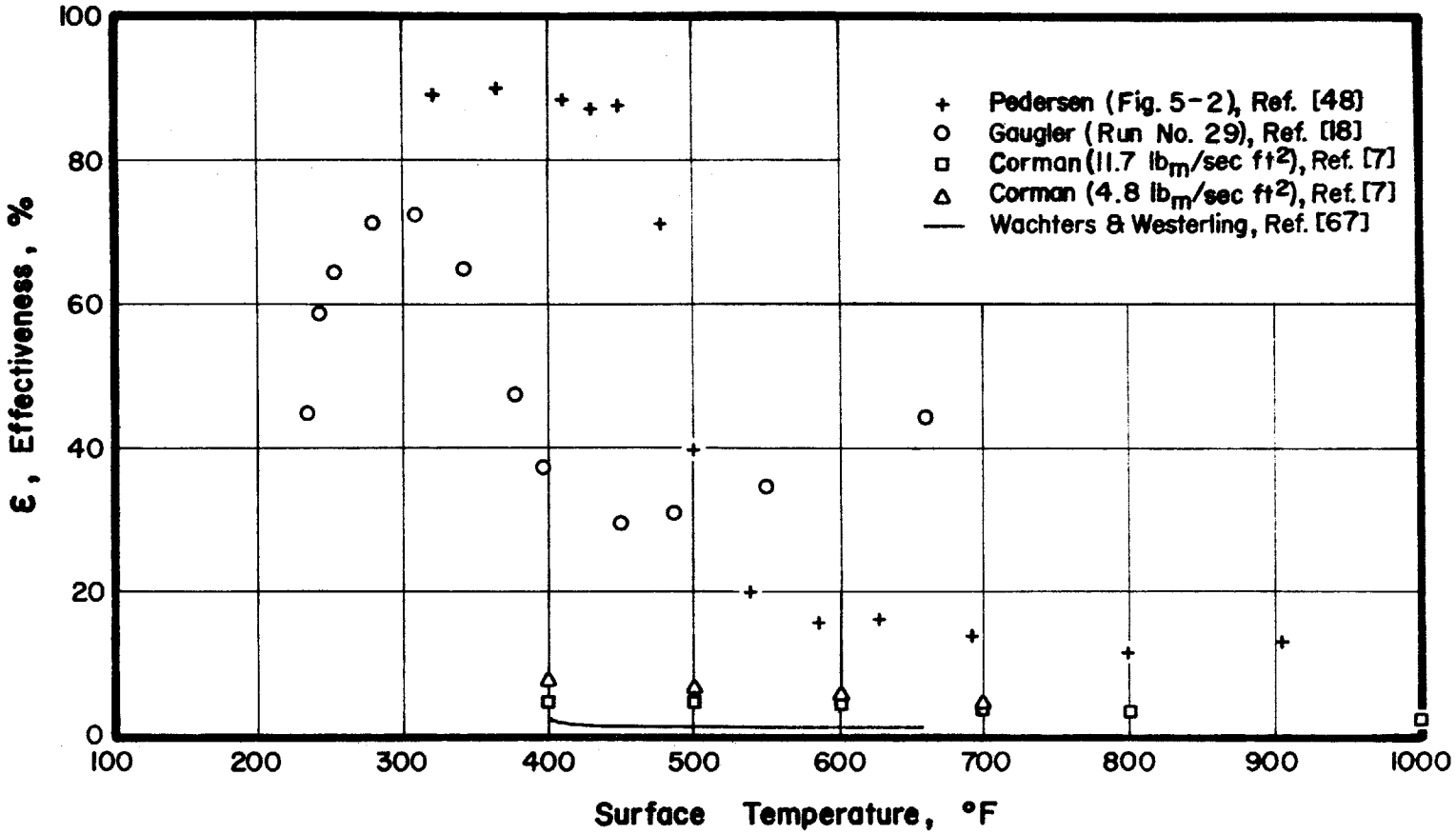

Figure 5.1 Effectiveness vs. Surface Temperature

$$\varepsilon = \frac{Q}{m\left[H_{\ell g} + C_{p\ell}(T_{sat} - T_{\ell})\right]} \tag{5.4}$$

where

Q = heat transferred per drop,

m = mass of drop $\left(m = \frac{\pi}{6} a^3 \rho_{\ell}\right)$,

$H_{\ell g}$ = latent heat of evaporation,

$C_{p\ell}$ = liquid specific heat,

T_{ℓ} = liquid (drop) temperature,

and T_{sat} = saturation temperature.

The effectiveness of evaporation measured by Pedersen was generally higher than the corresponding values measured by the other investigators (Figure 5.1). This may be due to the dry air atmosphere used by Pedersen rather than a saturated steam atmosphere as suggested by Groeneveld (1972).

Figure 5.1 clearly demonstrates the effect of the wall (surface) temperature on the evaporation of the deposited drops. It is evident from this figure that the wall cooling due to the direct removal of heat as latent vaporization heat of deposited drops is much less significant at the higher wall temperature.

Toda (1972) studied a heat transfer cooling phenomenon by mist drops on a heated surface at a temperature above the saturation temperature. Drops were sprayed by any method, collided with the heated surface, and cooled it by their evaporation. It was revealed that the heat transfer characteristics of mist cooling can be classified into the three regions, according to the thermal behavior of liquid film formed from mist drops on

the heated surface:

(a) low surface temperature region,

(b) high surface temperature region,

(c) combination of (a) and (b).

Toda developed the semi-theoretical equations for the time-averaged heat flux for three regions listed above which included four experimentally determined constants. His theory is in good agreement with his experimental data.

A comprehensive study of the evaporation of the liquid drop deposited on the wall has been performed by Iloeje (1974). He assumed that after a drop was deposited on the wall, nucleation and bubble growth from liquid drop take place (pool boiling model assumed). At the end of bubble growth period, a part of the liquid drop is ejected into the main stream by escaping vapor bubbles and a part is left on the wall to evaporate (see Figure 44 of his thesis where proposed model is drawn). His analytical procedure which involves several assumptions [32] gives heat transferred to a single drop as

$$Q = C_0 C_1 \frac{\pi a^2}{4} \left(\frac{\rho_\ell}{\rho_g} \right) \frac{R_v \sigma \rho_\ell C_{p\ell} T_{sat}^2}{0.213 P_\ell H_{\ell g}} \qquad (5.4a)$$

where

R_v = gas constant,

σ = surface tension,

$C_{p\ell}$ = liquid specific heat,

P_ℓ = liquid pressure,

a = average drop diameter in dispersed flow as defined by Forslund [17],

and C_0 and C_1 are constants with values of 0.683 and 0.455, respectively. The value of Q calculated from Eq. (5.4a) is only a few percent of the maximum value which is given as $Q_{max} = \frac{\pi a^3}{6} \rho_\ell H_{\ell g}$. This makes Iloeje's expression applicable only in the very high temperature region ($T_w >> T_{min}$, T_{min} = minimum film boiling temperature).

The successive states of drop-wall interaction are shown in Figure 5.2 This figure was made after analyzing available experimental results [10,63, 47,44,2,67,48,46] related to the deposition of the drop and its evaporation on the heating wall.

At the high wall temperature and high drop impact velocity, tiny drops rebound on the wall with little cooling action until the wall temperature is reduced to a certain value (the minimum film boiling temperature) at which point the drops wet the wall with a significant cooling action [10] (Figure 5.2a). For the same condition the large drop behavior as shown in Figure 5.2b where a part of drop is ejected into the main stream by escaping vapor bubbles [46,10].

In the high temperature region and low impact velocity ($v_0 < 6.5$ ft/s) the liquid film formed from the deposited drop is found to be in a film boiling-line state (Figure 5.2c) in which a vapor layer is formed between the liquid film and the heated surface [46,63]. The evaporation of the liquid film on the liquid-vapor layer interface is induced by convective heat transfer through the vapor layer and radiation heat transfer from the heated wall.

The low wall temperature and low impact velocity case is shown on

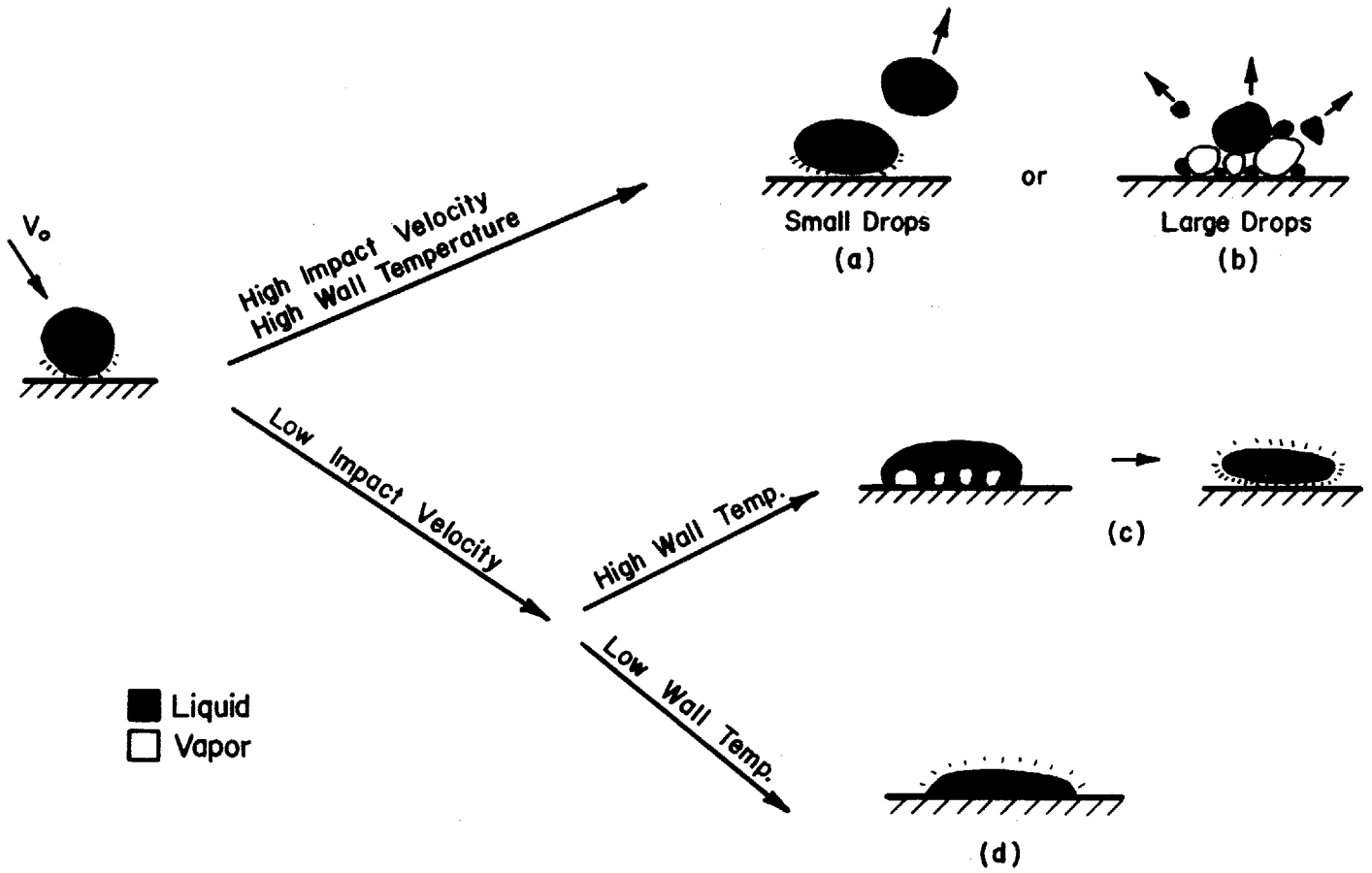

Figure 5.2 Successive States of Liquid Drop - Wall Interaction

Figure 5.2d where the liquid film evaporates from the liquid-vapor interface. At the initial stage of formation of a liquid film on a heated wall, heat is transferred by conduction from the heated wall to the liquid film. When the superheated thermal layer in the liquid film is fully developed, evaporation of the liquid film at the liquid-vapor interface takes place. This liquid-vapor interface moves with time [63,46].

Not all possible states of the drop-wall interaction are covered in Figure 5.2. Only the most frequently observed states are shown.

The list of variables that have a certain influence on the wall-drop heat transfer includes:

- wall temperature,
- nature of the fluid,
- drop impact velocity,
- nature of the heating wall and coupling of fluid and wall,
- drop temperature,
- surface state of heating wall (microughness, oxidation, etc.).

The "behavior" and the further existence of the liquid film formed from the deposited drop is mostly prescribed by the wall temperature (Figures 5.1 and 5.2). The wall temperature is the most important variable associated with this problem.

The data for water obtained by Pedersen [48] show that drop impact velocity is the dominant variable affecting drop heat transfer in the very high temperature region ($T_w \simeq T_{min} + 500°F$). The effectiveness of the drop evaporation as defined by Eq. (5.4) was very low ($\varepsilon \simeq 5\%$) for the above range

of the wall temperature. The increase in ε (about 100%) due to the increase in the impact velocity does not increase significantly the total heat transfer to the liquid in the case of dispersed flow [$(q/A)_d$, Eq. (5.1)] since the drop deposition flux (number of drops deposited per unit area of the wall per unit time) is very low in such a high temperature region. In the region of high drop deposition flux and high ε (the wall temperature in the vicinity of and below the minimum film boiling temperature) even small increases in ε due to increases in drop impact velocity will significantly increase total heat transfer to the liquid [$(q/A)_d$, Eq. (5.1)].

Oxide films and crud [32] can reduce the effective liquid drop-surface contact angle and liquid contacting the surface will spread over a wider area, increasing the heat transfer directly to liquid in spite of a high surface thermal resistance layer created by the oxide.

The wall microughness increases the heat transfer to liquid drop. When a liquid drop hits the wall it is possible that it will be dragged along the wall due to its velocity in the flow direction (see Table 2). Therefore, the liquid wets the wall penetrating into the microscopic surface depressions and heats up rapidly, beginning on very fast evaporation [32,10].

The effect of the drop temperature (drop subcooling) on the drop heat transfer is mentioned in reference [48]. The drop subcooling increases the heat transfer since it lowers the contact boundary temperature (liquid drop-wall contact boundary temperature) as shown by Eq. (5.2).

Decreasing the contact angle (the contact angle between the wall and

the liquid drop is measured through the liquid) increases the wettability of the surface, which in turn increases the heat transfer to drop. As shown in Figure 5.2, the contact angle is important for the case (d) (low wall temperature, $T_w < T_{min}$) and less important for cases (a), (b), and (c) (high wall temperature), where there is not full contact of the liquid with wall.

The wall-drop heat transfer under stationary vapor conditions (a sessile drop or drop impinging upon a wall [48,63,47]) and under flowing vapor conditions (a drop deposited from the vapor stream [10,44,16]) are, to a certain extent, different processes. The presence of a vapor and drop velocity parallel to the wall, for example as in Figure 5.2c, will reduce the vapor layer thickness between drop and wall, thus increasing the heat transfer through this layer. The successive states of drop-wall interaction shown in Figure 5.2 have been observed in both cases (with and without vapor flow). Of course this does not eliminate the need for the caution that should be exercised in extrapolating the data for these two cases [32,16].

The experimental data and proposed correlation for Q (heat transferred to a single drop evaporating on the wall) available in the literature [62,48,10,44,16] were analyzed in deriving $(q/A)_d$. The relation between Q and $(q/A)_d$ will be shown in the next section. When incorporated into our heat transfer prediction scheme none of the correlations for Q provided satisfactory prediction of our experimental data. All the experimental data for Q [63,47,44,48,18,67,7,10] show the exponential decay in Q with increase of wall temperature (Figure 5.1). Using this information, we

introduced the following simple expression for the heat transferred to a single drop on the wall, deposited from the fluid stream:

$$Q = \frac{\pi a^3}{6} \rho_\ell H_{\ell g} \; e^{1-(T_w/T_{sat})^2} \tag{5.5}$$

Although this expression included only the nature of the fluid and the wall temperature as variables, it provided good prediction of the experimental data obtained by the author. This will be shown below.

5.2 Drop Deposition Flux and $(q/A)_d$

The deposition of a drop in dispersed flow with heat addition has been analyzed in Chapter IV. The mass flux of liquid drops migrating toward the wall, entering the laminar sublayer, is by definition

$$M = v_0(1 - \alpha)\rho_\ell \tag{5.6}$$

where

M = mass flux (lb/ft^2hr),

α = void fraction (by homogeneous model),

ρ_ℓ = liquid density,

and $v_0 = 0.15 \frac{Gx}{\alpha\rho_g} \sqrt{f_g/2}$, drop deposition velocity, Eq. (4.44).

The mass flux of liquid drops at the wall [32] is then

$$M_w = v_0(1 - \alpha)\rho_\ell f \tag{5.6a}$$

where f is the mass fraction of the drops entering the laminar sublayer which reach the wall, Eq. (4.46).

The drop deposition flux (the number of the drops deposited per unit area of the wall per unit time) is then

$$N = \frac{M_w}{\frac{\pi}{6}\bar{a}^3 \rho_\ell} = \frac{6v_0(1-\alpha)}{\pi \bar{a}^3} f \quad \left[\frac{\#\ \text{drops}}{\text{ft}^2\text{-hr}}\right] \tag{5.7}$$

where $\bar{a}$ = average drop diameter for $a_c < a < a_m$, defined by Eq. (3.11). Applying Eq. (5.5), the heat transfer from the wall to the liquid drops is

$$(q/A)_d = N \cdot Q = v_0(1-\alpha)\rho_\ell H_{\ell g} f \; e^{1-(T_w/T_{sat})^2} \tag{5.8}$$

The equivalent procedure to the above, in deriving $(q/A)_d$, is presented in Appendix V-1.

5.3 Heat Transfer to Vapor, $(q/A)_v$

Heat transfer from the wall to the bulk vapor component of the dispersed flow is given by the McAdams equation, using a vapor flow Reynolds number,

$$(q/A)_v = 0.023 \frac{k_g}{D} Re^{0.8} Pr^{0.4} (T_w - T_{sat}) \tag{5.9}$$

where $Re = \frac{GxD}{\alpha \mu_g}$.

Fluid properties are calculated at bulk vapor temperature. It was assumed in the above equation that the surface void fraction α_s (percentage of the wall area available for the heat transfer to the vapor flow) was equal to unity (Appendix V-2).

5.4 Radiation Heat Transfer, $(q/A)_r$

In dispersed flow with heat addition the heated wall is also cooled by radiation. It is given as the sum of the radiation heat transfer from the surface to the liquid drops and to the vapor,

$$(q/A)_r = \mathcal{F}_{we}\,\sigma\,(T_w^4 - T_{sat}^4) + \mathcal{F}_{wv}\,\sigma\,(T_w^4 - T_{sat}^4) \qquad (5.10)$$

assuming that the liquid drops and vapor are at the saturation temperature. $\mathcal{F}_{we}$ and $\mathcal{F}_{wv}$ are gray body factors between the wall and drops and between the wall and vapor, respectively. σ is the Stefan-Boltzman constant. The evaluation of $\mathcal{F}_{we}$ and $\mathcal{F}_{wv}$ was presented in ref. [60] where dispersed system was assumed gray and diffuse, the absorption and emission of the mixture was incorporated into the network analysis by treating the system as an enclosure filled by a radiating gas and a cloud of liquid drops. Details of this analysis are omitted here as $(q/A)_r$ was negligible in the nitrogen dispersed flow under consideration (Table 3).

TABLE 3. Value of $(q/A)_r/(q/A)_v$ at T_w = 740°R and G = 120,000 lbm/ft^{2}hr, x = 0.50

Transient Test Section Material	$(q/A)_r/(q/A)_v$
Copper	0.0083
Aluminum 1100	0.0016
Inconel 600	0.0102

The emissivity of the test section surface is given in reference [41].

5.5 Total Heat Flux, q/A

The total heat transfer from the wall to the dispersed flow under consideration can be calculated for the given mass flux, vapor quality, and system pressure, using Eq. (5.8), developed in this study, and Eq. (5.9),

$$q/A = v_0(1 - \alpha)\rho_\ell H_{\ell g} f \; e^{1 - (T_w/T_{sat})^2} + \tag{5.11}$$

$$+ \; 0.023 \frac{k_g}{D} \; Re^{0.8} \; Pr^{0.4} \; (T_w - T_{sat})$$

The comparison of Eq. (5.11) with the experimental data obtained by the author, for a relatively wide range of mass fluxes and vapor qualities, is presented in Figures 5.3 - 5.12. The minimum value of q/A [Eq. (5.11)] corresponds to the minimum film boiling temperature (the rewet wall superheat). The equation (5.11) represents a well-known boiling curve for specified values of mass flux, vapor quality, and system pressure. It covers a low and high wall superheat dispersed flow heat transfer, i.e., flow transition boiling and flow film boiling, respectively. The effect of the mass flux and vapor quality on q/A, given by Eq. (5.11), is as follows:

(a) When the mass flux increases (constant vapor quality assumed), q/A increases and T_{min} increases.

(b) When the vapor quality increases (constant mass flux assumed), $(q/A)_d$ decreases, $(q/A)_v$ increases, and T_{min} decreases. This affects q/A in such a way that q/A increases in the high

temperature region (film boiling region) and decreases in the low temperature region (transition boiling region).

These conclusions are experimentally supported (Figures 5.3 - 5.12) within the experimental error of the data (Appendix II-1).

5.6 Value of C, Equation (3.5)

The values of C in Eq. (3.5), selected for the prediction of the experimental data in Figures 5.3 - 5.12, are summarized in Figure 5.13. Figure 5.13 shows that C increases when the mass flux and vapor quality increase. In references [12,57], where Nukiyawa-Tanazawa equation [Eq. (3.4)] was applied for calculation of $\bar{a}$ (mean drop diameter), the vapor velocity was at least ten times higher than in our case. We may assume that C will approach unity in our case but at very high values of G (mass velocity) and x (vapor quality), since at such high values of G and x the vapor velocity will be very high, i.e., we will be approaching the conditions similar to those for which the Nukiyawa-Tanazawa equation was developed.

From Figure 5.13 one can see that the value of C is larger at higher mass velocity. It does not mean that drops are smaller at lower values of G; it simply shows that at a lower value of G, the conditions concerning vapor velocity are further from the conditions of the Nukiyawa-Tanazawa equation and the numerical correction of the equation (3.4) is larger.

The effect of gravity on the drop size in our experiment and the experiments relevant to ours [58] is probably very important as the vapor velocity

is not very high. Also, the effect of the drop evaporation (heat and mass transfer at the drop interface) on the drop size can be very important. Neither of these two effects, gravity or evaporation, are included or considered in the Nukiyawa-Tanazawa analysis [12,68].

The value of C affects the value of $\bar{a}$ [mean drop diameter, Eq. (3.5)], while the drop size distribution is affected by $\bar{a}$ [Eq. (3.7)]. The drop cooling rate at the wall is affected by $P(a)$ [Eq. (5.8)], etc. All this emphasizes the importance of knowing the actual value of the mean drop diameter in predicting the heat transfer in a dispersed flow.

The prediction of our experimental data with constant value of $C = 0.26$ is analyzed in Appendix V-3. Since the predictions in Figures V-2, V-4, V-10 are not good, the constant value of C is not recommended. It is important to mention that C is not a dimensionless parameter, as is evident from Eq. (3.5).

5.7 Thermal Non-Equilibrium in Dispersed Flow

A significant degree of thermal non-equilibrium can exist in a dispersed flow, i.e., a vapor can be superheated. The vapor temperature is, in that case, given by energy balance between the evaporating liquid and superheating vapor,

$$x_E H_{\ell g} = x \left[H_{\ell g} + C_{pg}(T_v - T_{sat}) \right] \qquad (5.12)$$

where

T_v = vapor temperature,

x = actual quality,

and x_E = equilibrium quality.

The actual quality, the ratio of mass flow of vapor to total mass flow, is less than or equal to the value calculated from the equilibrium energy balance (equilibrium quality) for the case of a dispersed flow. In order to find T_v from Eq. (5.12) we need one more relation between x and x_E. Forslund (1966) experimentally obtained the relation between x and x_E for nitrogen (Figure 19, ref. [17]). Plummer (1974) deduced the relation between x and x_E using Forslund's data. Applying Forslund's data or relation suggested by Plummer (Eq. (4.1), ref. [50]), T_v can be calculated from Eq. (5.12). Groeneveld (1972) proposed the relation between the actual and equilibrium quality which is based on the large number of the experimental data (Eq. (4), ref. [24]). Knowing T_v, the driving force for the convection heat transfer [second term, Eq. (5.11)] is $(T_w - T_v)$ instead of $(T_w - T_{sat})$.

The analysis of the drop deposition presented in Chapter IV is also valid for the case when vapor is superheated, since the assumption of the linear temperature distribution inside the laminar sublayer holds as well as when vapor was not superheated.

In the experimental data reported in this study (Figures 5.3 - 5.12), no thermal non-equilibrium was observed since the equilibrium vapor qualities were relatively low and the preheater section was very long (Figure 2.1, Section 2.1), so that the preheater flux was low.

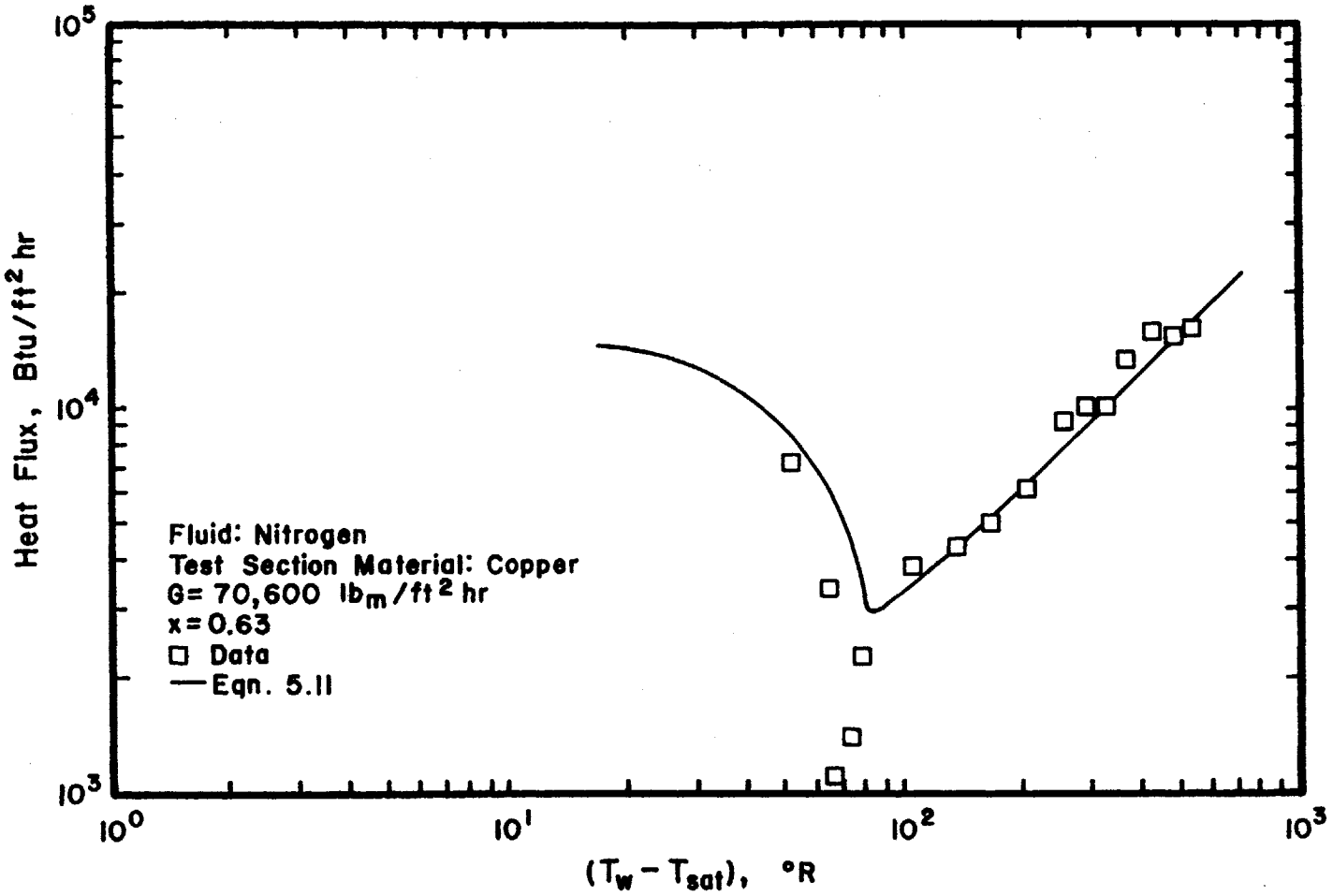

Figure 5.3 Heat Flux vs. Wall Superheat

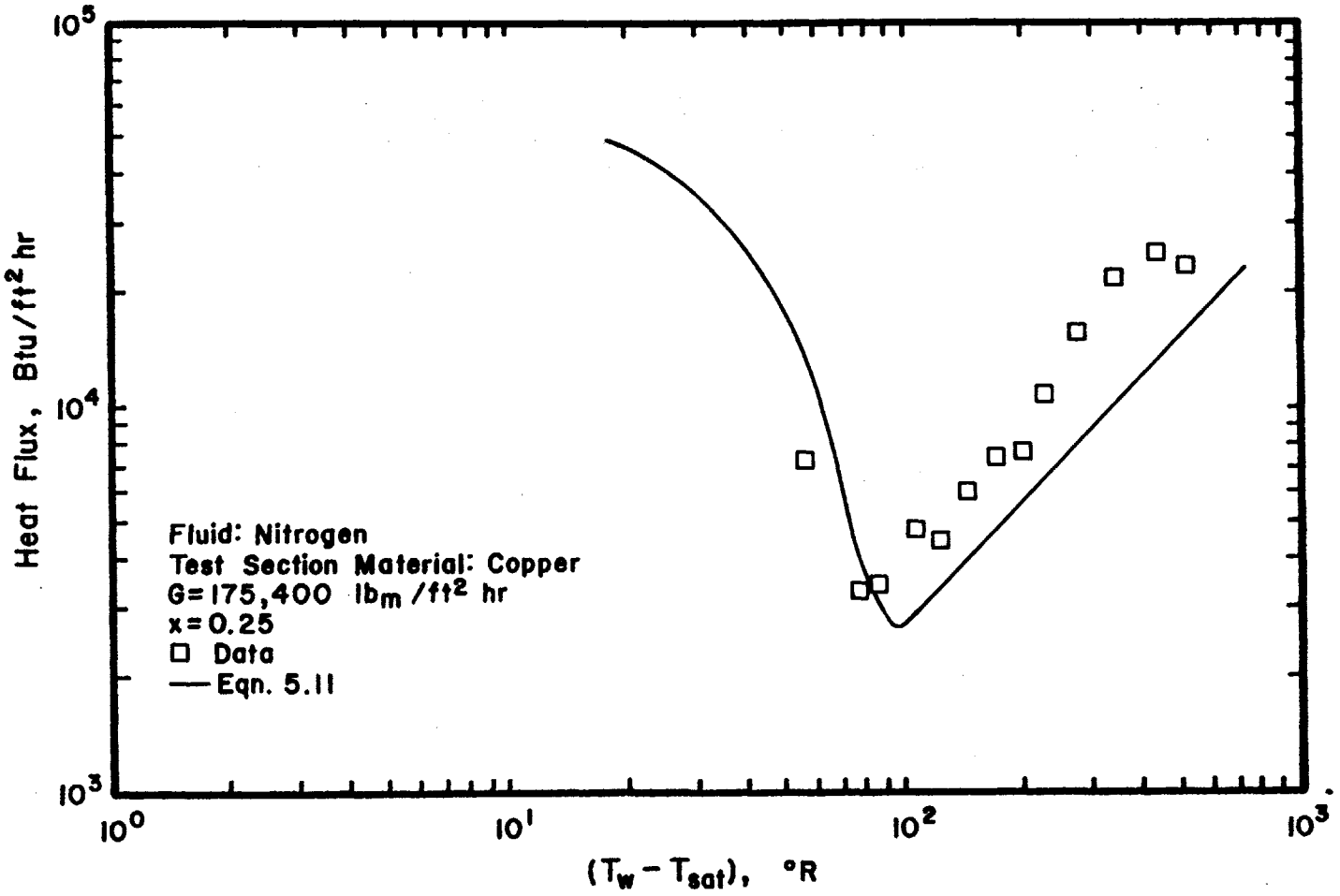

Figure 5.4 Heat Flux vs. Wall Superheat

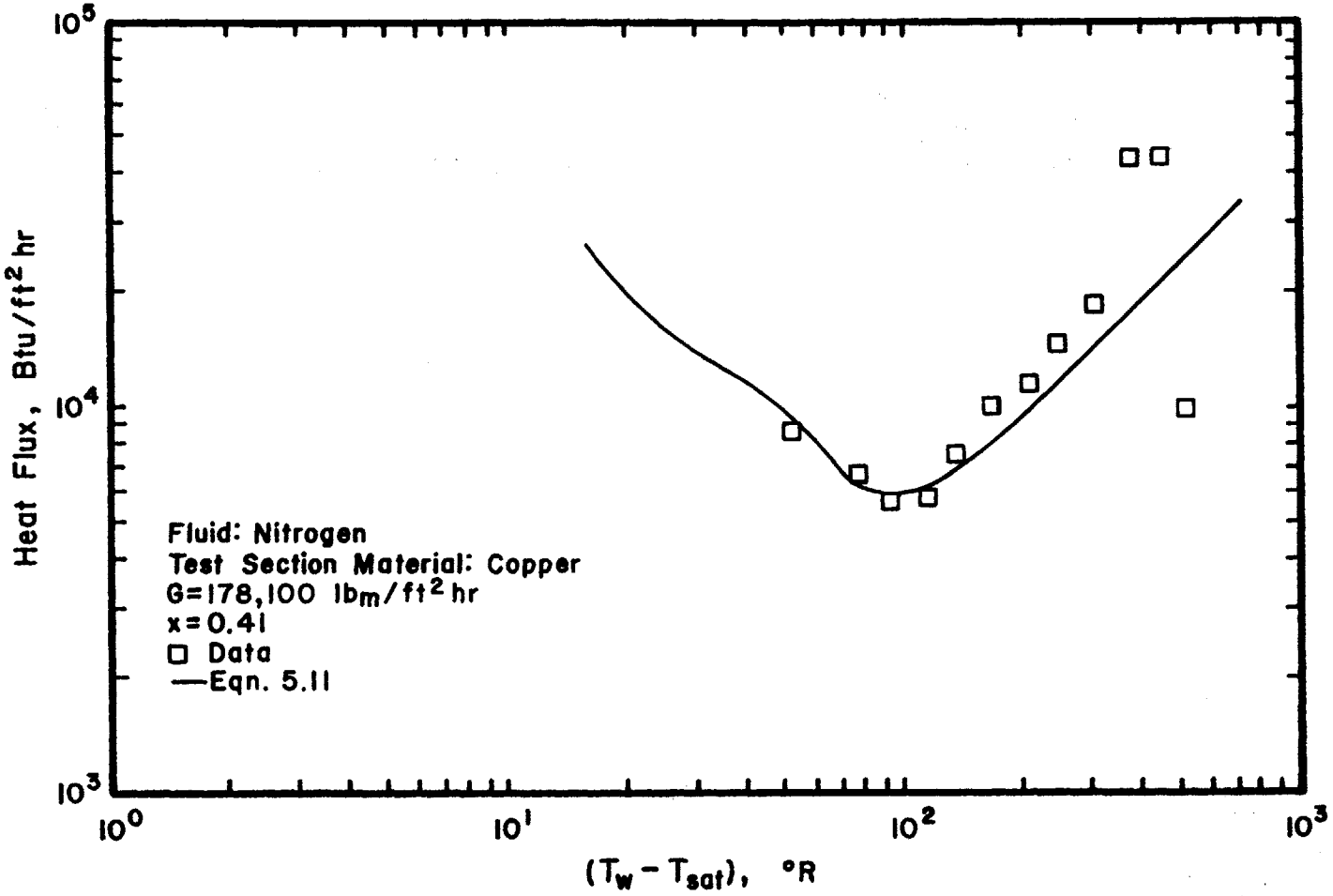

Figure 5.5 Heat Flux vs. Wall Superheat

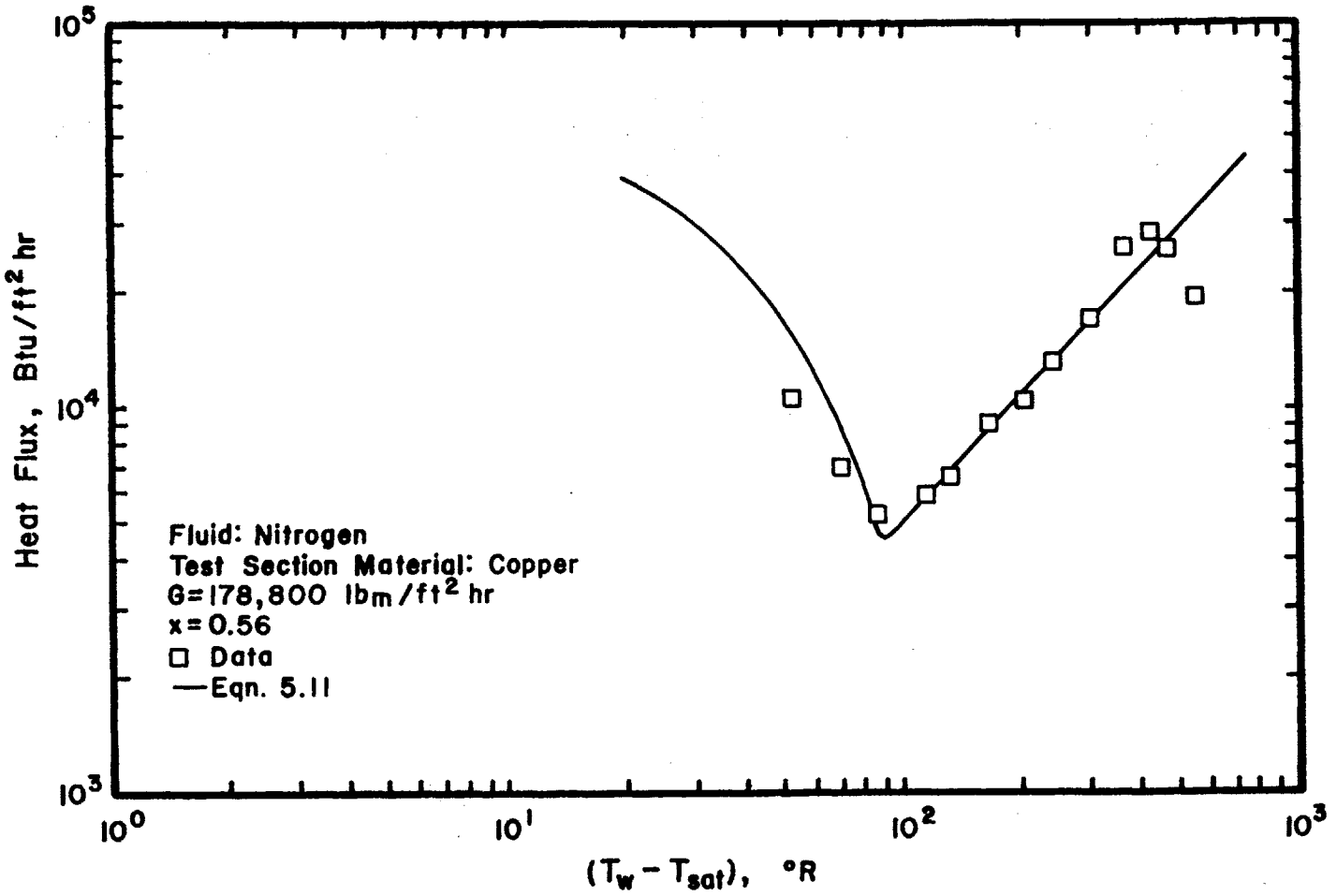

Figure 5.6 Heat Flux vs. Wall Superheat

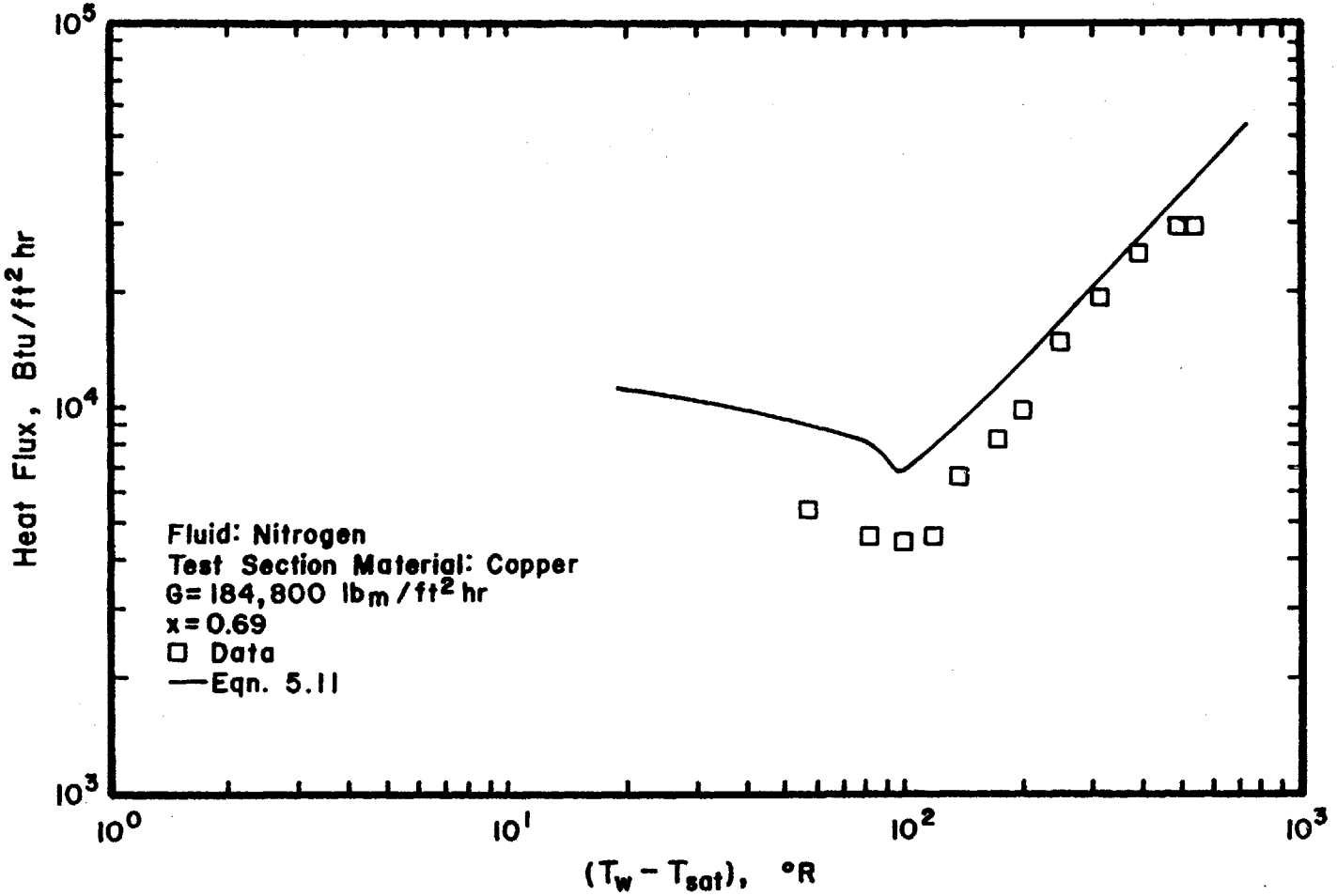

Figure 5.7 Heat Flux vs. Wall Superheat

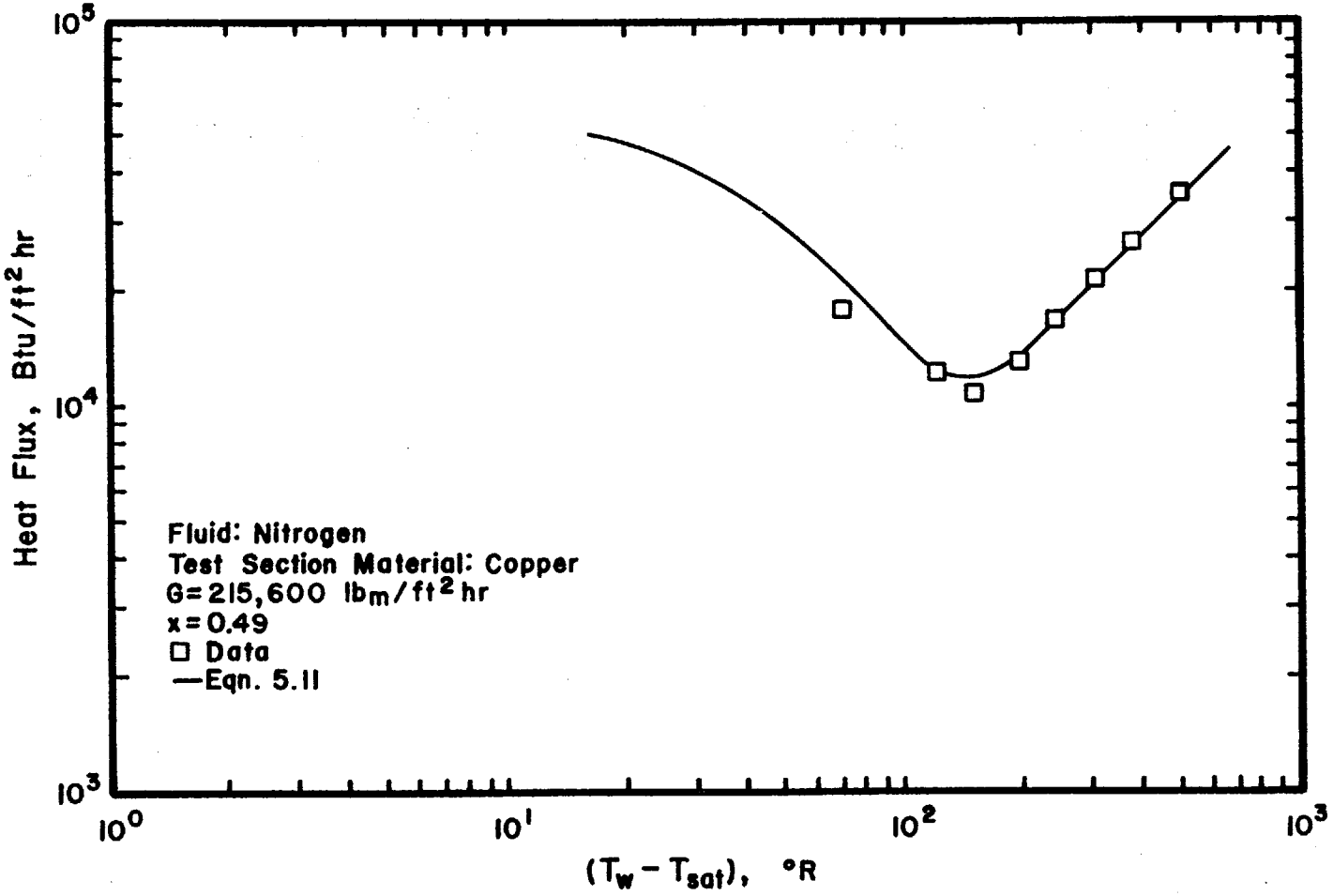

Figure 5.8 Heat Flux vs. Wall Superheat

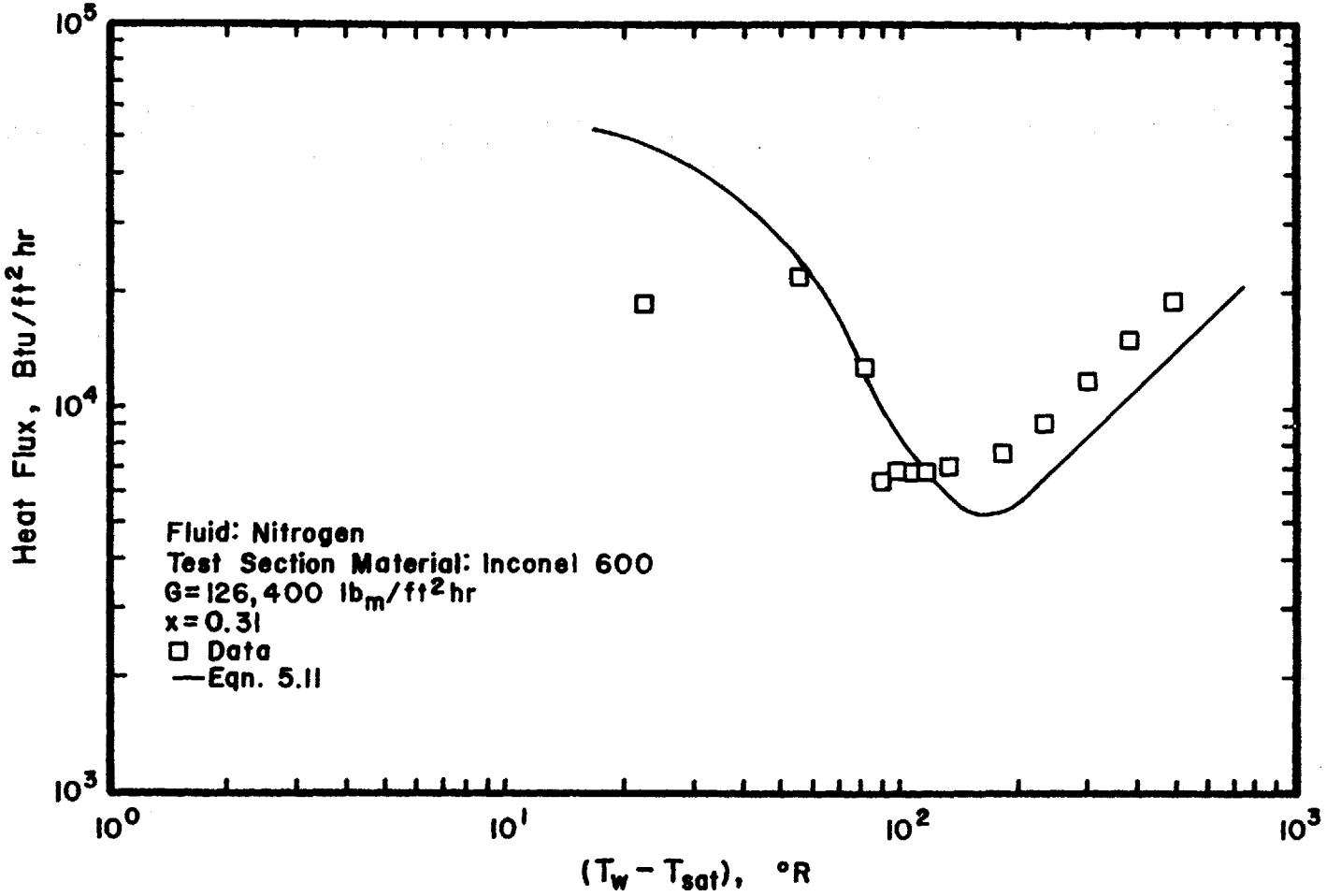

Figure 5.9 Heat Flux vs. Wall Superheat

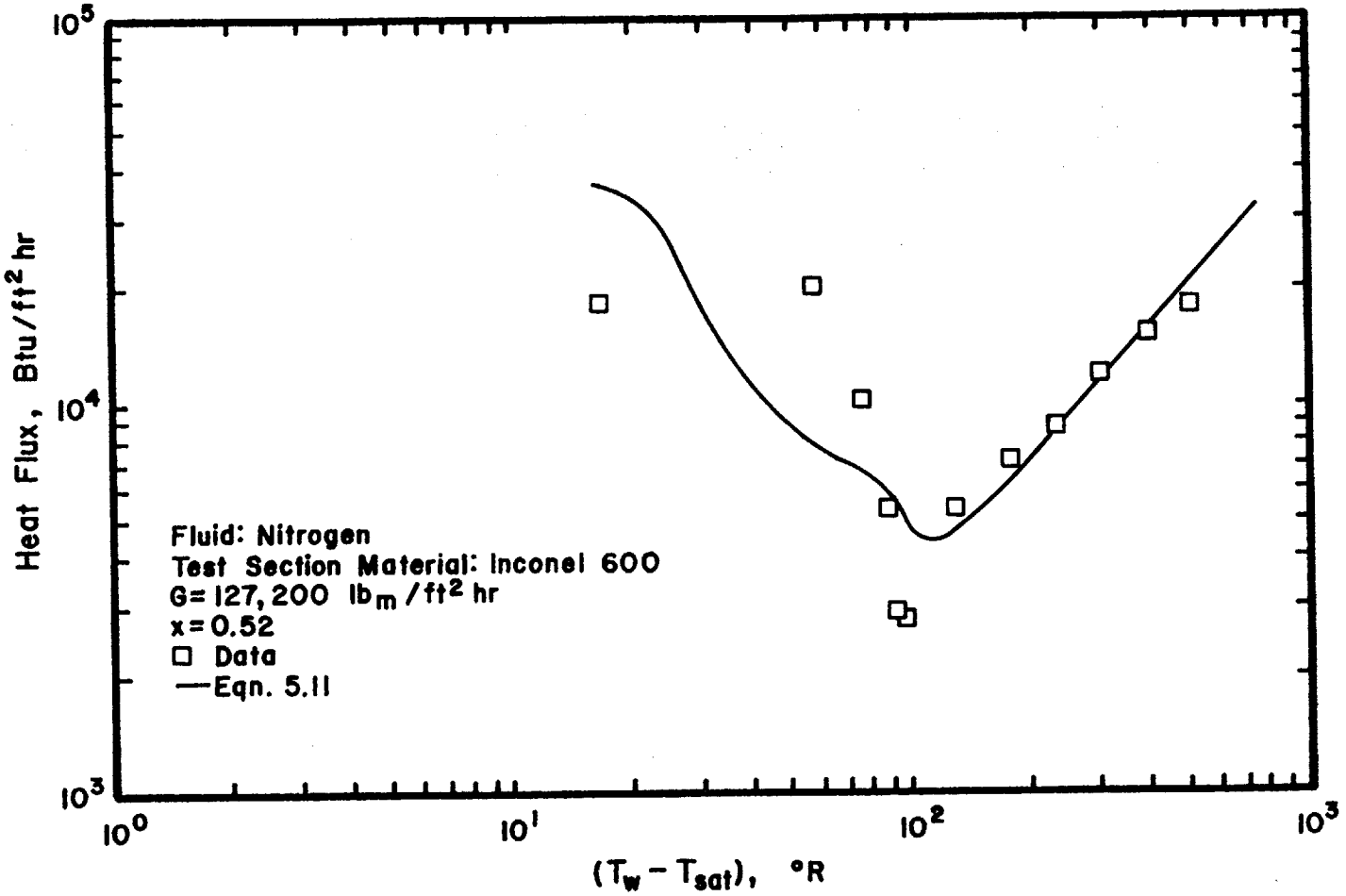

Figure 5.10 Heat Flux vs. Wall Superheat

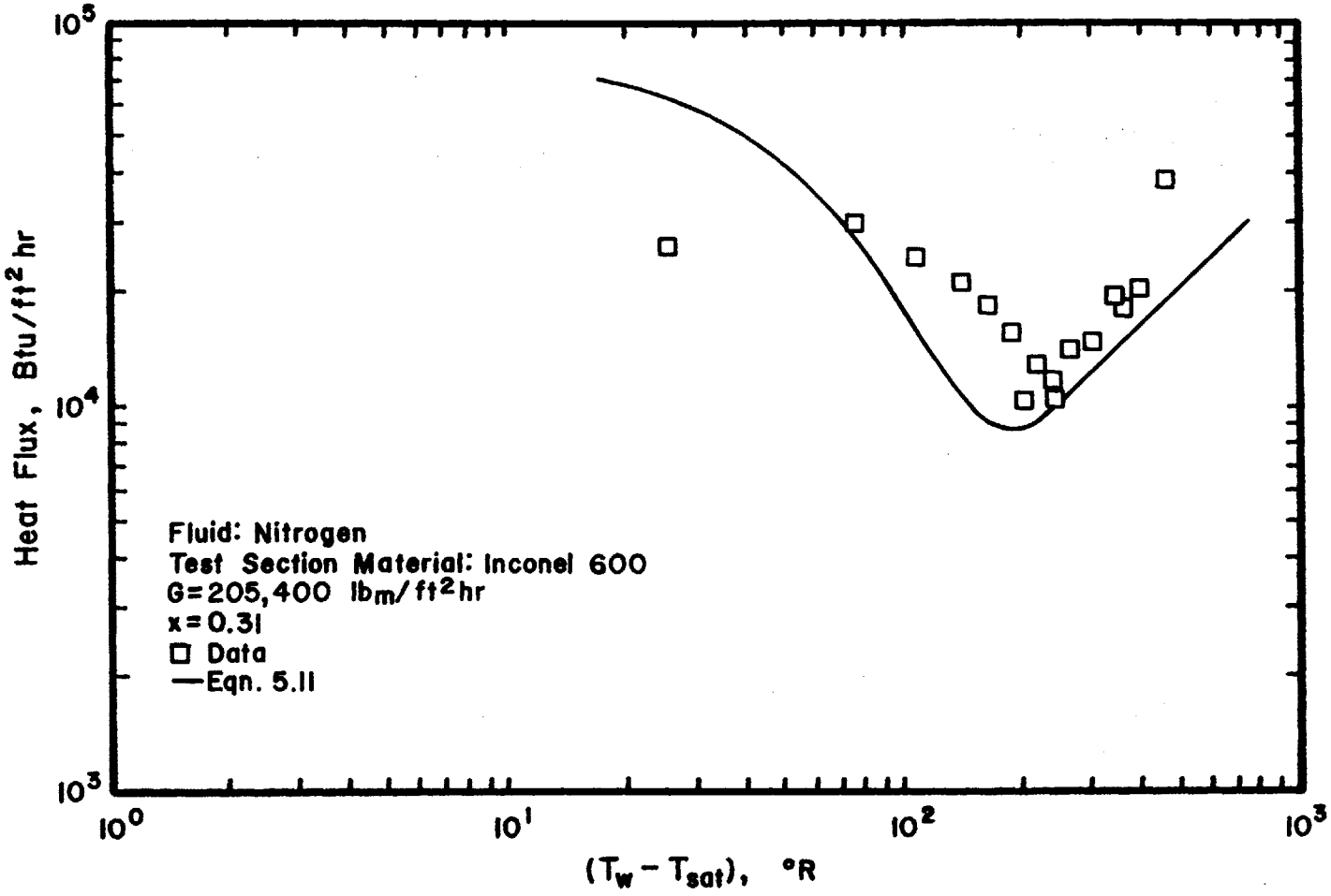

Figure 5.11 Heat Flux vs. Wall Superheat

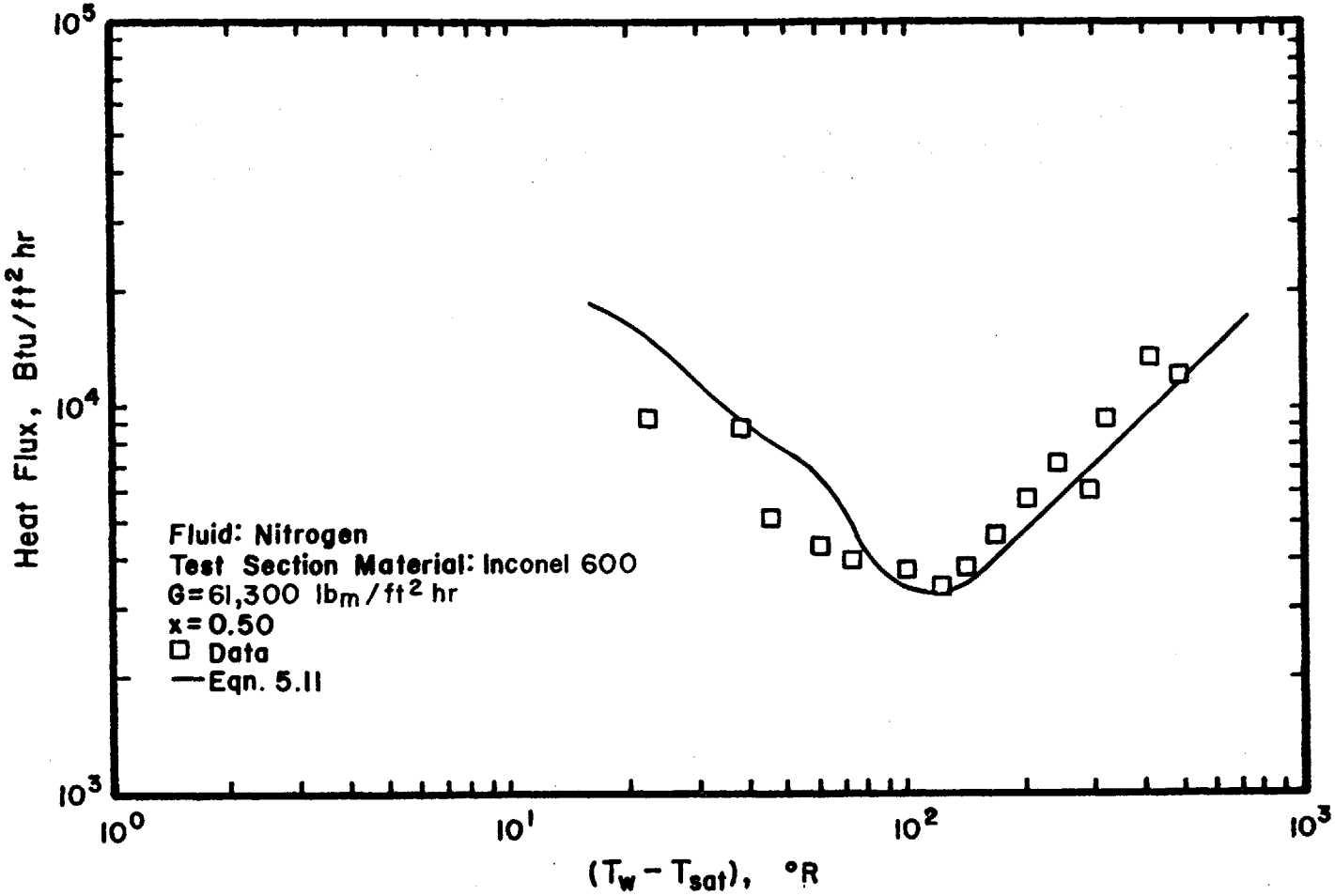

Figure 5.12 Heat Flux vs. Wall Superheat

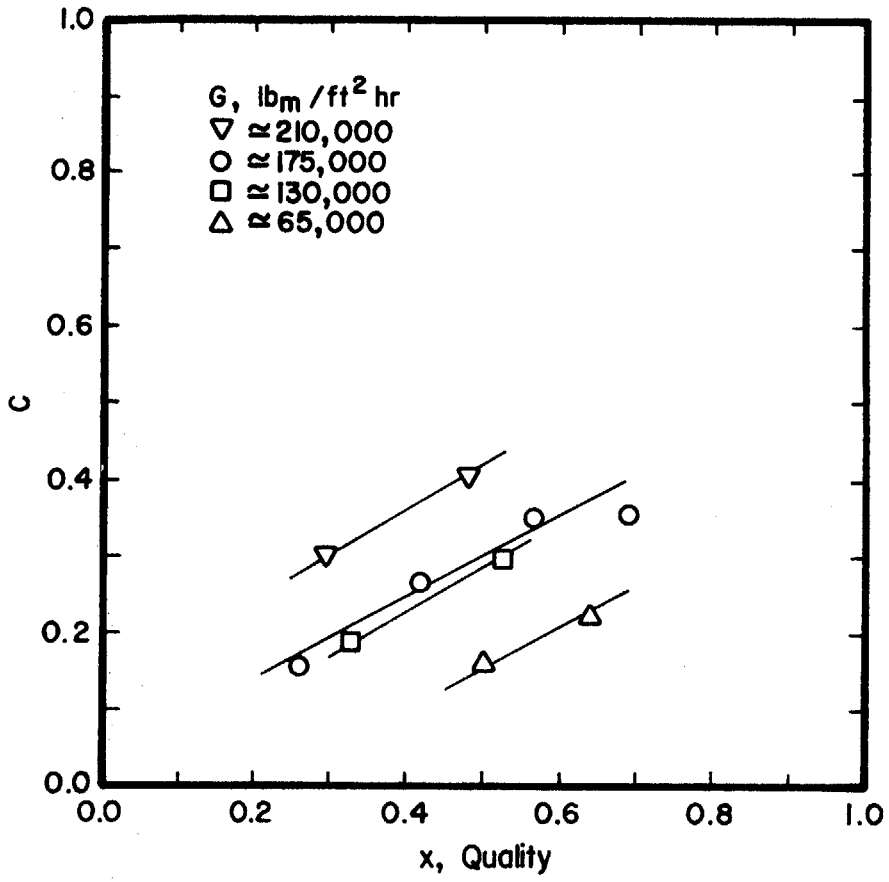

Figure 5.13 Mean Drop Diameter Correction Factor vs. Quality (Eqn. 3.5)

CHAPTER VI: SUMMARY AND CONCLUSIONS

1. The experimental and theoretical analysis of the dispersed flow heat transfer was performed in this study.
2. The obtained experimental data (Figures 5.3 - 5.12) are with small experimental error (Appendix II-1) and cover both the transition boiling and the film boiling regions.
3. The characterization of a drop size and a drop size distribution in a dispersed flow in terms of a mass flux and vapor quality was performed (Chapter III). Equations for the maximum drop diameter [Eq. (3.3)], the average drop diameter [Eq. (3.5)] and the drop size distribution [Eq. (3.7)] were utilized for the description of the structure of the dispersed flow and the analysis of drop-wall interaction.
4. The above equations for the maximum drop diameter, average drop diameter, and drop size distribution indicate that, for the higher mass fluxes and vapor qualities, the drops are smaller (Figures 3.1, 3.2, 3.3). This is in agreement with the experimental data for the drop size and the drop size distribution reported by several investigators [58,10,16].
5. The deposition of liquid drops in a dispersed flow was studied (Chapter IV). The expression for the reaction force on the drop due to non-uniform drop evaporation inside the laminar sublayer was developed [Eq. (4.31)]. This force, as well as other forces acting on the drop inside the laminar sublayer--lift, drag, gravity, buoyancy, and inertia--was analyzed and the trajectories for the drop were calculated.

6. The trajectory of the drop inside the laminar sublayer is prescribed by the magnitude of the forces mentioned above. The effects of the drop diameter, deposition velocity, slip ratio, wall temperature, and flow Reynolds number on the drop trajectory were examined.

7. The drop deposition model developed in this study (Chapter IV) explains the mechanism of drop deposition in dispersed flow including vapor-drop interaction. The model predicts:
   (a) the decrease of drop deposition rate (number of drops deposited per unit area of the wall and unit time) with increase of the wall temperature;
   (b) the increase of drop deposition rate with increase of the mass flux;
   (c) the decrease of drop deposition rate with increase of the vapor quality.

8. In the literature available, the analyzed experimental data for Q (heat transferred to liquid drop evaporating on the wall) indicated that the wall temperature has the most significant effect on Q. An expression for Q was introduced in this thesis [Eq. (5.5)]. It provided good prediction of our experimental data as discussed in Section 5.5. The effects of the drop impact velocity, drop temperature, contact angle, and surface state of heating wall (microughness, oxidation) on Q were summarized in Section 5.1.

9. Based on the analysis of the structure of dispersed flow, drop deposition and drop-wall heat transfer, the relation, Eq.(5.8), for the heat

flux to the liquid drops was developed.

10. The total heat transfer to the dispersed flow considered in this study was given as the sum of the heat transfer to liquid drops $(q/A)_d$, and heat transfer to the vapor component of the flow $(q/A)_r$, i.e. [Eq. (5.11)],

$$q/A = v_0(1 - \alpha)\rho_\ell H_{\ell g} f\, e^{1-(T_w/T_{sat})^2} + 0.023 \frac{k_g}{D} Re^{0.8} Pr^{0.4} (T_w - T_{sat})$$

since the radiation heat transfer was negligible (Table 3). The comparison of the experimental data with the prediction by the above equation was shown in Figures 5.3 - 5.12. Figures 5.3 - 5.12 show that the above equation is capable of predicting the experimental data.

11. The effect of the mass flux and vapor quality on q/A, given by the above equation, was as follows:

    (a) When the mass flux increases (constant vapor quality assumed), q/A increases and T_{min} (minimum film boiling temperature) increases.

    (b) When the vapor quality increases (constant mass flux assumed), $(q/A)_d$ decreases, $(q/A)_v$ increases, and T_{min} decreases. This affects q/A in such a way that q/A increases in the high temperature region (film boiling region) and decreases in the low temperature region (transition boiling region).

These conclusions are experimentally supported (Figures 5.3 - 5.12) within the experimental error of the data (Appendix II-1).

12. Our extensive analysis of drop trajectories indicated that the drops that entered laminar sublayer and did not penetrate it, i.e., were returned to the main stream, did not penetrate very far into the laminar sublayer (Figures 4.3-4.7a). Therefore, we concluded that there was no appreciable heat transfer from the wall to these drops. This was confirmed by the fact that the experimental data were predicted without including this component of heat transfer which was proposed in reference [32].

13. By comparing the predictions of the experimental data in Figures 5.3 - 5.12 to the predictions of the same data, but with constant value of C, in Figures V.1 - V.10, one can see that the prediction [Eq. (5.11)] is very sensitive on the value of C [Eq. (3.5)], especially in the vicinity of and below the minimum film boiling temperature. The value of C affects the value of $\bar{a}$ [mean drop diameter, Eq. (3.5)]. The drop size distribution $P(a)$ is affected by $\bar{a}$. The drop cooling rate at the wall is affected by $P(a)$.

    From the above it was concluded that the actual knowledge of the mean drop diameter in dispersed flow is of the extreme importance in predicting the heat transfer in a dispersed flow.

14. Additional work on the average drop size in dispersed flow and mechanism of the heat transfer to single drop deposited on the wall from the fluid stream will improve the work presented in this thesis.

REFERENCES

1. Bailey, G.H. et al., Dynamic Equations and Solutions for Particles Undergoing Mass Transfer, Brit. Chem. Eng., Vol. 15, No. 7, pp. 912-916 (1970).
2. Baumeister, K.J. et al., A Generalized Correlation of Vaporization Times of Drops in Film Boiling on a Flat Plate, Third International Heat Transfer Conference, AIChE, Chicago (1966).
3. Bennett, A.W. et al., Heat Transfer to Steam-Water Mixtures Flowing in Uniformly Heated Tubes in which the CHF has been Exceeded, AERE-R-5373 (1967).
4. Bird, et al., Transport Phenomena, J. Wiley and Sons, Inc., 1960.
5. Brenner, H., Hydrodynamic Resistance of Particles at Small Reynolds Numbers, Advances in Chemical Engineering, pp. 287-439 (1966).
6. Collier, J.G., Convective Boiling and Condensation, McGraw-Hill, 1972.
7. Corman, J.C., Water Cooling of a Thin, High Temperature Metal Strip, Ph.D. Thesis, Carnegie Institute of Technology (1966).
8. Cousins, L.B. and Hewitt, G.F., Liquid Phase Mass Transfer in Annular Two-Phase Flow: Droplet Deposition and Liquid Entrainment, AERE-R-5657, U.K.A.E.A., Harwell (1968).
9. Cumo, M. et al., On Two-Phase Highly Dispersed Flows, ASME Paper 73-HT-18 (1973).
10. Cumo, M. et al, Advances in Heat Transfer--A Collection of Papers, CNEN-RT/ING (72) 19, (1972).

11. Deich, M.E. and Ignat'evskaya, L.E., Characteristics of the Motion of a Drop in a Two-Phase Boundary Layer on a Flat Plate, Tepl. Vys. Tem., Vol. 9, No. 2, pp. 335-340 (1971).

12. Deich, M.E. and Filippov, G.A., Gas Dynamics of Two-Phase Media (in Russian), Energiya (1968).

13. Denson, C.D.; Christiansen, E.B.; and Salt, D.L., Particles Migration in Shear Fields, AIChE Journal, Vol. 12, No. 3, pp. 589-595 (1966).

14. Era, A. et al., Heat Transfer Data in the Liquid Deficient Region for Steam-Water Mixtures at 70 kg/cm^2 Flowing in Tubular and Annular Conditions, CISE-R-184, Milan (1966).

15. Farmer, R.; Griffith, P.; and Rohsenow, W.M., Liquid Droplet Deposition in Two-Phase Flow, ASME Paper No. 70-HT-1 (1970).

16. Ferrari, G., Private communication.

17. Forslund, R.P. and Rohsenow, W.M., Thermal Non-Equilibrium in Dispersed Flow Film Boiling in a Vertical Tube, MIT Report No. 75312-44 (1966).

18. Gangler, R.E., An Experimental Study of Spray Cooling of High Temperature Surfaces, Ph.D. Thesis, Carnegie Institute of Technology (1966).

19. Gauvin, W.H.; Katta, S.; and Knelman, F.H., Drop Trajectory Predictions and their Importance in the Design of Spray Drayers, Int. J. Multiphase Flow. Vol. 1, pp. 793-816 (1975).

20. Goldsmith, H.L. and Mason, S.G., Colloid Sci. Vol. 17, p. 458 (1962).

21. Gottfried, B.S. et al., The Leidenfrost Phenomenon: Film Boiling of Liquid Droplets on a Flat Plate, I. J. Heat Mass Transfer, Vol. 9, pp. 1167-1187 (1966).

22. Goldstein, S., Modern Developments in Fluid Dynamics, Clarendon, Oxford, pp. 83, 492, 1938.

23. Groeneveld, D.C., The Thermal Behavior of a Heated Surface at and Beyond Dryout, AECL-4309 (1972).

24. Groeneveld, D.C., Post Dryout Heat Transfer: Physical Mechanisms and a Survey of Prediction Methods, Nuclear Engineering and Design, Vol. 32, pp. 283-294 (1975).

25. Harper, E.Y. and Chang, I-Dee, Maximum Dissipation Resulting from Lift in a Slow Viscous Shear Flow, J. Fluid Mech., Vol. 33, Part 2, pp. 209-225 (1968).

26. Herkenrath, H. et al., Heat Transfer in Water with Forced Circulation in 140-250 Bar Pressure Range, EUP 3658d (1967).

27. Hinze, J.O., Fundamentals of the Hydrodynamic Mechanism of Splitting in Dispersion Processes, AIChE Journal, Vol. 1, p. 289 (1955).

28. Hidy, G.M. and Brock, J.R., The Dynamics of Aerocolloidal Systems, Pergamon Press, 1970.

29. Hottel, H.C. and Stewart, McC., Space Requirement for the Combustion of Pulvurized Coal, Industrial and Engineering Chemistry, Vol. 32, pp. 719-730 (1940).

30. Hughes, R. and Gilliland, E., Chem. Eng. Progr., Vol. 48, p. 497 (1952).

31. Hynek, S.J. et al., Forced Convection, Dispersed-Flow Film Boiling, MIT Report No. 70586-63 (1969).

32. Iloeje, O.C. et al., A Study of Wall Rewet and Heat Transfer in Dispersed Vertical Flow, MIT Report No. 72718-92 (1974).

33. Isshiki, N. Theoretical and Experimental Study on Atomization of Liquid Drop in High Speed Gas Stream, Report No. 35, Transportation Technical Research Institute, Tokyo (1959).

34. Kirillov, P.L. and Smogalev, I.P., Effect of Drop Size on Mass Transfer in a Two-Phase Flow (in Russian), Teplotiz. Vis. Temp., Vol. 11, No. 6 (1973).

35. Kohlman, D.L. and Mollo-Christensen, E., Measurement of Drag of Cylinders and Spheres in a Couette-Flow Channel, The Physics of Fluids, Vol. 8, No. 6, pp. 1013-1017 (1965).

36. Kondic, N.N., Lateral Motion of Individual Particles in Channel Flow-Effect of Diffusion and Interaction Forces, Transactions of ASME, J. Heat Transfer, pp. 419-428, September (1970).

37. Laverty, W.F. and Rohsenow, W.M., Film Boiling of Saturated Liquid Flowing Upward through a Heated Tube: High Vapor Quality Range, MIT, EPL Report No. 9857-32 (1964).

38. Lewis, J.P. et al., Boiling Heat Transfer to Liquid Hydrogen and Nitrogen in Forced Flow, NASA-TN-D-1314 (1962).

39. Liu, Y.H. and Ilori, T.W., On the Theory of Aerosol Deposition in Turbulent Pipe Flow, University of Minnesota, Minneapolis, Particle Technology Laboratory Publ. No. 210 (1973).

40. Marchaterre, J.F. and Hogland, B.W., Correlation for Two-Phase Flow, Nucleonics, p. 142, August (1962).

41. McAdams, W.H., Heat Transmission, McGraw-Hill, 1954.

42. MacVean, S.S., unpublished work, Dartmouth College, Hanover (see also ref. [68]), 1957.

43. McCormack, P.D. and Crane, L., Physical Fluid Dynamics, Academic Press, 1973.

44. McGinnis, F.K. and Holman, J.P., Individual Droplet Heat Transfer Rates for Splattering on Hot Surfaces, Int. J. Heat Mass Transfer, Vol. 12, p. 95-108 (1969).

45. Mikic, B.B., Conduction Heat Tranfser--Class Notes, MIT (1974).

46. Nishio, S. and Hirata, M., An Experimental Study of the Dynamic Behavior of a Liquid Drop Deposited Upon a Heated Surface, Technical Report and Private communication, Dept. of Mechanical Engineering, University of Tokyo (1975).

47. Parker, J.D. and Grosh, R.J., Heat Transfer to a Mist Flow, Report ANL-6291 (1961).

48. Pedersen, C.O., The Dynamics and Heat Transfer Characteristics of Water Droplets Impinging Upon a Heated Surface, Ph.D. Thesis, Carnegie Institute of Technology (1967).

49. Probert, R.P., The Influence of Particle Size and Distribution in the Combustion of Oil Droplets, Philosophical Magazine, Vol. 37, pp. 94-105 (1946).

50. Plummer, D.N. et al., Post Critical Heat Transfer to Flowing Liquid in a Vertical Tube, MIT Report No. 72718-91 (1974).

51. Repetti, R.V. and Leonard, E.F., Serge-Silberberg Annulus Formation: A Possible Explanation, Nature, Vol. 203, pp. 1346-1348 (1964).

52. Rubinow, S.I. and Keller, J.B., The Transverse Force on a Spinning Sphere Moving in a Viscous Fluid, J. Fluid Mech. Vol. 11, pp. 447-459 (1961).

53. Rouhiainen, P.O. and Stachiewicz, J.W., On the Deposition of Small Particles From Turbulent Streams, Transactions of ASME, J. of Heat Transfer, pp. 169-177, September (1970).

54. Saffman, P.G., The Lift on a Small Sphere in a Shear Flow, J. Fluid Mech., Vol. 22, Part 2, pp. 385-400 (1965).

55. Schmidt, K.R., Wärmetechnische Untersuchungen an hoch Belasteten Kesselheizflächen, Mitteilungen der Vereinigung der Grosskessel-bezitzer, pp. 391-401 (1959).

56. Shapiro, A.H. and Erickson, A.J., On the Changing Size Spectrum of Particle Clouds Undergoing Evaporation, Combustion, or Acceleration, Trans. ASME, Vol. 79, p. 775 (1957).

57. Shapiro, A.H. et al., The Aerothermopressor--A Device for Improving the Performance of a Gas-Turbine Power Plant, ASME Paper No. 55-SA-65 (1955).

58. Snyder, G.A., Determination of the Drop Size Distribution in Two-Phase, Boiling Flow, B.Sc. Thesis, MIT (1959).

59. Soo, S.L., Fluid Dynamics of Multiphase Systems, Blaisdell Pub. Co., 1967.

60. Sun, K.H. et al., Calculations of Combined Radiation and Convection Heat Transfer in Rod Bundles Under Emergency Cooling Conditions, ASME Paper 75-HT-64 (1975).

61. Swanson, W.M., The Magnus Effect: A Summary of Investigations to Date, Transactions of the ASME, J. Basic Engineering, pp. 461-470, September (1961).

62. Swenson, H.S. et al., The Effects of Nucleate Boiling versus Film Boiling on Heat Transfer in Power Boiler Tubes, ASME Paper 61-W-201 (1961).

63. Toda, S., A Study of Mist Cooling, Heat Transfer, Japanese Research, Vol. 1, No. 3, p. 39 (1972).

64. Tong, L.S. and Young, J.D., A Phenomenological Transition and Film Boiling Heat Transfer Correlation, Proceedings of the Fifth International Heat Transfer Conference, Tokyo, IV, pp. 120-124 (1974).

65. Tong, L.S., Boiling Heat Transfer and Two-Phase Flow, John Wiley and Sons, 1965.

66. Von Glahn, U.H. and Lewis, J.P., Nucleate and Film Boiling Studies with Liquid Hydrogen, Advances in Cryogenic Engineering, edited by K.D. Timmerhaus, Vol. 5, pp. 262-269, Plenum Press, N.Y., 1960.

67. Wachters, L.H.J. and Westerling, N.A.J., The Heat Transfer from a Hot Wall to Impinging Water Drops in the Spheroidal State, Chem. Eng. Sci., Vol. 21, p. 1047-1056 (1966).

68. Wallis, G.B., One-Dimensional Two-Phase Flow, McGraw-Hill, 1969.

69. Walters, H.H., Single Tube Heat Transfer Tests with Liquid Hydrogen, Advances in Cryogenic Engineering, edited by K.D. Timmerhaus, Vol. 6, pp. 509-516, Plenum Press, N.Y., 1961.

70. Waldmann, L. and Schmitt, K.H., Thermophoresis and Diffusiophoresis of Aerosols, Ch. 6, Aerosol Science, Ed. by C.N. Davies, Academic Press, 1966.

APPENDIX: II-1

II.1 Calculation of the Maximum Experimental Errors in (q/A) due to the Axial Conduction in the Transient Test Section

A detailed drawing of the transient test section design is given on Figure II-2. This design is a modification of an earlier design (Figure 6 of ref. [1]†) which was tested and found to have certain deficiencies concerning extraneous heat additions. It has been verified experimentally that the design in Fig. II-2 still has some problems with heat losses or gains. Appendix A, ref. [1], gives a total estimation of the heat losses or gains of the transient test section. The maximum errors in (q/A) due to the axial conduction losses for the data shown in Figures 5.3 - 5.12 are presented in Table 4. These errors are in the vicinity of the minimum film boiling temperature, T_{min} . For example, the error in heat flux for data on Figure 5-3, Table 4, is 18% for $T = T_{min}$ but for $T = T_{min} + 30°R$ and $T = T_{min} - 30°R$ the errors are $1 \times 10^{-2}\%$ and 5.0%, respectively.

The effect of the axial conduction on the experimentally obtained boiling curve is summarized in Figure II-1. More about the axial conduction effect on the minimum slope point of $T(t)$ curve, Eq. (2.1), [or (q/A) vs. wall superheat curve] can be found in references [1] and [2].

---

†Numbers in parentheses refer to references, found at the end of Appendix.

TABLE 4: Maximum Experimental Errors in (q/A) due to the Axial Conduction

Data in Figure #	ε (%)
5.3	18.0
5.4	2.70
5.5	2.29
5.6	3.30
5.7	12.6
5.8	1.0×10^{-3}
5.9	1.0×10^{-3}
5.10	1.0×10^{-3}
5.11	1.0×10^{-3}
5.12	1.0×10^{-3}

ε = maximum estimated error due to the axial conduction during quench interval

$$\varepsilon \equiv \frac{q'}{M\, C_p \frac{dT}{dt}}\ 100$$

q' = $0.063(T_{PBB} - T)$, heat gains in Btu/hr (Eq. (A.15), ref. [1]),

M = mass of the transient test section,

C_p = specific heat of the transient test section,

T = temperature of the transient test section,

t = time,

T_{PBB} = "preheater brass base" temperature (see Figure II-2).

NOTE: T and T_{PBB} are recorded during quench period.

II.2 Determination of System Variables and Experimental Errors

The important system variables calculated in the experimental program are mass flux, equilibrium quality to the transient section, and the saturation temperature of liquid nitrogen at the transient section [1]. The uncertainties in these are related to the independent quantities which go into their evaluation. The equation used in the determination of the quantities described above and the errors for each are presented in Appendix B, reference [1].

REFERENCES

1. Plummer, D.N. et al, Post Critical Heat Transfer to Flowing Liquid in a Vertical Tube, MIT Report 72178-91, (1974).
2. Iloeje, O.C. et al, A Study of Wall Rewet and Heat Transfer in Dispersed Vertical Flow, MIT Report 72718-92 (1974).

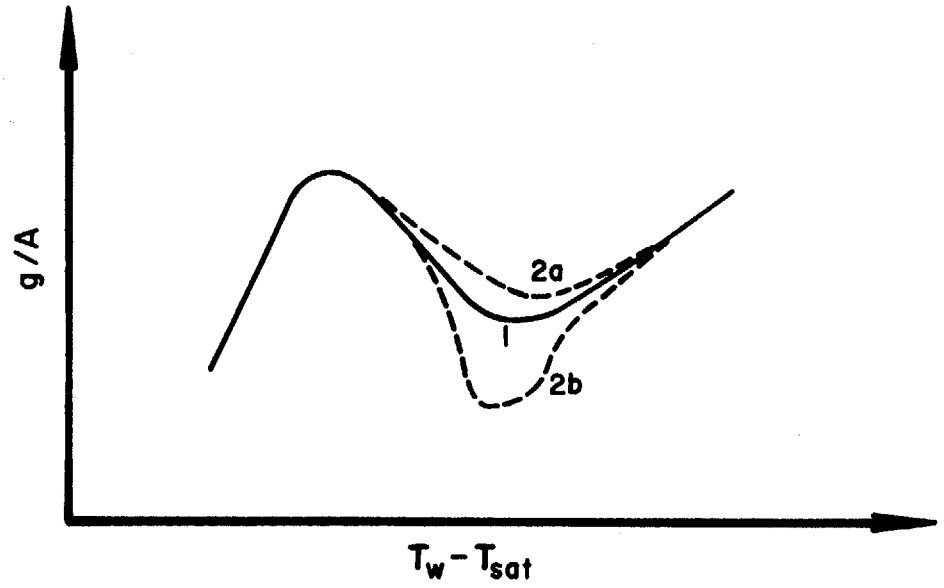

Figure II-1 The Effect of the Axial Conductance on the Experimentally Obtained Boiling Curve

1. Boiling Curve Without Heat Conduction
2. Boiling Curve With Heat Conduction
   a. Conduction Heat Transfer from the Transient Test Section to Preheater (Heat Losses)
   b. Conduction Heat Transfer from the Preheater to the Transient Test Section (Heat Gains)

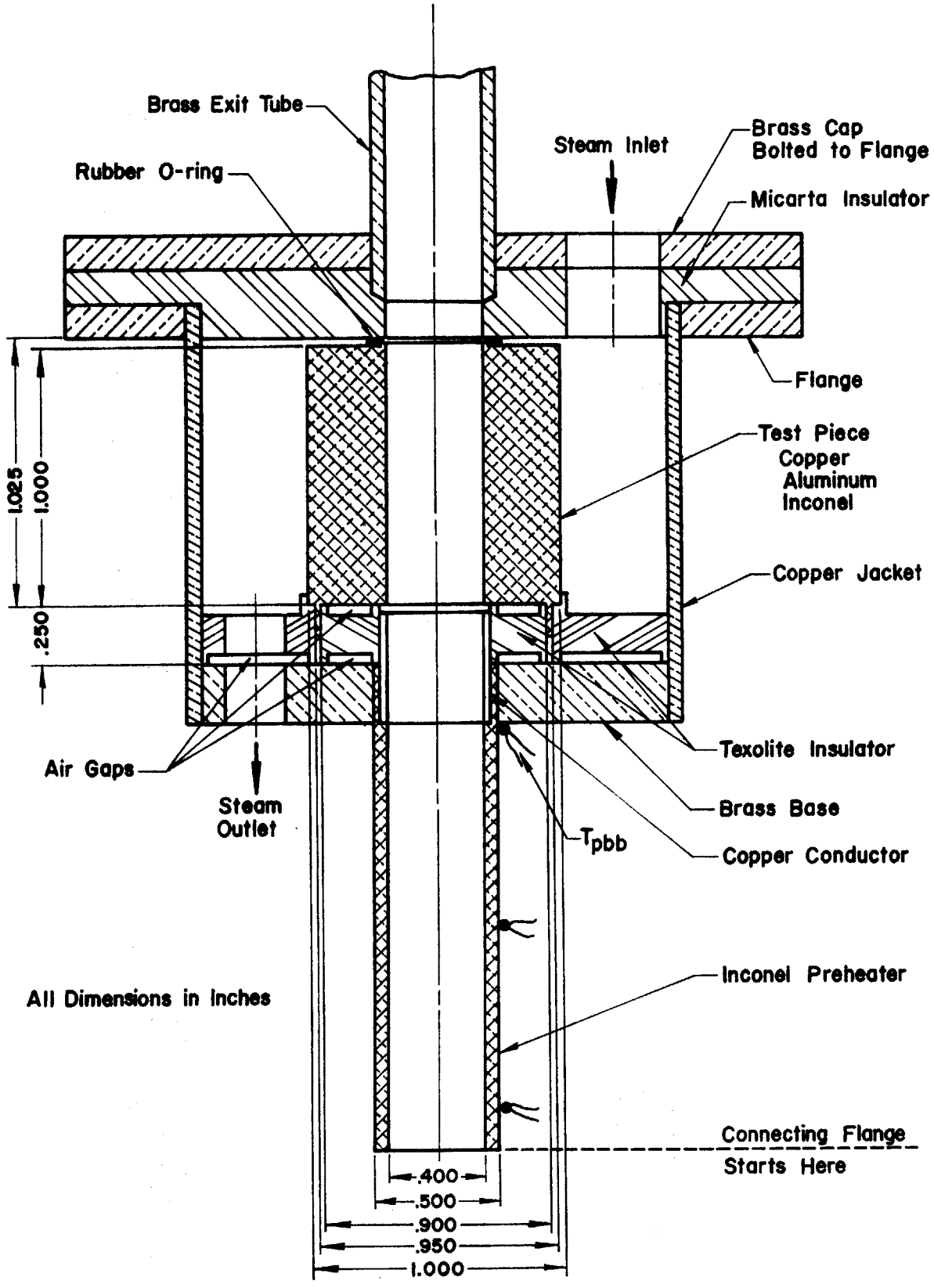

Figure II-2 Test Block Design

APPENDIX III-1:

SNYDER'S DATA ANALYSIS

For mass velocity $G = 4 \times 10^{-4}$ lb/sec, tube diameter $D = 0.18$ inches and quality $x = 0.7$ the experimental value for the most probable drop diameter was $a_{mp} = 42.2\mu m$(see Figure 1, page 9 of Snyder's thesis, ref. [1]†). Applying Eq. (3.6) the mean drop diameter $\bar{a}$ is then

$$\bar{a} = 2a_{mp} = 84.4\ \mu m$$

A calculated value for $\bar{a}$, from Eq. (3.4) for the above conditions, was $\bar{a} = 336\mu m$. The correction factor C, Eq. (3.5), is then

$$C = \frac{84.4}{336} = 0.3984$$

i.e., the theoretical value for $\bar{a}$ is almost four times larger than the experimental value.

REFERENCES

1. Snyder, G.A., Determination of Drop Size, Distribution in Two-Phase Boiling Flow, B.Sc. Thesis, MIT, 1959.

---

†Refers to reference at the end of this Appendix.

APPENDIX III-2

Note that for a given G and x,

$$V_g = \frac{G\,x}{\rho_g \alpha} \tag{III-2.1}$$

and

$$V_g = \frac{G(1 - x)}{\rho_\ell (1 - \alpha)} \tag{III-2.2}$$

where

$$\alpha = \frac{x}{x + \frac{\rho_g}{\rho_\ell}\, s(1 - x)} \tag{III-2.3}$$

The slip ratio S is given in Refs. [1,2] for a specified G and x. Fluid properties are evaluated at the saturation temperature.

REFERENCES

1. Plummer, D.N. et al., Post Critical Heat Transfer to Flowing Liquid in a Vertical Tube, MIT Report No. 72718-91 (1974).
2. Hynek, S.J. et al., Forced Convection Dispersed Flow Film Boiling, MIT Report No. 70586-63 (1969).

APPENDIX: IV-1

SOLUTION OF DIFFERENTIAL EQUATIONS (4.39a,b)

By introducing the following substitutions:

$$U = U_0 \frac{y}{\delta} \quad ; \quad A \equiv \frac{3}{8} \frac{\rho_g}{\rho_\ell} \frac{U_0}{\delta} \quad ; \quad B \equiv \frac{18\mu_g}{\rho_\ell a^2} \quad ; \quad C \equiv B \frac{U_0}{\delta} \quad ;$$

$$D \equiv \frac{(\rho_\ell - \rho_g)g}{\rho_\ell} \quad ; \quad E \equiv 3 \frac{h^2(T_w - T_s)^2}{H_{\ell g}^2 \rho_\ell \rho_g a^2} \quad ; \quad F \equiv (AU_0 - E) \frac{1}{\delta} \quad ;$$

$$\frac{dx}{dt} = x' \quad ; \quad \frac{d^2x}{dt^2} = x'' \quad ; \quad \frac{dy}{dt} = y' \quad ; \text{ and } \quad \frac{d^2y}{dy^2} = y''$$

the system of equations (4.39a,b) becomes:

$$x'' = Ay' - Bx' + Cy - D \qquad \text{(IV-1.1)}$$

$$y'' = -Ax' - By' + Fy + E \qquad \text{(IV-1.2)}$$

As explained in section 4.3 the following initial boundary conditions are used:

$$x(t=0) = 0 \qquad \text{(IV-1.3)}$$

$$y(t=0) = \delta \qquad \text{(IV-1.4)}$$

$$x'(t=0) = u_0 \qquad \text{(IV-1.5)}$$

$$y'(t=0) = v_0 \qquad \text{(IV-1.6)}$$

From Eq. (IV-1.2) by differentiation:

$$y''' = -Ax'' - By'' + Fy' \qquad \text{(IV-1.7)}$$

Also, from Eq. (IV-1.2),

$$x' = -\frac{1}{A}y'' - \frac{B}{A}y' + \frac{F}{A}y + \frac{E}{A} \qquad \text{(IV-1.8)}$$

From Eqs. (IV-1.1) and (IV-1.8),

$$x'' = \frac{B}{A}y'' + \left(\frac{B^2}{A} + A\right)y' + \left(C - \frac{FB}{A}\right)y - \left(\frac{BE}{A} + D\right) \qquad \text{(IV-1.9)}$$

From Eqs. (IV-1.7) and (IV-1.9),

$$y''' + 2By'' + (B^2 + A^2 - F)y' + (CA - FB)y - (BE + DA) = 0 \qquad \text{(IV-1.10)}$$

The solution of the last equation is

$$y = c_1e^{r_1t} + c_2e^{r_2t} + c_3e^{r_3t} + (BE + DA)/(CA - FB) \qquad \text{(IV-1.11)}$$

where r_1, r_2, r_3 are roots of the characteristic polynomial which corresponds to Eq. (IV-1.10) and c_1, c_2, c_3 are constants.

From Eq. (IV-1.11),

$$y' = c_1r_1e^{r_1t} + c_2r_2e^{r_2t} + c_3r_3e^{r_3t} \qquad \text{(IV-1.12)}$$

$$y'' = c_1r_1^2e^{r_1t} + c_2r_2^2e^{r_2t} + c_3r_3^2e^{r_3t} \qquad \text{(IV-1.13)}$$

From Eqs. (IV-1.8), (IV-1.12), and (IV-1.13),

$$x' = \frac{c_1}{A}(F - Br_1 - r_1^2)e^{r_1 t} + \frac{c_2}{A}(F - Br_2 - r_2^2)e^{r_2 t} + \frac{c_3}{A}(F - r_3 - r_3^2)e^{r_3 t} + \frac{F}{A}\left(\frac{BE + DA}{CA - FB}\right) + \frac{E}{A} \tag{IV-1.14}$$

From Eq. (IV-1.14),

$$x = \frac{c_1}{r_1 A}(F - Br_1 - r_1^2)e^{r_1 t} + \frac{c_2}{r_2 A}(F - Br_2 - r_2^2)e^{r_2 t} + \frac{c_3}{r_3 A}(F - r_3 - r_3^2)e^{r_3 t} + \left[\frac{F}{A}\left(\frac{BE + DA}{CA - FB}\right) + \frac{E}{A}\right]t + c_4 \tag{IV-1.15}$$

Note that

x = axial position of drop [Eq. (IV-1.15)];

y = radial position of drop [Eq. (IV-1.11)];

x' = drop velocity in x direction [Eq. (IV-1.14)];

y' = drop velocity in y direction [Eq. (IV-1.12)].

Four numerical constants, c_1 , c_2 , c_3 and c_4 are now determined by the method of determinants using initial boundary conditions given by Eqs. (IV-1.3)-(IV-1.6) (Appendix V-4).

APPENDIX: IV-2

As v_1 and v_2 are given by Eqs. (4.26) and (4.27), then Eq. (4.30) can be written in the following form:

$$F_{cy} = \frac{A}{4} \rho_g \left(v_2^2 - v_1^2 \right) \qquad \text{(IV-2.1)}$$

By substituting Eqs. (4.28) and (4.29) into the above equation, we have

$$F_{cy} = \frac{\pi a^2 h^2}{4 H_{\ell g}^2 \rho_g} (T_w - T_s)^2 \frac{a}{\delta} \left(1 - \frac{y}{\delta} \right)$$

APPENDIX: IV-3

Rubinow-Keller's force is given by Eq. (4.7). Saffman's force is given by the sum of Eqs. (4.15) and (4.15a). The ratio of Saffman to Rubinow-Keller force, RF , is calculated for different drop size at certain values of flow parameters, Tables 5 and 6.

TABLE 5. Values of RF at G = 60,000 lb/ft^{2}hr, x = 0.50

a [microns]	RF
1	19.4
5	4.68
10	2.84
100	1.184
1000	1.0184

TABLE 6. Values of RF at G = 210,000 lb/ft^{2}hr, x = 0.50

a [microns]	RF
1	8.3
5	2.46
10	1.73
100	1.073
1000	1.0073

Note that the forces become numerically the same for the larger drops (a > 10μm).

APPENDIX: IV-4

In order to estimate the pressure increase in the vapor layer between the drop and heated wall (see figure VI-1 on the next page) the following approximate relation has been used:

$$P_A - P_0 \simeq \rho_g \, v_{A'}^2$$

where P_0 is ambient (system) pressure and P_A local pressure below the drop (point A, Figure IV-1) and $v_{A'}$ is the vapor velocity generated at the lower portion of the sphere given as

$$v_{A'} = \frac{k_g}{y} \frac{(T_w - T_s)}{H_{fg} \rho_g}$$

where y = current distance from the wall (Figure IV-1).

Figure IV-1 shows that the pressure below the drop increases when the drop is approaching the wall. Calculation was terminated at $y = 5\mu m$, i.e., the wall roughness of 5μm was assumed.† The change of the saturation temperature T_s and the latent heat of evaporation $H_{\ell g}$ due to the pressure increase for the performed calculation was negligible.

---

†In the process of generating drop trajectories inside the boundary layer (Section 4.4 explains this process), if the distance of the drop from the wall was less than or equal to 5 μm we assumed that the drop was deposited on the wall.

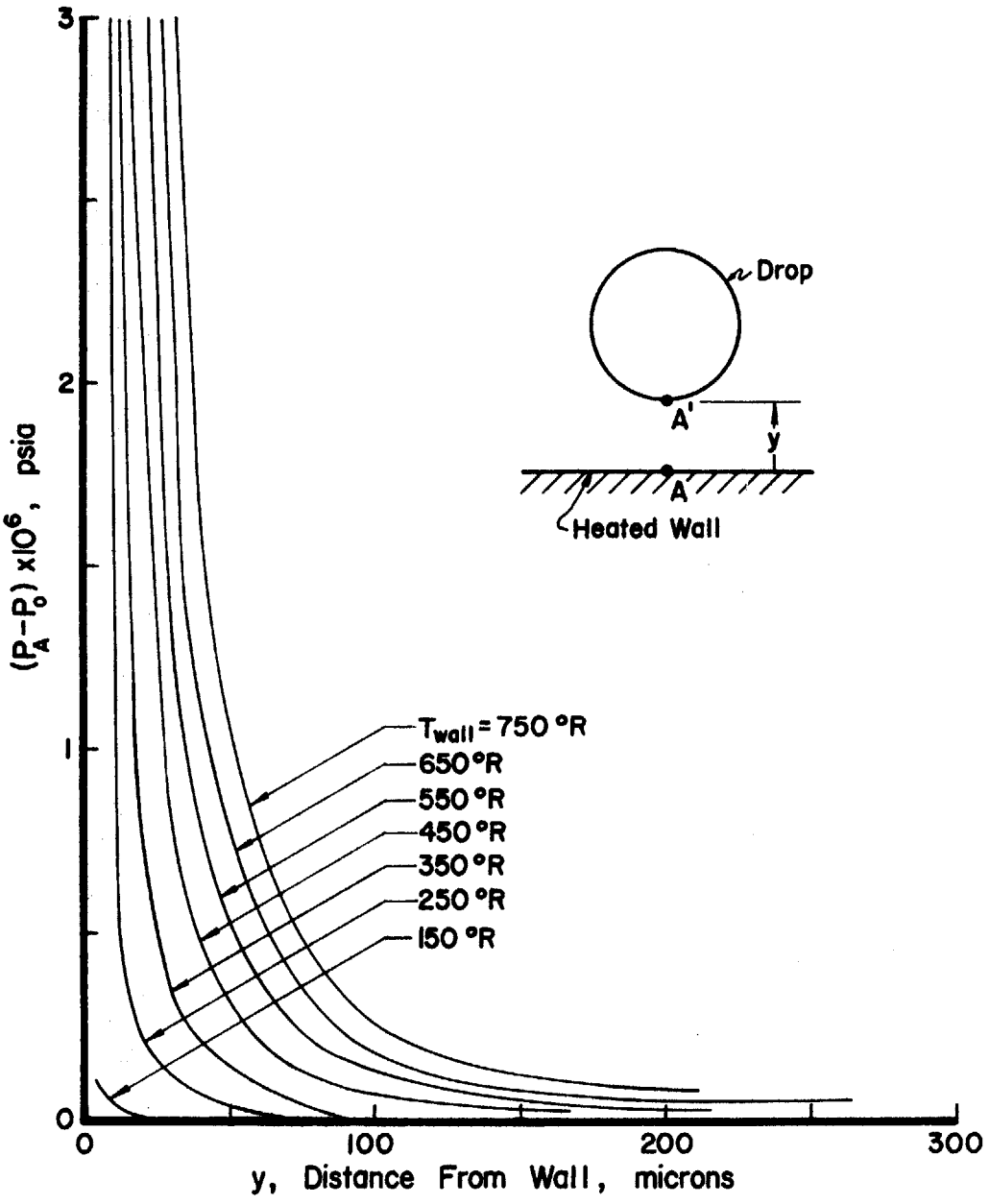

Figure IV-I The Pressure Increase Below a Drop Approaching a Heated Wall

APPENDIX: IV-5

The amount (mass) of vapor generated during deposition motion of the evaporating drop is approximately given by the following relation:

$$\sum m = \frac{\pi}{H_{\ell g}} \int_0^{t_0} a^2 h (T_v - T_s)\, dt \qquad \text{(IV-5.1)}$$

where a = drop diameter

h = heat transfer coefficient [Eq. (4.18)]

T_v = current vapor temperature

and t_0 = deposition time.

For a nitrogen drop of $a = 100\mu$ and $T_w = 640°R$ (note that $T_v = T_w$ at $t = t_0$) and $T_s = 140°R$ and $t_0 = 100$ ms (very conservative value),

$$\sum m = 2.33 \times 10^{-12} \text{ lb}$$

Since the mass of a drop with $a = 100\mu$ is $m = 1.0 \times 10^{-9}$ lb., then $\sum m/m \cdot 100 = 0.233\%$, which is very small.

APPENDIX: V-1

The mass flux of liquid drops migrating toward the wall, entering the laminar sublayer, is by definition

$$M = v_0(1 - \alpha)\rho_\ell \qquad [\text{lbm/ft}^2\text{hr}] \tag{V-1.1}$$

The drop deposition flux related to M is then

$$N = \frac{v_0(1 - \alpha)\,\rho_\ell}{\frac{\pi}{6}\rho_\ell \int_0^{a_m} a^3\, P(a)\, da} \tag{V-1.2}$$

where $$[N] = \left[\frac{\text{\# of drops of size } a\text{ , } 0 < a < a_m}{\text{ft}^2 \cdot \text{hr}}\right]$$

For a certain value of the wall temperature only drops having diameter $a > a_c$ (a_c is the deposition diameter, Chapter IV) will be deposited on the wall. The heat flux from the wall to the deposited drop is

$$(q/A)_d = N \int_{a_c}^{a_m} Q\, P(a)\, da \tag{V-1.3}$$

where Q = heat transferred per drop of any size, Eq. (5.5),

$P(a)$ = drop size distribution,

and a_m = maximum drop diameter, Eq. (3.3).

Substituting the values for Q and N [Eq. (V-1.2)]into Eq. (V-1.3),

$$(q/A) = v_0(1 - \alpha)\rho_\ell H_{\ell g}\, e^{1-(T_w/T_{sat})^2}\, \frac{\int_{a_c}^{a_m} a^3\, P(a)\, da}{\int_0^{a_m} a^3\, P(a)\, da} \qquad (V\text{-}1.4)$$

Since [Eq. (4.46)]

$$f \equiv \frac{\int_{a_c}^{a_m} a^3\, P(a)\, da}{\int_0^{a_m} a^3\, P(a)\, da} \qquad (V\text{-}1.5)$$

Eq. (5.8) and Eq. (V-1.4) are the same. Substituting the value for $P(a)$ [Eq. (3.7)] into Eq. (V-1.5) and performing the integration,

$$f = \left\{\left[\left(\frac{a_c}{\bar{a}}\right)^3 + \frac{3}{4}\left(\frac{a_c}{\bar{a}}\right)\right] \exp\left[-2\left(\frac{a_c}{\bar{a}}\right)^2\right] - \left[\left(\frac{a_m}{\bar{a}}\right)^3 + \frac{3}{4}\left(\frac{a_m}{\bar{a}}\right)\right] \exp\left[-2\left(\frac{a_m}{\bar{a}}\right)^2\right] + \right.$$

$$\left. + \frac{6}{16}\sqrt{\pi/2}\left[\operatorname{erf}\left(\sqrt{2}\,\frac{a_m}{\bar{a}}\right) - \operatorname{erf}\left(\sqrt{2}\,\frac{a_c}{\bar{a}}\right)\right]\right\}\left\{\frac{6}{16}\sqrt{\pi/2}\operatorname{erf}\left(\sqrt{2}\,\frac{a_m}{\bar{a}}\right) - \right.$$

$$\left. - \left[\left(\frac{a_m}{\bar{a}}\right)^3 + \frac{3}{4}\left(\frac{a_m}{\bar{a}}\right)\right] \exp\left[-2\left(\frac{a_m}{\bar{a}}\right)^2\right]\right\}^{-1} \qquad (V\text{-}1.6)$$

The values of a_m and $\bar{a}$ were given by Eqs. (3.3) and (3.5), respectively. The value of a_c was calculated for the particular value of the wall temperature as explained in Chapter IV.

APPENDIX: V-2

Void fraction α can be defined as the ratio of the gas (vapor) flow area to the total flow area. If a homogeneous void distribution is assumed, then α is the ratio of gas phase area to any area inside the flow. In Chapter IV we concluded that not all drops entering the boundary layer penetrate it so the surface void fraction α_s is generally less than α as defined above. Having this in mind we may write the following relation between the homogeneous and surface void fraction,

$$1 - \alpha_s = (1 - \alpha)f \qquad \text{(V-2.1)}$$

where f is now the surface cumulative factor given by Eq. (4.46) for $n = 2$. From Eq. (V-2.1),

$$\alpha_s = 1 - f(1 - \alpha) \qquad \text{(V-2.2)}$$

In fully-developed dispersed flow the minimum value for α is about 0.8. For the relatively low wall superheat ($T_w \simeq T_{min}$), f is a few tenths of one, so for all practical purposes, $\alpha_s = 1$.

APPENDIX: V-3

The value of $C = 0.26$ is used to predict the data in Figure V-1 to V-10. The prediction in Figures V-2, V-4, V-10 is not good.

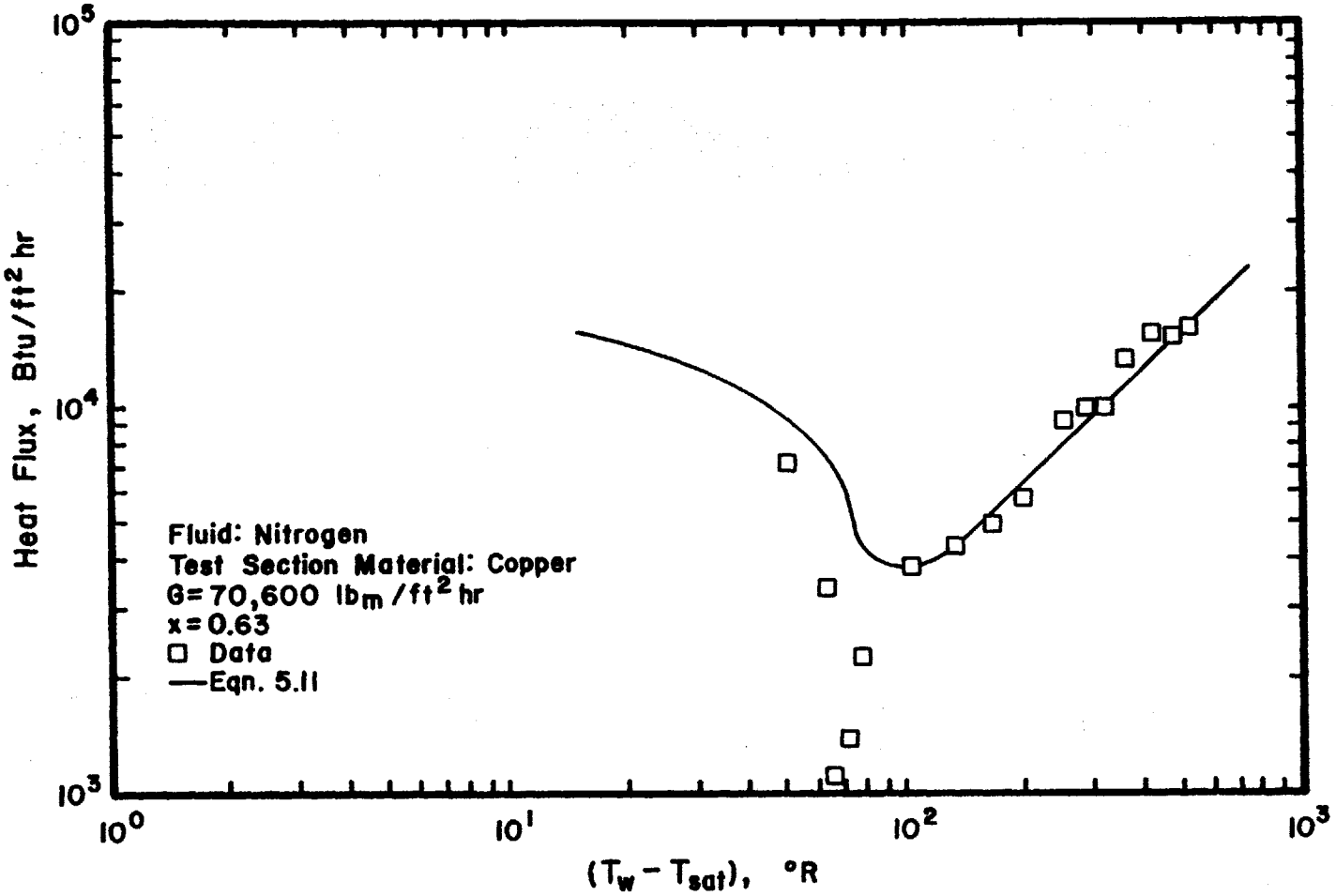

Figure V-1 Heat Flux vs. Wall Superheat

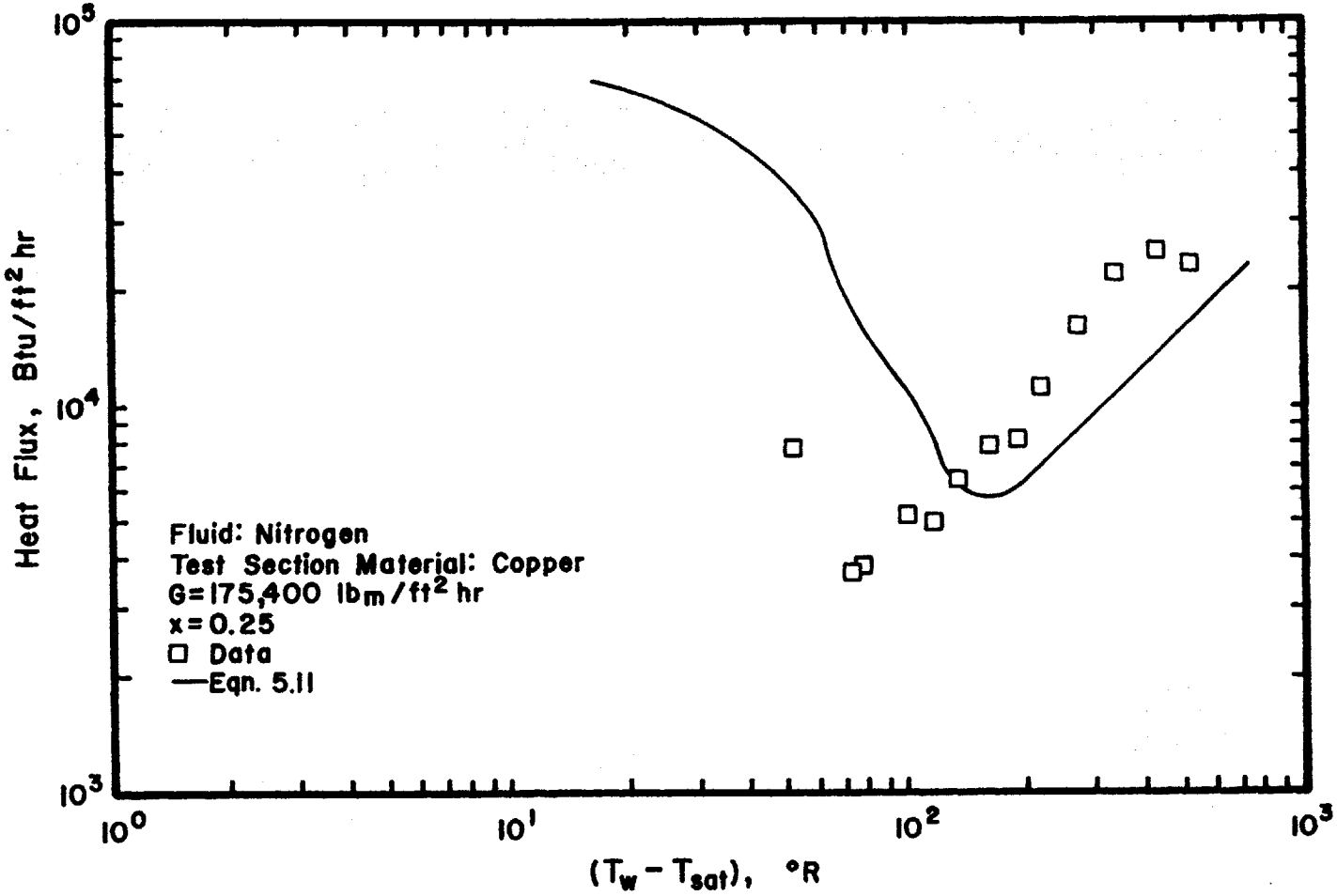

Figure V-2 Heat Flux vs. Wall Superheat

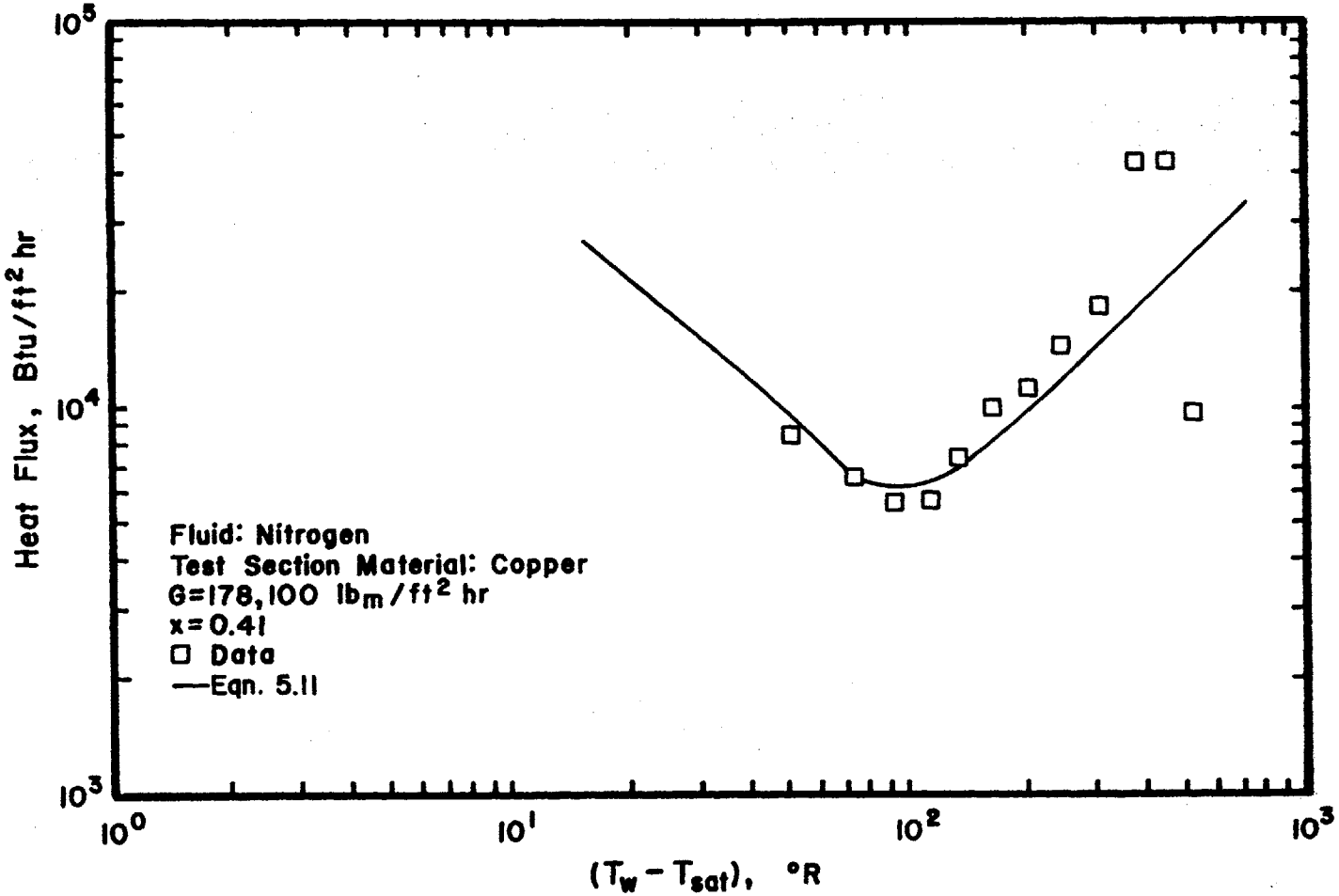

Figure V-3 Heat Flux vs. Wall Superheat

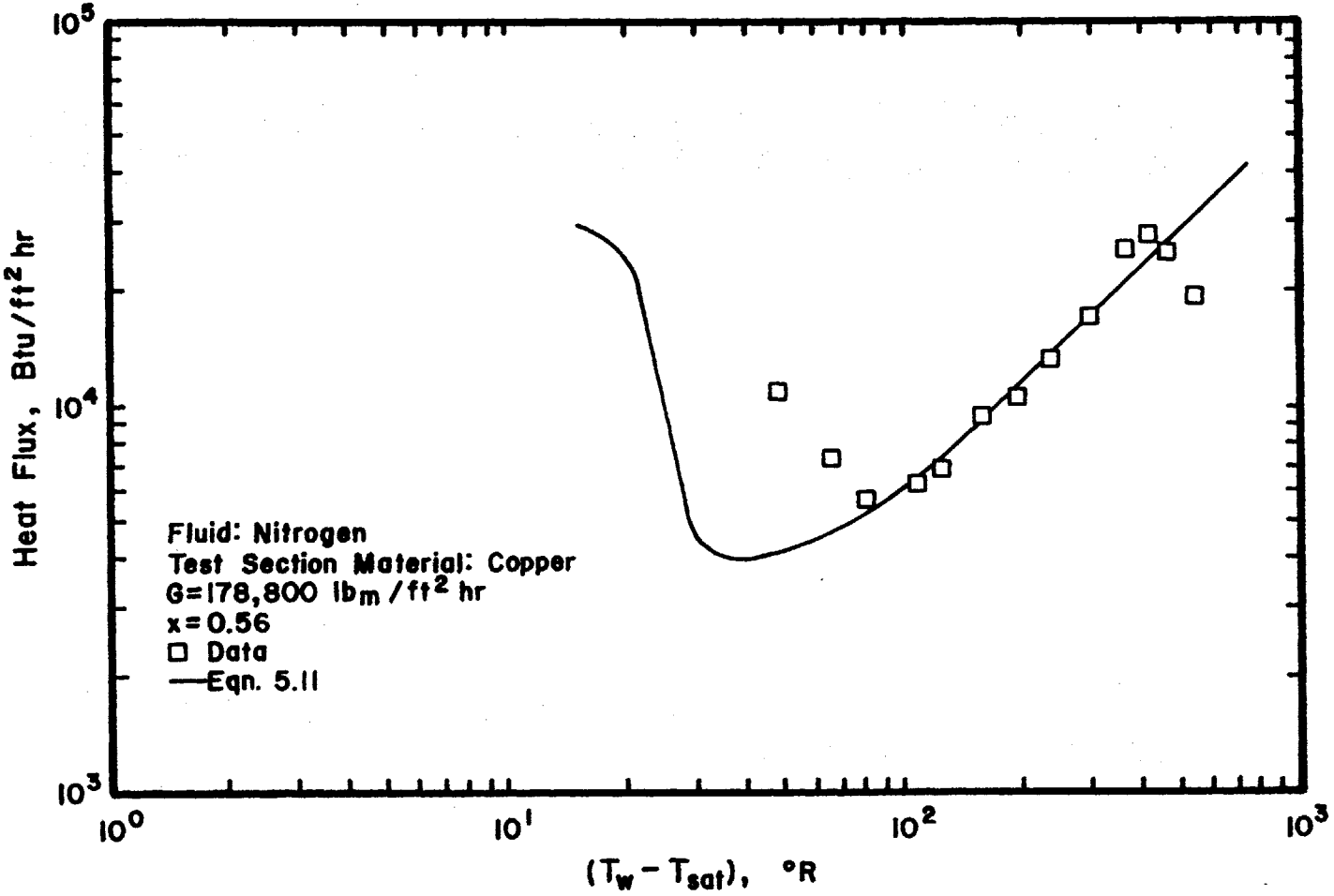

Figure V-4 Heat Flux vs. Wall Superheat

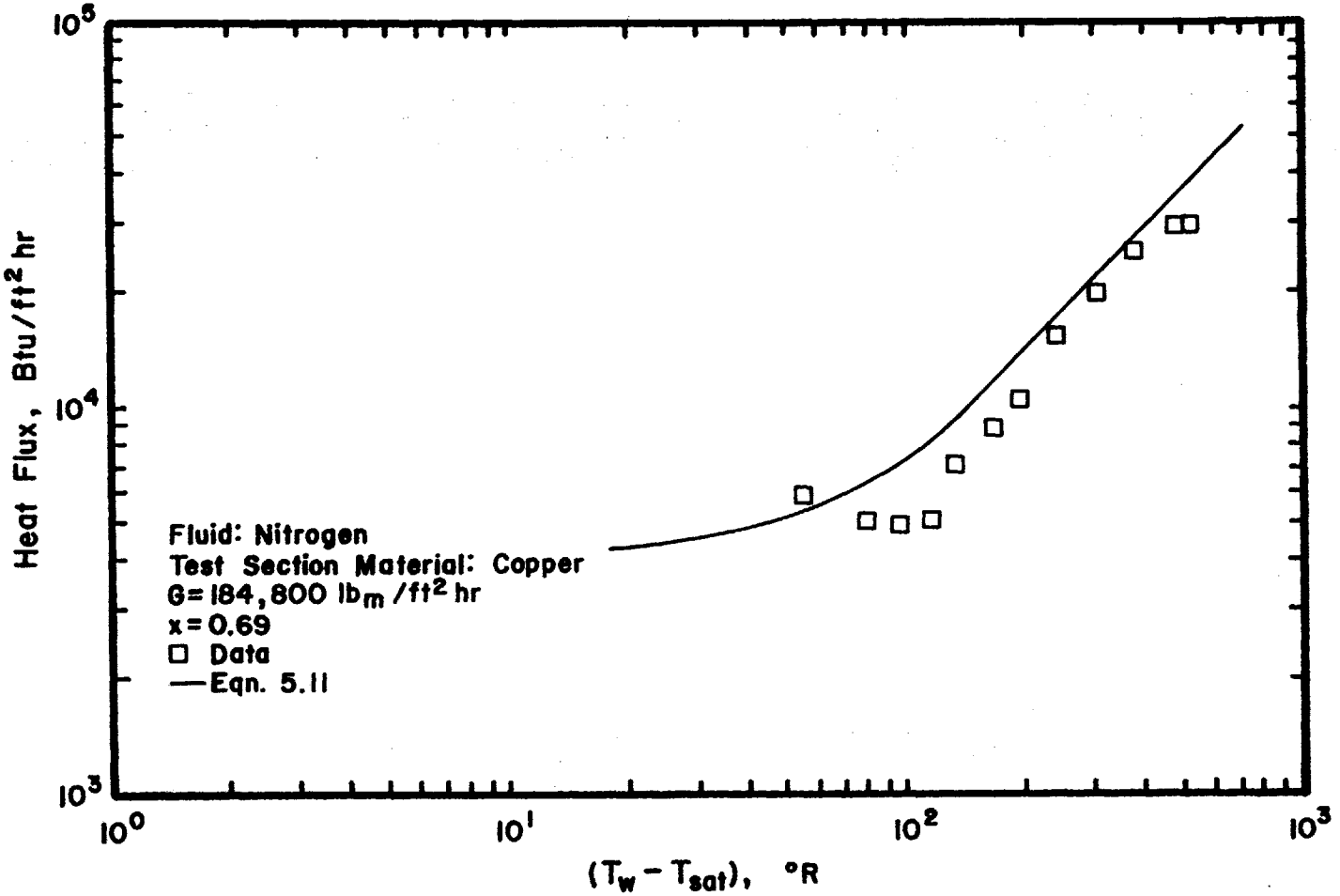

Figure V-5 Heat Flux vs. Wall Superheat

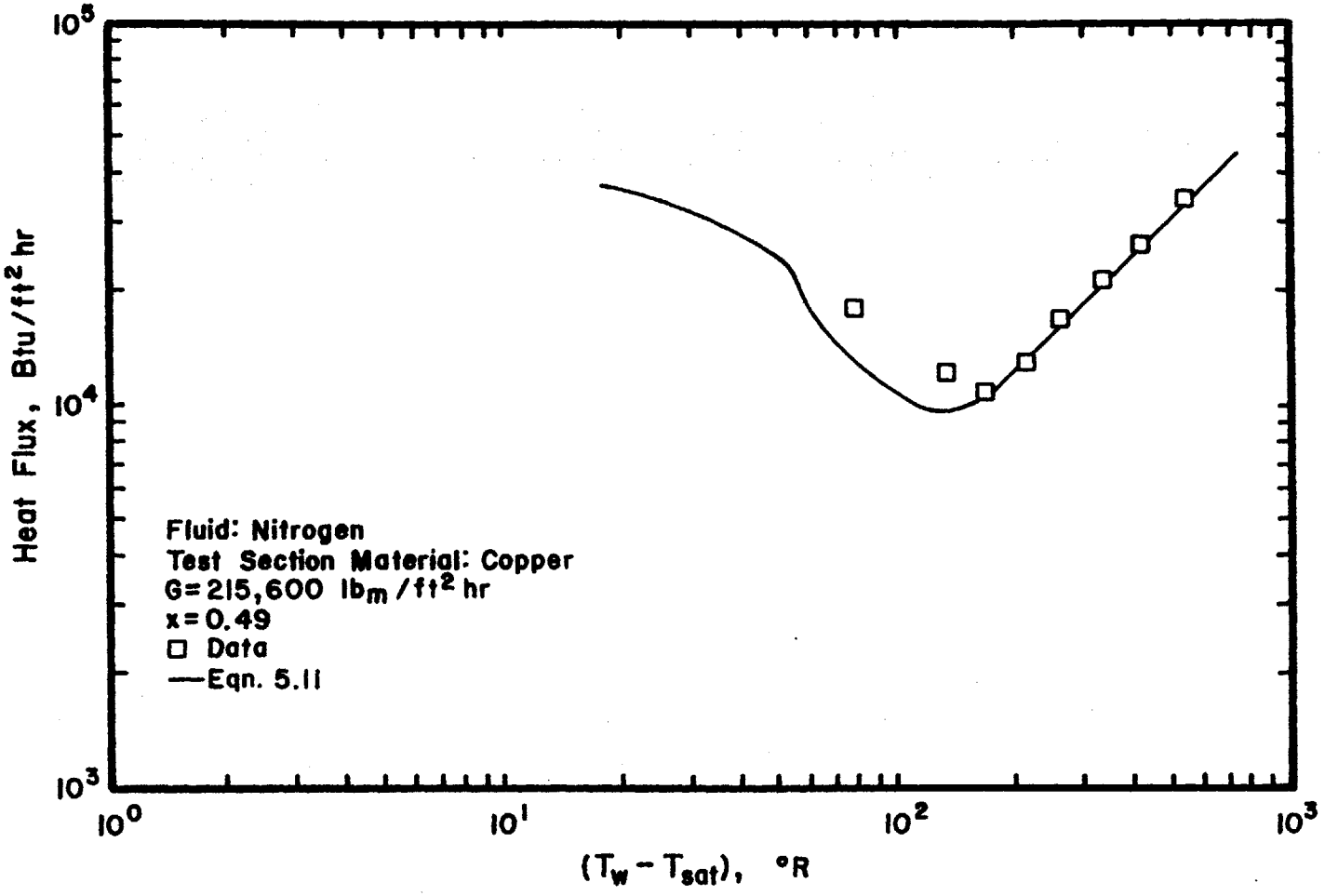

Figure V-6 Heat Flux vs. Wall Superheat

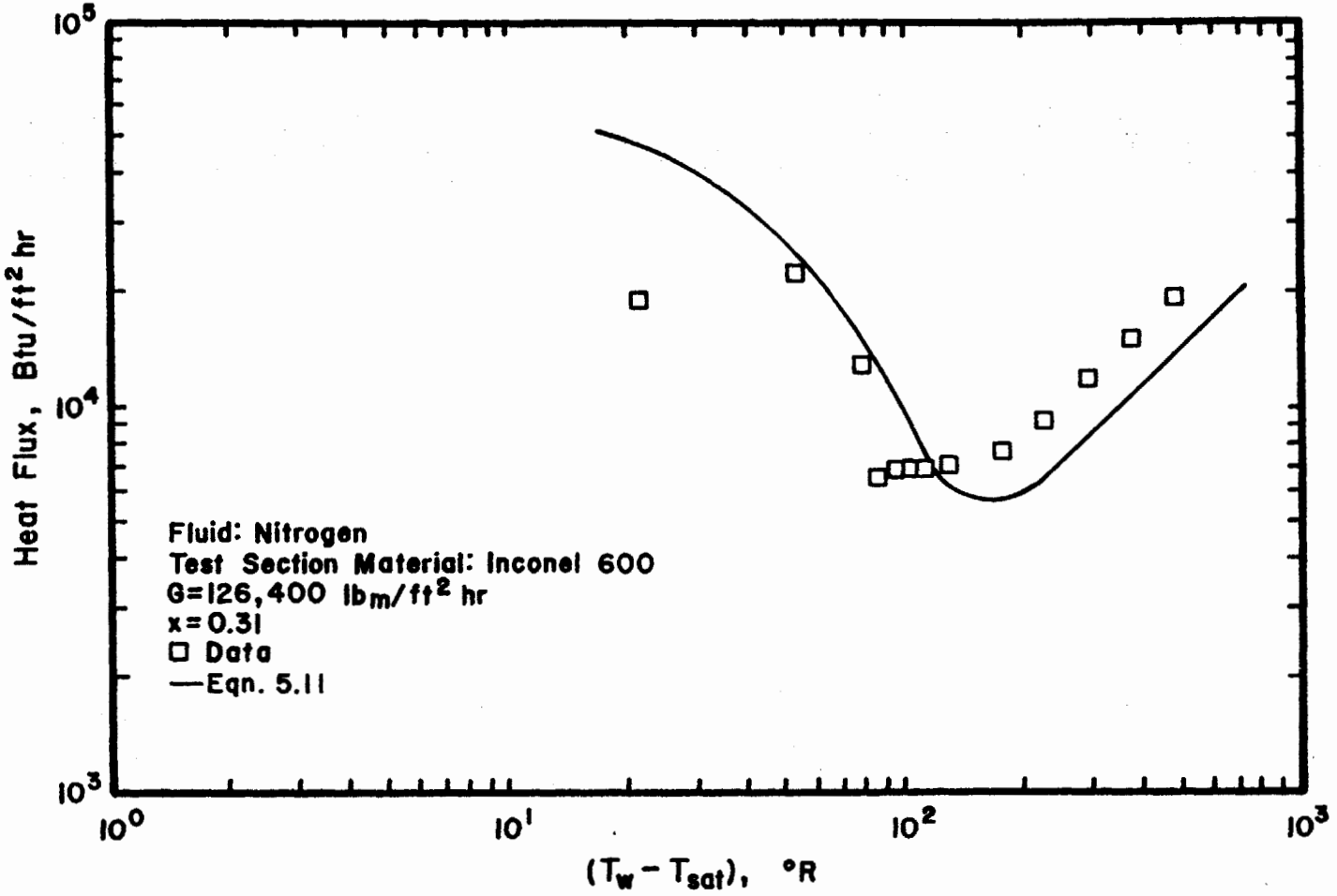

Figure V-7 Heat Flux vs. Wall Superheat

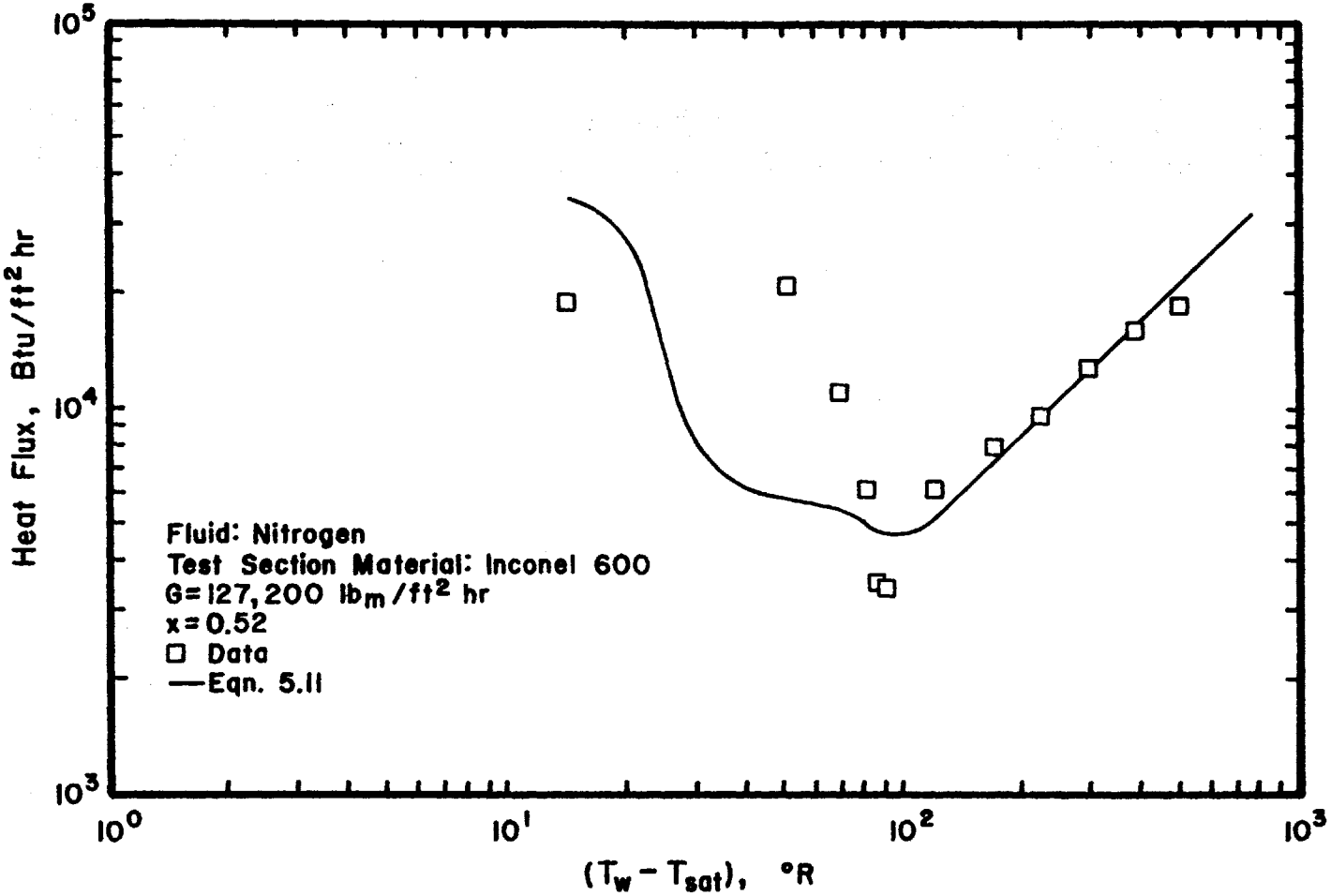

Figure V-8 Heat Flux vs. Wall Superheat

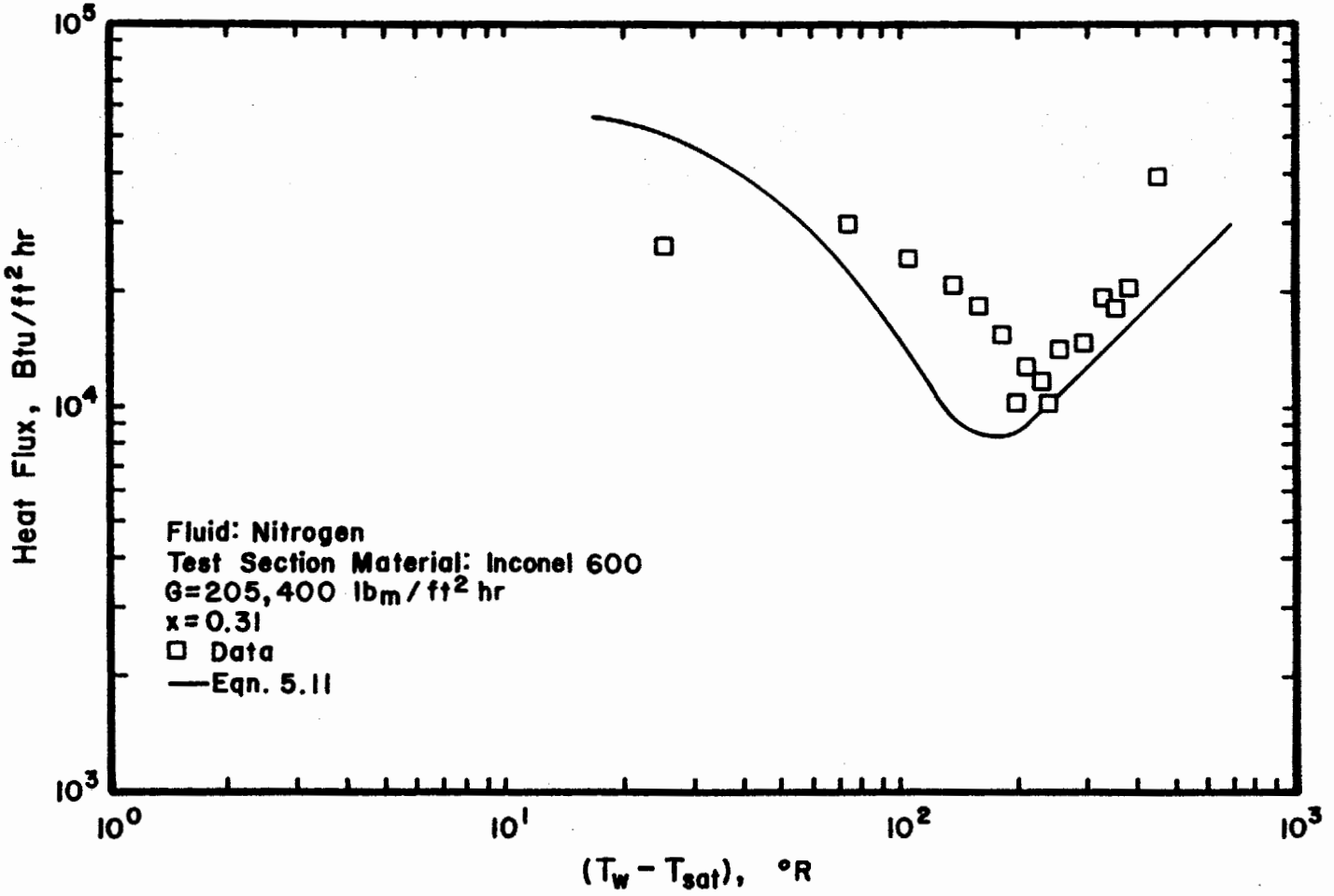

Figure V-9 Heat Flux vs. Wall Superheat

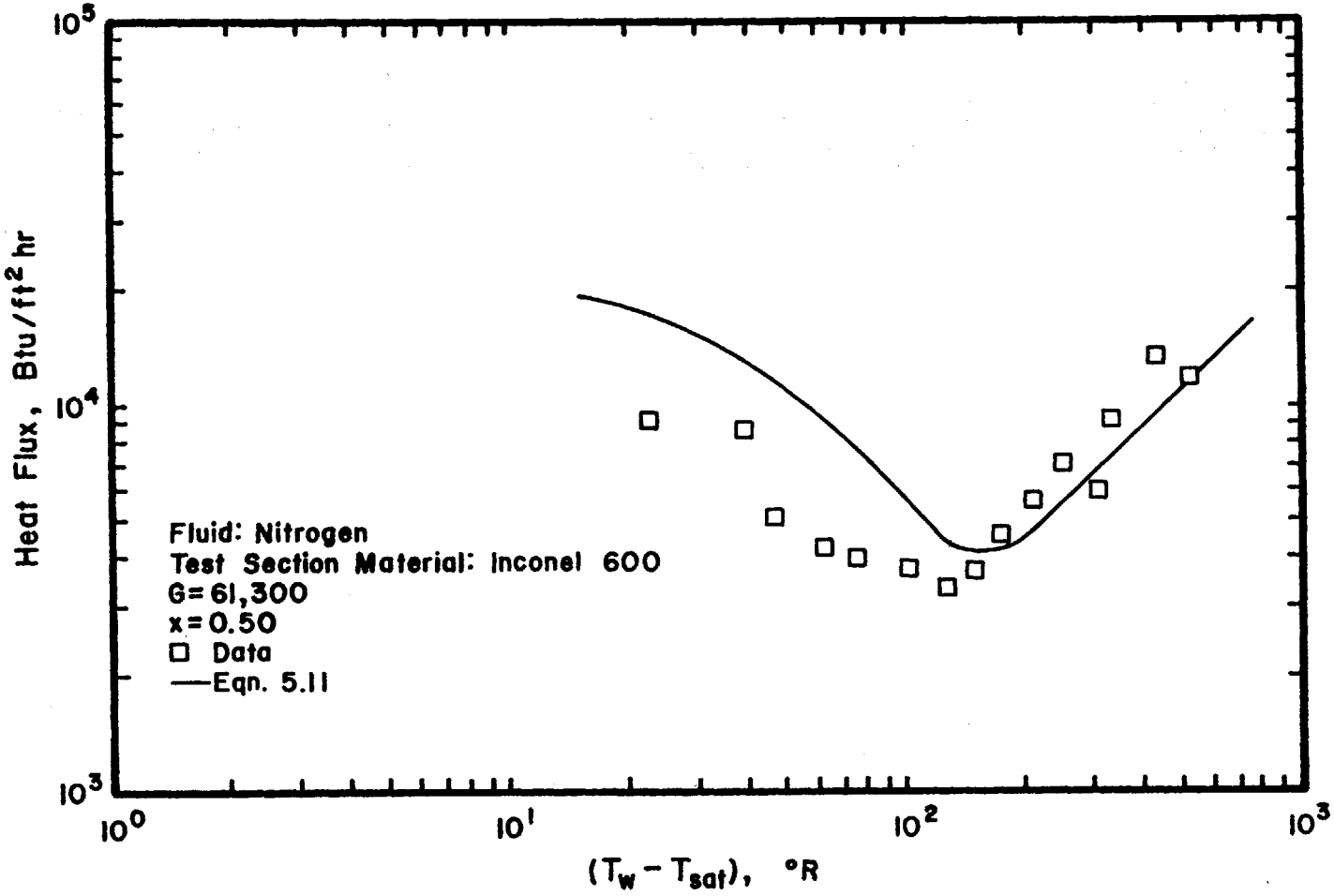

Figure V-10 Heat Flux vs. Wall Superheat

APPENDIX V-4

COMPUTER PROGRAM LISTING

```
C     DISPERSED FLOW HEAT TRANSFER                                          PGM10001
C                                                                           PGM10002
C     PROGRAM CALCULATES HEAT FLUX VS. WALL SUPERHEAT FOR GIVEN             PGM10003
C     MASS FLUX AND VAPOR QUALITY                                           PGM10004
C                                                                           PGM10005
      REAL KGV,MUGV,KGL,M,M2,K1,K2                                          PGM10006
      READ(8,1) KGV,MUGV,RHOG,RHCL                                          PGM10007
      READ(8,1) CPG,CPL,HFG,TSAT                                            PGM10008
      READ(8,1) SIGMA,RV,P,KGL                                              PGM10009
      READ(8,11) AL,AG,VIS                                                  PGM10010
      READ(8,111) GM,XE,S1,SLIP,D                                           PGM10011
      READ(8,112) PI,GC,WE,DCRI                                             PGM10012
    1 FORMAT(4F10.6)                                                        PGM10013
   11 FORMAT(3F10.6)                                                        PGM10014
  111 FORMAT(5F10.6)                                                        PGM10015
  112 FORMAT(4F10.6)                                                        PGM10016
    4 FORMAT(1X,F15.3,E20.5)                                                PGM10017
C                                                                           PGM10018
C     THE VALUES OF SLIP FOR PREDICTIONS IN FIGURES 5.3-5.12 WERE           PGM10019
C     BETWEEN 1.3 TO 1.1. IT WAS OBTAINED FROM MODIFIED RESULTS             PGM10020
C     OF REF(50) FOR FULLY DEVELOPED DISPERSED FLOW                         PGM10021
C                                                                           PGM10022
C     S1 IS A SIMBOL FOR C IN FIGURE 5.13 SO VALUES OF S1 CAN BE            PGM10023
C     OBTAINED FROM FIGURE 5.13                                             PGM10024
C                                                                           PGM10025
C     DATA PROPERTY FOR NITROGEN, REF(32) PAGE 207                          PGM10026
C                                                                           PGM10027
C     KGV-VAPOR CONDUCTIVITY (BTU/FT-HR-R)                                  PGM10028
C     KGL-LIQUID CONDUCTIVITY (BTU/FT-HR-R)                                 PGM10029
C     MUGV-VAPOR D. VISCOCITY (LBM/FT-HR)                                   PGM10030
C     VIS-VAPOR C. VISCOCITY (FT2/HR)                                       PGM10031
C     XSCL(I)-ARRAY CONTAINING SCALE FOR THE AXES                           PGM10032
C     RHOL-LIQUID DENSITY (LBM/FT3)                                         PGM10033
C     RHOG-VAPOR DENSITY (LBM/FT3)                                          PGM10034
C     CPG-VAPOR SPEC. HEAT (BTU/LBM-R)                                      PGM10035
C     CPL-LIQUID SPEC. HEAT (BTU/LBM-R)                                     PGM10036
```

```
C      HFG-LATENT HEAT(BTU/LBM)                                                  PGM10037
C      TSAT-SATURATION TEMPERATURE (R)                                           PGM10038
C      SIGMA-SURFACE TENSION (LBF/FT)                                            PGM10039
C      RV-GAS CONSTANT (BTU/LBM-R)                                               PGM10040
C      P-SISTEM PRESSURE (LBF/FT2)                                               PGM10041
C      AL-LIQUID THER. DIFFUSIVITY (FT2/HR)                                      PGM10042
C      AG-VAPOR THER. DIFFUSIVITY (FT2/HR)                                       PGM10043
C      D-TUBE DIAMETER (FT)                                                      PGM10044
C      XE-EQULIBRIUM QUALITY                                                     PGM10045
C      VN-DROPS DEPOSITION VELOSITY (FT/HR)                                      PGM10046
C      M-LIQUID DEPOSITION FLUX (LBM/HR-FT2)                                     PGM10047
C      TCHF-INITIAL VALUE OF WALL TEMPERATURE                                    PGM10048
C      ALFAE-VOID FRACTION BASED ON XE                                           PGM10049
C      SLIP-SLIP (VG/VL)                                                         PGM10050
C      VG-VAPOR VELOSITY (FT/HR)                                                 PGM10051
C      VL-LIQUID VELOSITY (FT/HR)                                                PGM10052
C      WE-WEBER NUMBER                                                           PGM10053
C      RE-REYNOLDS NUMBER                                                        PGM10054
C      PR-PRANDTL NUMBER                                                         PGM10055
C      DM-MAXIMUM DROP DIAMETER (FT)                                             PGM10056
C      DAV-AVERAGE(MEAN) DROP DIAMETER (FT)                                      PGM10057
C      DMP-MOST PROBABLE DROP DIAMETER (FT)                                      PGM10058
C      DCR-DEPOSITED DROP DIAMETER GIVEN BY DROP DEPOSITION MODEL (FT)           PGM10059
C      TWAL-WALL TEMPERATURE                                                     PGM10060
C      DW-AVERAGE DROP DIAMETER FOR DEPOSITD DROPS (FT)                          PGM10061
C      DL-AVERAGE DROP DIAMETER FOR NOT DEPOSITED DROPS (FT)                     PGM10062
C      F-DEPOSITION FACTOR                                                       PGM10063
C      QD-HEAT TRANSFERED BY SINGLE DEPOSITED DROP (BTU)                         PGM10064
C      Q1-HEAT TRANSFER BY  DEPOSITED DROPS (BTU/FT2-HR)                         PGM10065
C      DELTA-BOUNDARY LAYER THICKNESS (FT)                                       PGM10066
C      Q2-HEAT TRANSFER BY NOT DEPOSITED DROPS (BTU/FT2-HR)                      PGM10067
C      TV-VAPOR TEMPERATURE (R)                                                  PGM10068
C      H-VAPOR HEAT TRANSFER COEFFICIENT (BTU/FT2-HR-R)                          PGM10069
C      Q3-HEAT TRANSFER BY VAPOR (BTU/FT2-HR)                                    PGM10070
C      QT-TOTAL HEAT FLUX TO FLUID (BTU/FT2-HR)                                  PGM10071
C      FR-VAPOR FRICTION FACTOR                                                  PGM10072
```

```
C      GC-ACCELERATION (CONVERSICN: (LBF)-(LBM-FT/HR2) )                    PGM10073
C      GM-MASS FLUX (LBM/FT2-HR)                                            PGM10074
C      K2-KONSTANT                                                          PGM10075
C      DCRI-INITIAL VALUE FOR DROP SIZE                                     PGM10076
C                                                                           PGM10077
       TCHF=TSAT+10.                                                        PGM10078
       ALFAE=XE/(XE+SLIP*(RHOG/RHOL)*(1.-XE))                               PGM10079
       VG=GM*XE/(RHOG*ALFAE)                                                PGM10080
       VL=GM*(1.-XE)/(RHOL*(1.-ALFAE))                                      PGM10081
       RE=RHOG*VG*D/MUGV                                                    PGM10082
       FR=0.0791/(RE**0.25)                                                 PGM10083
       VN=0.15*VG*SQRT(FR/2.)                                               PGM10084
       DELTA=D*EXP(-SQRT(2./(36.*FR)))/2.                                   PGM10085
       DELTA=K2*DELTA                                                       PGM10086
       DM=7.5*SIGMA*GC/(RHOG*(VG-VL)**2)                                    PGM10087
       DV1=(VG-VL)/(3600.*3.28)                                             PGM10088
       SIGMA1=3.28*SIGMA                                                    PGM10089
       GAMAL=RHOL*35.314                                                    PGM10090
       DAV=(1.83/DV1)*SQRT(SIGMA1/GAMAL)*3.28                               PGM10091
       DAV=S1*DAV                                                           PGM10092
       DMP=DAV/2.                                                           PGM10093
       TWAL=TCHF                                                            PGM10094
       DCR=10.*3.28E-6                                                      PGM10095
       DO 4 J=1,75                                                          PGM10096
       DSAVE=DCR                                                            PGM10097
C                                                                           PGM10098
       CALL ENG(VG,VL,VN,TWAL,DEITA,DCR,KGV,MUGV,RHOL,RHOG,HFG,CPG,TSAT,D   PGM10099
      1)                                                                    PGM10100
C                                                                           PGM10101
       IF(DCR.LT.DSAVE) DCR=DSAVE                                           PGM10102
       DCR1=DCR/DAV                                                         PGM10103
       DM1=DM/DAV                                                           PGM10104
       IF(DCR1.GE.8.66) GO TO 599                                           PGM10105
       IF(DM1.GE.8.66) GO TO 598                                            PGM10106
       F=(((DCR/DAV)**3+0.75*(DCR/DAV))*EXP(-2.*(DCR/DAV)**2)-              PGM10107
      1((DM/DAV)**3+0.75*(DM/DAV))*EXP(-2.*(DM/DAV)**2)+                    PGM10108
```

```
     2  0.47*(ERF(1.41*DM/DAV)-ERF(1.41*DCR/DAV)))/                        PGM10109
     3 (-((DM/DAV)**3+0.75*(DM/DAV))*EXP(-2.*(DM/DAV)**2)+                 PGM10110
     4 0.47*ERF(1.41*DM/DAV))                                              PGM10111
      IF(DCR.GE.DM) F=0.                                                   PGM10112
      DW=DAV**3*(((DCR/DAV)**3+0.75*(DCR/DAV))*EXP(-2.*(DCR/DAV)**2)-      PGM10113
     1 ((DM/DAV)**3+0.75*(DM/DAV))*EXP(-2.*(DM/DAV)**2)+                   PGM10114
     2 0.47*(ERF(1.41*DM/DAV)-ERF(1.41*DCR/DAV)))/                         PGM10115
     3 (EXP(-2.*(DCR/DAV)**2)-EXP(-2.*(DM/DAV)**2))                        PGM10116
      DW=DW**0.333                                                         PGM10117
      GO TO 59                                                             PGM10118
  598 CONTINUE                                                             PGM10119
      F=((DCR1**3+0.75*DCR1)*EXP(-2.*DCR1**2)+0.47*(ERF(1.41*DM1)-         PGM10120
     1 ERF(1.41*DCR1)))/(0.47*ERF(1.41*DM1))                               PGM10121
      DW=DAV**3*((DCR1**3+0.75*DCR1)*EXP(-2.*DCR1**2)+0.47*(ERF(1.41*      PGM10122
     1 DM1)-ERF(1.41*DCR1)))/EXP(-2.*DCR1**2)                              PGM10123
      DW=DW**0.333                                                         PGM10124
      GO TO 59                                                             PGM10125
  599 CONTINUE                                                             PGM10126
      F=(ERF(1.41*DM1)-ERF(1.41*DCR1))/ERF(1.41*DM1)                       PGM10127
      DW=0.47*DAV**3*(ERF(1.41*DM1)-ERF(1.41*DCR1))                        PGM10128
      DW=DW**0.333                                                         PGM10129
   59 CONTINUE                                                             PGM10130
C                                                                          PGM10131
      QD=DW**3*RHCL*PI*HFG/6.                                              PGM10132
      EFEC=EXP(1.-(TWAL/TSAT)**2)                                          PGM10133
      QD=QD*EFEC                                                           PGM10134
      M=RHOL*VN*(1.-ALFAE)                                                 PGM10135
      IF(DCR.GE.DM) F=0.                                                   PGM10136
      Q1=M*F*QD/(RHOL*DW**3*PI/6.)                                         PGM10137
      PR=MUGV*CPG/KGV                                                      PGM10138
      H=0.023*(KGV/D)*(RE**0.8)*(PR**0.4)                                  PGM10139
      TV=TSAT                                                              PGM10140
      Q3=H*(TWAL-TV)*ALFAE                                                 PGM10141
      Q3=H*(TWAL-TV)                                                       PGM10142
      QT=Q1+Q3                                                             PGM10143
      DELT=TWAL-TSAT                                                       PGM10144
```

```
      WRITE(5,3) DELT,QT                                          PGM10145
    4 TWAL=TWAL+10.                                               PGM10146
      END                                                         PGM10147
```

```
C     THE SUBROUTINE ENG CALCULATES DEPOSITION DIAMETER VS. WALL                PGM20001
C     TEMPERATURE BY GENERATING DROP  TRAJECTORIES INSIDE THE                   PGM20002
C     BOUNDARY LAYER. THE DETAILES CONCERNING DROP TRAJECTORY                   PGM20003
C     CAN BE OBTAINED BY SIMPLY CALLING TMS,X,Y,U,V.                            PGM20004
C                                                                               PGM20005
C     TMS-TIME(MSEC)                                                            PGM20006
C     X-AXIAL POSITION OF DROP (EQUATION 4-1.15)                                PGM20007
C     Y-RADIAL POSITION OF DROP (4-1.11)                                        PGM20008
C     V-RADIAL DROP VELOSITY (EQUATION 4-1.12)                                  PGM20009
C     AXIAL DROP VELOSITY (EQUATION 4-1.14)                                     PGM20010
C                                                                               PGM20011
      SUBROUTINE ENG(VG,VL,VN,TWAL,DELTA,DCR,KGV,MUGV,RHOL,RHOG,HFG,CPG,        PGM20012
     1 TSAT,D)                                                                  PGM20013
C                                                                               PGM20014
      REAL KGV,MUGV ,KSI                                                        PGM20015
      DIMENSION XCOF(4),COF(4),ROOTR(3),ROOTI(3),Y(1000)                        PGM20016
      UV=VG                                                                     PGM20017
      UO=VL                                                                     PGM20018
C                                                                               PGM20019
C     DATA FOR DCRI(IN MICRONS),PI,AND G ARE NEEDED                             PGM20020
C                                                                               PGM20021
      PI=PI                                                                     PGM20022
      DIAM=DCRI                                                                 PGM20023
      G=GC                                                                      PGM20024
      DIAM1=DIAM/(3.28E-6)                                                      PGM20025
      DELTA1=DELTA/(3.28E-6)                                                    PGM20026
      Y(1)=DELTA                                                                PGM20027
      DO 8 J=1,100                                                              PGM20028
      YP=DELTA+0.95*DELTA                                                       PGM20029
C                                                                               PGM20030
C     NOTE FOLLOWING INDENTITIES FROM APPENDIX 4-1                              PGM20031
C     A=A                                                                       PGM20032
C     B=B                                                                       PGM20033
C     C=C                                                                       PGM20034
C     Q=D                                                                       PGM20035
C     ALFA=E                                                                    PGM20036
```

```
C       BETA=F                                                                  PGM20037
C                                                                               PGM20038
        A=3.*RHOG*UV/(8.*RHOL*DELTA)                                            PGM20039
        B=18.*MUGV/(RHOL*DIAM**2)                                               PGM20040
        C=B*UV/DELTA                                                            PGM20041
        Q=(RHOL-RHOG)*G/RHOL                                                    PGM20042
        H=2.6*KGV/DIAM                                                          PGM20043
        ALFA=3.*H**2*(TWAL-TSAT)**2/(HFG**2*RHOL*RHOG*DELTA)                    PGM20044
        BETA=(A*UV-ALFA)/DELTA                                                  PGM20045
        A1=(3.*(B**2-BETA-A**2)-4.*B**2)/3.                                     PGM20046
        B1=(16.*B**3-18.*B*(B**2-BETA-A**2)+27.*(C*A-BETA*B))/27.               PGM20047
        R=B1**2/4.+A1**3/27.                                                    PGM20048
        XCOF(1)=A*C-BETA*B                                                      PGM20049
        XCOF(2)=B**2-BETA+A**2                                                  PGM20050
        XCOF(3)=2.*B                                                            PGM20051
        XCOF(4)=1.                                                              PGM20052
        CALL BAIRS(XCOF,COF,3,ROOTR,ROOTI,IER)                                  PGM20053
        R1R=ROOTR(1)                                                            PGM20054
        R1I=ROOTI(1)                                                            PGM20055
        R2R=ROOTR(2)                                                            PGM20056
        R2I=ROOTI(2)                                                            PGM20057
        R3R=ROOTR(3)                                                            PGM20058
        R3I=ROOTI(3)                                                            PGM20059
        TMS=1.                                                                  PGM20060
        DO 1 I=2,1000                                                           PGM20061
        TS=TMS/1000.                                                            PGM20062
        S=TS/3600.                                                              PGM20063
        CO=C*A-BETA*B                                                           PGM20064
        IF(CO-0.) 98,97,98                                                      PGM20065
   97   R2=-A**2+BETA                                                           PGM20066
        IF(R2-0.) 94,95,96                                                      PGM20067
   96   CONTINUE                                                                PGM20068
C                                                                               PGM20069
C       ROOTS ARE REAL AND DIFFERENT                                            PGM20070
C                                                                               PGM20071
        R01=-B+SQRT(-A**2+BETA)                                                 PGM20072
```

```
      R02=-B-SQRT(-A**2+BETA)                                                  PGM20073
      A10=DELTA+2.*B*(B*ALFA+Q*A)/((B**2+A**2-BETA)**2)                        PGM20074
      A20=-(VN+(B*ALFA+Q*A)/(B**2+A**2-BETA))                                  PGM20075
      A40=UO+(2.*BETA*B*(B*ALFA+Q*A)/(A*(B**2+A**2-BETA)**2))+(B*(B*ALFA       PGM20076
     1 +Q*A)/(A*(B**2+A**2-BETA)))-ALFA/A                                      PGM20077
      A13=1./(B**2+A**2-BETA)                                                  PGM20078
      A31=(BETA-B*R01-R01**2)/(R01*A)                                          PGM20079
      A32=(BETA-B*R02-R02**2)/(R02*A)                                          PGM20080
      A41=A31*R01                                                              PGM20081
      A42=A32*R02                                                              PGM20082
      A43=A13*BETA/A                                                           PGM20083
      DC=-R02*A43+R01*A43-A13*R01*A42+A13*A41*R02                              PGM20084
      DC1=-A10*A43*R02+A20*A43-A13*A20*A42+A13*A40*R02                         PGM20085
      DC2=-A20*A43+A10*R01*A43-A13*R01*A40+A13*A20*A41                         PGM20086
      DC3=-A40*R02+A42*A20+A40*R01-A20*A41-A10*R01*A42+A10*R02*A41             PGM20087
      DC4=A20*A32*A43-A20*A31*A43+A13*R01*A32*A40-A13*R02*A31*A40+             PGM20088
     1  A13*A20*A31*A42-A13*A20*A41*A32-A10*R01*A32*A43+A10*R02*A31*A43        PGM20089
      C1=DC1/DC                                                                PGM20090
      C2=DC2/DC                                                                PGM20091
      C3=DC3/DC                                                                PGM20092
      C4=DC4/DC                                                                PGM20093
      Y(I)=                                                                    PGM20094
     1  C1*EXP(R01*S)+C2*EXP(R02*S)+((B*ALFA+Q*A)/(B**2+A**2-BETA))*S+          PGM20095
     1  A13*C3-2.*B*(B*ALFA+Q*A)/((B**2+A**2-BETA)**2)                         PGM20096
      X=C1*A31*EXP(R01*S)+C2*A32*EXP(R02*S)+(BETA*(B*ALFA+Q*A)/((B**2+         PGM20097
     1  A**2-BETA)*2.*A))*S**2+(A43*C3-A40+UO)*S+C4                            PGM20098
      V=C1*R01*EXP(R01*S)+C2*R02*EXP(R02*S)+(B*ALFA+Q*A)/(B**2+A**2-           PGM20099
     1  BETA)                                                                  PGM20100
      U=C1*A41*EXP(R01*S)+C2*A42*EXP(R02*S)+(BETA*(B*ALFA+Q*A)/(B**2+          PGM20101
     1  A**2-BETA))*S/A+A43*C3-A40+UO                                          PGM20102
      GO TO 44                                                                 PGM20103
   95 CONTINUE                                                                 PGM20104
C                                                                              PGM20105
C     CASE ROORS ARE REAL AND EQUAL                                            PGM20106
C                                                                              PGM20107
      A10=DELTA+2.*B*(B*ALFA+Q*A)/((B**2+A**2-BETA)**2)                        PGM20108
```

```
      A20=-(VN+(B*ALFA+Q*A)/(B**2+A**2-BETA))                                    PGM20109
      A40=UO+2.*BETA*B*(B*ALFA+Q*A)/(A*(B**2+A**2-BETA)**2)+                     PGM20110
     1 B*(B*ALFA+Q*A)/(A*(B**2+A**2-BETA))-ALFA/A                               PGM20111
      A13=1./(B**2+A**2-BETA)                                                   PGM20112
      A32=-(1./A-BETA/(A*B**2))                                                 PGM20113
      A43=BETA/(A*(B**2+A**2-BETA))                                             PGM20114
      DC=-A43+A13*B**2/A+A13*BETA/A                                             PGM20115
      DC1=-A10*A43-A13*A20*B/A+A13*A40                                          PGM20116
      DC2=-A20*A43-A10*B*A43+A13*B*A40+A13*A20*BETA/A                           PGM20117
      DC3=-A40+A20*B/A+A10*B**2/A+A10*BETA/A                                    PGM20118
      DC4=A20*A32*A43-A13*B*A32*A40+A13*A40*BETA/(A*B)-A13*A20*BETA/            PGM20119
     1 (A**2)-A13*A20*A32*BETA/A+A10*B A32*A43-A10*A43*BETA/(A*B)               PGM20120
      C1=DC1/DC                                                                 PGM20121
      C2=DC2/DC                                                                 PGM20122
      C3=DC3/DC                                                                 PGM20123
      C4=DC4/DC                                                                 PGM20124
      Y(I)=                                                                     PGM20125
     1   (C1+C2*S)*EXP(-B*S)+((B*ALFA+Q*A)/(B**2+A**2-BETA))*S+A13*C3-          PGM20126
     1   2.*B*(B*ALFA+Q*A)/((B**2+A**2-BETA)**2)                                PGM20127
      X=-((C1*BETA+C2*B)/(A*B))*EXP(-B*S)-(C2*BETA/(B*A))*(S+1./B)*             PGM20128
     1   EXP(-B*S)+(BETA*(B*ALFA+Q*A)/(2.*A*(B**2+A**2-BETA)))*S**2+            PGM20129
     2   (A43*C3-A40+UO)*S+C4                                                   PGM20130
      V=(C2-C1*B-C2*B*S)*EXP(-B*S)+(B*ALFA+Q*A)/(B**2+A**2-BETA)                PGM20131
      U=((C1*BETA+C2*B)/A)*EXP(-B*S)+(C2*BETA*S/A)*EXP(-B*S)+(BETA*             PGM20132
     1 (B*ALFA+Q*A)/(A*(B**2+A**2-BETA)))*S+A43*C3-A40+UO                       PGM20133
      GO TO 44                                                                  PGM20134
   94 CONTINUE                                                                  PGM20135
C                                                                               PGM20136
C     ROOTS ARE COMPLEX NUMBERS                                                 PGM20137
C                                                                               PGM20138
      KSI=SQRT(+A**2-BETA)                                                      PGM20139
      A10=DELTA+2.*B*(B*ALFA+Q*A)/((B**2+A**2-BETA)**2)                         PGM20140
      A20=-(VN+(B*ALFA+Q*A)/(B**2+A**2-BETA))                                   PGM20141
      A40=UO+2.*BETA*B*(B*ALFA+Q*A)/(A*(B**2+A**2-BETA)**2)+                    PGM20142
     1 B*(B*ALFA+Q*A)/(A*(B**2+A**2-BETA))-ALFA/A                               PGM20143
      A13=1./(B**2+A**2-BETA)                                                   PGM20144
```

```
      A31=-BETA*B/(A*(B**2+KSI**2))                                          PGM20145
      A32=KSI*(A**2-B**2)/(A*(B**2+KSI**2))                                  PGM20146
      A42=B*KSI/A                                                            PGM20147
      A43=BETA*A13/A                                                         PGM20148
      DC=-KSI*A43+A13*B*A42-A13*KSI*A                                        PGM20149
      DC1=-A10*KSI*A43-A13*A20*A42+A13*KSI*A40                               PGM20150
      DC2=-A20*A43-A10*B*A43+A13*B*A40-A13*A*A20                             PGM20151
      DC3=-KSI*A40+A20*A42+A10*B*A42-A10*KSI*A                               PGM20152
      DC4=A20*A32*A43-A13*B*A32*A40-A13*KSI*A31*A40+A13*A20*A31*A42+         PGM20153
     1  A13*A20*A*A32+A10*B*A32*A43+A10*KSI*A31*A43                          PGM20154
      C1=DC1/DC                                                              PGM20155
      C2=DC2/DC                                                              PGM20156
      C3=DC3/DC                                                              PGM20157
      C4=DC4/DC                                                              PGM20158
      Y(I)=                                                                  PGM20159
     1   (C1*COS(KSI*S)+C2*SIN(KSI*S))*EXP(-B*S)+((B*ALFA+Q*A)/(B**2+        PGM20160
     1 A**2-BETA))*S+A13*C3-2.*B*(B*ALFA+Q*A)/((B**2+A**2-BETA)**2)          PGM20161
      X=((C2*A+B*KSI*C1/A)*(B*SIN(KSI*S)+KSI*COS(KSI*S))+(B*KSI*C2/A-        PGM20162
     1 C1*A)*(KSI*SIN(KSI*S)-B*COS(KSI*S)))*EXP(-B*S)/(B**2-KSI**2)+         PGM20163
     2 (BETA*(B*ALFA+Q*A)/(2.*A*(B**2+A**2-BETA)))*S**2+(C3*A43-A40+         PGM20164
     3 UO)*S+C4                                                              PGM20165
      V=((C2*KSI-B*C1)*COS(KSI*S)-(C1*KSI+B*C2)*SIN(KSI*S))*EXP(-B*S)+       PGM20166
     1 (B*ALFA+Q*A)/(B**2+A**2-BETA)                                         PGM20167
      U=(-(C2*A+B*KSI*C1/A)*SIN(KSI*S)+(B*KSI*C2/A-C1*A)*COS(KSI*S))         PGM20168
     1  *EXP(-B*S)+(BETA*(B*ALFA+Q*A)/(A*(B**2+A**2-BETA)))*S+C3*A43-A40      PGM20169
     2  +UO                                                                  PGM20170
      GO TO 44                                                               PGM20171
   98 CONTINUE                                                               PGM20172
      IF(R2I.NE.0.0.AND.R3I.NE.0.) GO TO 61                                  PGM20173
      IF(R1R.EQ.0.) GO TO 50                                                 PGM20174
      IF(R2R.NE.0.) GO TO 800                                                PGM20175
      R2R=R1R                                                                PGM20176
      R1R=0.                                                                 PGM20177
      GO TO 50                                                               PGM20178
  800 IF(R3R.NE.0.) GO TO 60                                                 PGM20179
      R3R=R1R                                                                PGM20180
```

```
      R1R=0.                                                                    PGM20181
   50 CONTINUE                                                                  PGM20182
C                                                                               PGM20183
C     CASE R1R=0.                                                               PGM20184
C                                                                               PGM20185
      A10=DELTA-(B*ALFA+Q*A)/(C*A-BETA*B)                                       PGM20186
      A32=(BETA-B*R2R-R2R**2)/(R2R*A)                                           PGM20187
      A33=(BETA-B*R3R-R3R**2)/(R3R*A)                                           PGM20188
      A42=(BETA-B*R2R-R2R**2)/A                                                 PGM20189
      A43=(BETA-B*R3R-R3R**2)/A                                                 PGM20190
      A40=UO-(BETA*(B*ALFA+Q*A)/(C*A-BETA*B)+ALFA)/A                            PGM20191
      DC=-R2R*A43+R3R*A42-R3R*BETA/A+R2R*BETA/A                                 PGM20192
      DC1=-A10*R2R*A43+A10*R3R*A42-VN*A43-R3R*A40+VN*A42+R2R*A40                PGM20193
      DC2=VN*A43+A40*R3R-A10*R3R*BETA/A-VN*BETA/A                               PGM20194
      DC3=-R2R*A40-VN*A42+VN*BETA/A+A10*R2R*BETA/A                              PGM20195
      DC4=R2R*A33*A40-R3R*A32*A40-VN*A32*A43+VN*A42*A33-                        PGM20196
     1  VN*A33*BETA/A+VN*A32*BETA/A-A10*R2R*A33*BETA/A+R3R*A10*A32*              PGM20197
     2BETA/A                                                                    PGM20198
      C1=DC1/DC                                                                 PGM20199
      C2=DC2/DC                                                                 PGM20200
      C3=DC3/DC                                                                 PGM20201
      C4=DC4/DC                                                                 PGM20202
      Y(I)=                                                                     PGM20203
     1  C1+C2*EXP(R2R*S)+C3*EXP(R3R*S)+(B*ALFA+Q*A)/(C*A-BETA*B)                PGM20204
      X=C2*A32*EXP(R2R*S)+C3*A33*EXP(R3R*S)+(BETA*(B*ALFA+Q*A)/(C*A-            PGM20205
     1 BETA*B)+ALFA+BETA*C1)*S/A+C4                                             PGM20206
      V=C2*R2R*EXP(R2R*S)+C3*R3R*EXP(R3R*S)                                     PGM20207
      U=C1*BETA/A+C2*A42*EXP(R2R*S)+C3*A43*EXP(R3R*S)+(BETA*(B*ALFA+Q*A)        PGM20208
     1 /(C*A-BETA*B)+ALFA)/A                                                    PGM20209
      GO TO 44                                                                  PGM20210
   60 CONTINUE                                                                  PGM20211
C                                                                               PGM20212
C     NO ZERO ROOTS                                                             PGM20213
C                                                                               PGM20214
      A10=DELTA-(B*ALFA+Q*A)/(C*A-BETA*B)                                       PGM20215
      A40=UO-(BETA*((B*ALFA+Q*A)/(C*A-BETA*B))+ALFA)/A                          PGM20216
```

```
      A31=(BETA-B*R1R-R1R**2)/(R1R*A)                                    PGM20217
      A32=(BETA-B*R2R-R2R**2)/(R2R*A)                                    PGM20218
      A33=(BETA-B*R3R-R3R**2)/(R3R*A)                                    PGM20219
      A41=(BETA-B*R1R-R1R**2)/A                                          PGM20220
      A42=(BETA-B*R2R-R2R**2)/A                                          PGM20221
      A43=(BETA-B*R3R-R3R**2)/A                                          PGM20222
      DC=-R2R*A43+R3R*A42+R1R*A43-R3R*A41-R1R*A42+R2R*A41                PGM20223
      DC1=-A10*R2R*A43+A10*R3R*A42-VN*A43-R3R*A40+VN*A42+R2R*A40         PGM20224
      DC2=VN*A43+R3R*A40+A10*R1R*A43-A10*R3R*A41-R1R*A40-VN*A41          PGM20225
      DC3=-R2R*A40-VN*A42+R1R*A40+VN*A41-A10*R1R*A42+A10*R2R*A41         PGM20226
      DC4=R2R*A33*A40-R3R*A32*A40-VN*A32*A43+VN*A42*A33-R1R*A33*A40+     PGM20227
     4R3R*A31*A40+VN*A31*A43-VN*A41*A33+R1R*A32*A40-R2R*A31*A40-         PGM20228
     5VN*A31*A42+VN*A41*A32-A10*A32*A43*R1R+A10*A42*A33*R1R+             PGM20229
     6A10*R2R*A31*A43-A10*R2R*A41*A33-A10*R3R*A31*A42+A10*R3R*A41*A32    PGM20230
      C1=DC1/DC                                                          PGM20231
      C2=DC2/DC                                                          PGM20232
      C3=DC3/DC                                                          PGM20233
      C4=DC4/DC                                                          PGM20234
      IF((R1R*S).GE.150.) GO TO 100                                      PGM20235
      IF((R2R*S).GE.150.) GO TO 100                                      PGM20236
      IF((R3R*S).GE.150.) GO TO 100                                      PGM20237
      XO1=0.                                                             PGM20238
      IF(((R1R*S)+120.).GE.0.) XO1=EXP(R1R*S)                            PGM20239
      XO2=0.                                                             PGM20240
      IF(((R2R*S)+120.).GE.0.) XO2=EXP(R2R*S)                            PGM20241
      XO3=0.                                                             PGM20242
      IF(((R3R*S)+120.).GE.0.) XO3=EXP(R3R*S)                            PGM20243
      Y(I)=                                                              PGM20244
     1  C1*XO1+C2*XO2+C3*XO3+((B*ALFA+Q*A)/(C*A-BETA*B))                  PGM20245
      X=C1*A31*XO1+C2*A32*XO2+C3*A33*XO3+(BETA*(B*ALFA+Q*A)/(C*A-BETA*B) PGM20246
     1 +ALFA)*S/A+C4                                                     PGM20247
      V=C1*R1R*XO1+C2*R2R*XO2+C3*R3R*XO3                                 PGM20248
      U=C1*A41*XO1+C2*A42*XO2+C3*A43*XO3+(BETA*(B*ALFA+Q*A)/             PGM20249
     1 (C*A-BETA*B)+ALFA)/A                                              PGM20250
      GO TO 44                                                           PGM20251
   61 CONTINUE                                                           PGM20252
```

```
C                                                                       PGM20253
C       ROOTS ARE COMPLEX NUMBERS                                       PGM20254
C                                                                       PGM20255
      R2I=ABS(R2I)                                                      PGM20256
      A10=DELTA-(B*ALPA+Q*A)/(C*A-BETA*B)                               PGM20257
      A40=UO-(BETA*((B*ALPA+Q*A)/(C*A-BETA*B))+ALPA)/A                  PGM20258
      A41=(BETA-B*R1R-R1R**2)/A                                         PGM20259
      A42=(BETA-R2R**2+R2I**2-B*R2R)/A                                  PGM20260
      A43=-(B*R2I+2.*R2R*R2I)/A                                         PGM20261
      IF(R1R.EQ.0.) GO TO 100                                           PGM20262
      A31=A41/R1R                                                       PGM20263
      A32=(R2R*(BETA-R2R**2+R2I**2-B*R2R)-R2I*(2.*R2R*R2I+B*R2I))/      PGM20264
     1  (A*(R2R**2+R2I**2))                                             PGM20265
      A33=-(R2I*(BETA-R2R**2+R2I**2-B*R2R)+R2R*(B*R2I+2.*R2R*R2I))/     PGM20266
     2  (A*(R2R**2+R2I** 2))                                            PGM20267
      DC=-R2R*A43+R2I*A42+R1R*A43-R2I*A41                               PGM20268
      DC1=-A10*R2R*A43+A10*R2I*A42-VN*A43-R2I*A40                       PGM20269
      DC2=VN*A43+R2I*A40+A10*R1R*A43-A10*R2I*A41                        PGM20270
      DC3=-R2R*A40-VN*A42+A40*R1R+VN*A41-A10*R1R*A42+A10*R2R*A41        PGM20271
      DC4=R2R*A33*A40-R2I*A32*A40-VN*A32*A43+VN*A42*A33-R1R*A33*A40+    PGM20272
     1 R2I*A31*A40+VN*A31*A43-VN*A41*A33-A10*R1R*A32*A43+A10*R1R*A42*A33 PGM20273
     2 +A10*R2R*A31*A43-A10*R2R*A41*A33-A10*R2I*(A31*A42-A41*A32)       PGM20274
      C1=DC1/DC                                                         PGM20275
      C2=DC2/DC                                                         PGM20276
      C3=DC3/DC                                                         PGM20277
      C4=DC4/DC                                                         PGM20278
      EE1=R2R*C2+R2I*C3                                                 PGM20279
      GG1=R2R*C3-R2I*C2                                                 PGM20280
      EE=R2R*EE1+R2I*GG1                                                PGM20281
      GG=R2R*GG1-R2I*EE1                                                PGM20282
      AA=(BETA*C2-EE-B*EE1)/A                                           PGM20283
      BB=(BETA*C3-GG-B*GG1)/A                                           PGM20284
      Y(I)   =C1*EXP(R1R*S)+(C2*COS(R2I*S)+C3*SIN(R2I*S))*EXP(R2R*S)+   PGM20285
     1  (DELTA-A10)                                                     PGM20286
      V=C1*R1R*EXP(R1R*S)+(EE1*COS(R2I*S)+GG1*SIN(R2I*S))*EXP(R2R*S)    PGM20287
      X=C1*A31*EXP(R1R*S)+EXP(R2R*S)*((AA*R2R-R2I*BB)*COS(R2I*S)+       PGM20288
```

```
     1 (AA*R2I+BB*R2R)*SIN(R2I*S))/(R2R**2+R2I**2)+(UO-A40)*S+C4                PGM20289
       U=A41*C1*EXP(R1R*S)+(AA*COS(R2I*S)+BB*SIN(R2I*S))*EXP(R2R*S)+           PGM20290
     1 (UO-A40)                                                                PGM20291
    44 CONTINUE                                                                PGM20292
       IF(Y(I)-0.) 43,43,177                                                   PGM20293
    43 GO TO 18                                                                PGM20294
   177 IF(Y(I)-Y(I-1)) 1,8,8                                                   PGM20295
     1 TMS=TMS+1.                                                              PGM20296
       GO TO 8                                                                 PGM20297
   100 CONTINUE                                                                PGM20298
     8 DIAM=DIAM+10.*3.28E-6                                                   PGM20299
    18 DCR=DIAM                                                                PGM20300
       RETURN                                                                  PGM20301
       END                                                                     PGM20302
```

APPENDIX V-5

SUMMARY OF DISPERSED FLOW HEAT TRANSFER CALCULATION PRESENTED IN THIS STUDY

The total heat flux from the heated wall to dispersed flow is given by Eq. (5.11), i.e.,

$$q/A = v_0(1 - \alpha)\rho_\ell H_{\ell g} f\, e^{1-(T_w/T_{sat})^2} + 0.023 \frac{k_g}{D} Re^{0.8} Pr^{0.4}(T_w - T_{sat})$$

The units for v_0, T_w, and T_{sat} in this equation are

v_0 [=] ft/hr

T_w [=] °R

and T_{sat} [=] °R

The units for the fluid properties are listed on page 12.

For a given G and x, the slip ratio S ($S = V_g/V_\ell$) was calculated using technique introduced by Plummer [50] (Equation 4.12 on page 98 of Plummer's report was used to evaluate S) which is based on Hynek's study of dispersed flow film boiling [31].

Knowing S,

$$\alpha = \frac{x}{x + \frac{\rho_g}{\rho_\ell} S(1 - x)}$$

and then

$$V_g = \frac{Gx}{\alpha\rho_g}$$

$$V_\ell = \frac{G(1 - x)}{\rho_\ell(1 - \alpha)}$$

$$v_0 = 0.15\ U^* = 0.15\ \frac{Gx}{\alpha\rho_g}\ \sqrt{f_g/2} \quad \text{where} \quad f_g = 0.0791/Re^{0.25}$$

and

$$Re = \frac{GxD}{\alpha\mu_g}$$

Deposition factor f [note that $P(a)$ is given by Eq. (3.7)]:

$$f \equiv \frac{\int_{a_c}^{a_m} a^3\ P(a)\ da}{\int_0^{a_m} a^3\ P(a)\ da}$$

$$= \left\{\left[\left(\frac{a_c}{\bar{a}}\right)^3 + \frac{3}{4}\left(\frac{a_c}{\bar{a}}\right)\right]\ \exp\left[-2\left(\frac{a_c}{\bar{a}}\right)^2\right] - \left[\left(\frac{a_m}{\bar{a}}\right)^3 + \frac{3}{4}\left(\frac{a_m}{\bar{a}}\right)\right]\exp\left[-2\left(\frac{a_m}{\bar{a}}\right)^2\right] + \right.$$

$$\left. + \frac{6}{16}\sqrt{\pi/2}\left[\operatorname{erf}\left(\sqrt{2}\,\frac{a_m}{\bar{a}}\right) - \operatorname{erf}\left(\sqrt{2}\,\frac{a_c}{\bar{a}}\right)\right]\right\}\left\{\frac{6}{16}\sqrt{\pi/2}\ \operatorname{erf}\left(\sqrt{2}\,\frac{a_m}{\bar{a}}\right) - \right.$$

$$\left. - \left[\left(\frac{a_m}{\bar{a}}\right)^3 + \frac{3}{4}\left(\frac{a_m}{\bar{a}}\right)\right]\ \exp\left[-2\left(\frac{a_m}{\bar{a}}\right)^2\right]\right\}^{-1}$$

In order to find f we first calculate a_m, $\bar{a}$, and a_c.

Maximum drop diameter a_m:

$$a_m = \frac{We_c \ \sigma}{\rho_g (V_g - V_\ell)^2} \quad , \quad \text{where} \quad We_c = 7.5$$

Mean drop diameter $\bar{a}$:

$$\bar{a} = \frac{1.83 \ C}{(V_g - V_\ell)} \sqrt{\sigma / \gamma_\ell}$$

where for a given value of G and x, the value of C can be obtained from figure 5.13.

Deposition diameter a_c is calculated for the specified value of the wall temperature (note: a_c varies with T_w) by generating drop trajectories inside the boundary layer. The values of V_g, V_ℓ, and v_0 which we need to calculate a_c are already calculated above. Calculation of a_c is summarized in subroutine ENG on page 165. In the process of generating the drop trajectory, if the distance of the drop from the wall was less than or equal to 5 μm, we assumed that the drop is deposited on the wall (i.e., the wall roughness of 5 μm was assumed). Note that we do not need to know the drop size distribution $P(a)$ to calculate a_c as it was explained in Section 4.4.

BIOGRAPHICAL NOTE

Ejup N. Ganić was born and raised in Yugoslavia, and is a citizen of Yugoslavia. He attended the University of Belgrade during 1965-1972, receiving his B.S. and M.S. degrees in Chemical Engineering.

During 1971 he did his master's thesis research in the Thermal Physics Laboratory, Boris Kidric Institute of Nuclear Sciences, Belgrade. In June of 1972 he joined the Institute for Chemistry, Technology, and Metallurgy, Belgrade, where he still holds a post. He worked in Warsaw, Poland, during the summer of 1969, and in Birmingham, England, during the summer of 1970.

In September of 1973 he entered graduate school at MIT. From that time to date he has been a Research Assistant in the Heat Transfer Laboratory.

He is the author of several publications in the areas of heat transfer, applied mathematics, and energy conversion.

Mr. Ganić has a membership with the American Institute of Chemical Engineers, American Society of Mechanical Engineers, American Nuclear Society, and Sigma Xi.